NASA TECHNICAL NOTE

NASA TN D-2650

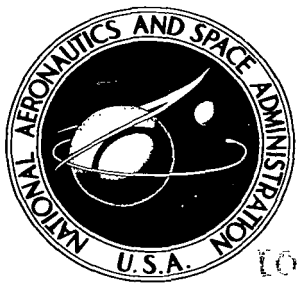

NASA TN D-2650

THEORETICAL BOUNDARIES AND INTERNAL CHARACTERISTICS OF EXHAUST PLUMES FROM THREE DIFFERENT SUPERSONIC NOZZLES

by Earl H. Andrews, Jr., Allen R. Vick, and Charlotte B. Craidon

Langley Research Center
Langley Station, Hampton, Va.

NATIONAL AERONAUTICS AND SPACE ADMINISTRATION • WASHINGTON, D. C. • MARCH 1965

THEORETICAL BOUNDARIES AND INTERNAL CHARACTERISTICS OF EXHAUST PLUMES FROM THREE DIFFERENT SUPERSONIC NOZZLES

By Earl H. Andrews, Jr., Allen R. Vick,
and Charlotte B. Craidon

Langley Research Center
Langley Station, Hampton, Va.

NATIONAL AERONAUTICS AND SPACE ADMINISTRATION

For sale by the Office of Technical Services, Department of Commerce,
Washington, D.C. 20230 -- Price $3.00

THEORETICAL BOUNDARIES AND INTERNAL CHARACTERISTICS OF EXHAUST PLUMES FROM THREE DIFFERENT SUPERSONIC NOZZLES

By Earl H. Andrews, Jr., Allen R. Vick,
and Charlotte B. Craidon
Langley Research Center

SUMMARY

Theoretical exhaust-plume calculations for nozzles exhausting into quiescent air have been performed to obtain exhaust-plume boundaries and internal characteristics within rocket exhaust plumes. The calculations were performed for three different supersonic nozzles over a range of ratios of nozzle-exit pressure to ambient pressure from approximately 10 to 10^6. Also included is a general study of exhaust-plume effects on a typical spacecraft which suggests several possible problem areas requiring further considerations.

The results from the theoretical calculations give exhaust-plume contours out to the maximum plume diameter and the internal characteristics within the plumes for the three different nozzles. The internal characteristics of the exhaust plumes include Mach number, density, and temperature, which are presented in the form of plume internal contour mappings.

INTRODUCTION

The operation of rocket motors at high altitudes and near-vacuum conditions results in a severely underexpanded flow of exhaust gases at the nozzle exit. The nozzle exhaust gases create large billowing exhaust plumes which are of concern (refs. 1 and 2). The areas of concern include the interference of the exhaust plume with the vehicle-to-ground radio-frequency communication signals, the impingement of exhaust gases upon adjacent surfaces with attendant heating and pressure loads, and the reverse-flow effects at the center of a cluster of nozzles. Considerable research is in progress to obtain further understanding of these problem areas with the purpose of preventing or accurately predicting their effects. (See, for example, refs. 3 to 8.)

A knowledge of the internal aerodynamic characteristics of exhaust plumes will assist in the prediction of: (1) plume impingement upon adjacent surfaces and other plumes; (2) the approximation of the magnitude of impingement forces upon adjacent surfaces by use of Newtonian flow theory (ref. 9); and (3) may simplify the prediction of the time of occurrence and the magnitude of signal

attenuation caused by the plume interfering with the vehicle-to-ground communication signals. The attenuation occurs when the nozzle exhaust plume becomes large enough to intercept the line of sight between the vehicle antenna and the ground tracking station.

The work reported herein was initiated to provide theoretical exhaust-plume characteristics which could be used in studies of exhaust-plume impingement and attenuation of radio-frequency signals passing through exhaust plumes. Theoretical calculations have been performed for three different supersonic nozzles: a circular-arc-expansion nozzle of high exit Mach number that is typical of a nozzle designed for space operations, and two conical-expansion nozzles of a lower exit Mach number suitable for lower-altitude operation. The calculations were performed with a computer program using the method of characteristics presented in reference 1 for a range of ratios of nozzle-exit pressure to ambient pressure from approximately 10 to 10^6. Internal-plume contour mappings of Mach number, density, and temperature for several values of the ratio of nozzle-exit pressure to ambient pressure were obtained by machine plotting. An interpolating computer program, which is presented in the appendix, produces the machine-plotting input from the results of the program for the method of characteristics. The method-of-characteristics program assumes a perfect gas exhausting into a quiescent medium and an isentropic flow throughout the exhaust plume. The isentropic-flow assumption is valid in the region of flow bounded by the internal shock of the plume and first Mach disk; however, slight errors are involved in the computations for the region from the internal shock out to the plume boundary. The assumption of a quiescent medium and isentropic flow greatly reduces the complexities and computation time of this computer program.

Also presented is a brief study of exhaust-plume effects on a typical spacecraft in order to determine whether possible problem areas exist which may require further consideration. The study was conducted on problems categorized in the following groups: exhaust-gas impingement, backflow of exhaust gases, and signal attenuation of the transmitting and receiving antennas.

SYMBOLS

M	Mach number
M_j	nozzle-exit Mach number
p_j	nozzle-exit static pressure
p_t	nozzle total pressure
p_∞	ambient pressure
r	perpendicular distance from jet axis
r_j	nozzle-exit radius

T	temperature
x	distance downstream from nozzle-exit plane
α_n	initial turning angle, measured between nozzle axis and tangent to jet boundary at nozzle lip
γ	ratio of specific heats
ρ	density
θ_n	nozzle half-angle
μ	Mach angle
μ_n	Mach angle corresponding to M_j
ν_n	Prandtl-Meyer expansion angle for nozzle-exit Mach number
ν_1	Prandtl-Meyer expansion angle for jet-boundary Mach number

Subscripts:

max	maximum
t	total or stagnation

MODELS AND ANALYTICAL PROCEDURE

The analytical investigation reported herein incorporates results from three supersonic nozzles. One nozzle is of a circular-arc design, and the other two are of a conical-nozzle design. (See fig. 1.) The nozzles are designated Nozzles I, II, and III as shown in figure 1. These nozzles are typical of those used for launch vehicles (nozzles II and III) and for spacecraft (nozzle I). Nozzles I and III are also representative of nozzles designed to obtain from ground tests attenuation measurements of radio-frequency signals passing through the nozzle-exhaust plume. The nozzle geometries are shown in the sketches of figure 1 and the conditions used in the theoretical computations are given in table I.

The method of characteristics as applied in the determination of a nozzle exhaust-plume boundary and the internal characteristic network of the plume requires that the point values of the nozzle leading characteristic line and corner-expansion fan be known. (See refs. 1 and 10.) The type of calculations performed to obtain the leading characteristic line and corner expansion fan was dictated by the nozzle geometries and operating conditions. That is, the leading-characteristic-line calculations are dependent upon nozzle values of M_j, θ_n, and γ, and the corner-expansion-fan calculations require that θ_n, μ_n, γ, and the μ corresponding to the nozzle-total-pressure ratio p_t/p_∞ be

known. For very small nozzles, viscous effects in the nozzle may influence the parameters at the exit (ref. 1); however, for the nozzles investigated herein, nozzle flow was assumed to be inviscid. The leading-characteristic-line and the corner-expansion-fan calculations are performed by means of brief digital computer programs whose output cards are the input data cards for a method-of-characteristics FORTRAN computer program (ref. 1) for determining the characteristic mesh of an exhaust plume. The programs and descriptive procedures are presented in the appendixes of reference 1.

The altitude range for each nozzle for which calculations have been made is presented in figure 2 as a function of the ratio of nozzle-exit pressure to ambient pressure $\left(p_j/p_\infty\right)$. The curves shown span the range of ambient pressures that may be obtained in the 60-foot-diameter vacuum sphere at the Langley Research Center. Nozzle I is representative of a design suitable for operation at the much higher pressure ratios of a space environment.

RESULTS AND DISCUSSION

Theoretical Calculations

Jet plume boundaries for nozzle exhausts expanding into quiescent air have been computed by use of the FORTRAN program presented in reference 1 which incorporates the method of characteristics using three-dimensional irrotational equations of flow. The characteristic network calculations yield the boundary coordinates and several additional internal-flow parameters, one of which is the local Mach number. From the local Mach number and the assumption that the ratio of specific heats (γ) is constant throughout the plume, other flow conditions such as local density and temperature ratios may be obtained. In order to plot contours of constant Mach number and/or other parameters, it is necessary to interpolate between consecutive points in the characteristic net. For this reason a program has been set up to have this step performed by the IBM 7090 electronic data processing system yielding punch cards of the output which can be used directly in machine plotting. This program, written in FORTRAN II language, is included in the appendix.

General details of exhaust plumes and the nomenclature used in identifying this material are shown in figure 3. There is little distinction between the identifying characteristics of exhaust plumes from either a conical or contoured nozzle other than the leading characteristic line (labeled L.C.), which is curved for a conical nozzle and straight for a contoured nozzle. A thorough discussion of these differences may be found in references 1 and 10. The results of the present computations, including free-jet boundaries and internal characteristics of the plume, are presented in figures 4 to 12 and are discussed in the following paragraphs.

Initial turning angle.- As any space-directed vehicle increases in altitude the decreasing ambient pressure results in an increasing ratio of nozzle-exit pressure to ambient pressure and, likewise, an increase in the amount of expansion of the exhaust gases upon emission from the nozzle. Other factors

affecting free-jet expansion are

M_j nozzle-exit Mach number

θ_n nozzle half-angle

γ ratio of specific heats

p_j nozzle-exit static pressure

p_∞ ambient pressure

These factors, determined by nozzle design and conditions in the combustion chamber, affect the expansion as shown in the following sketch:

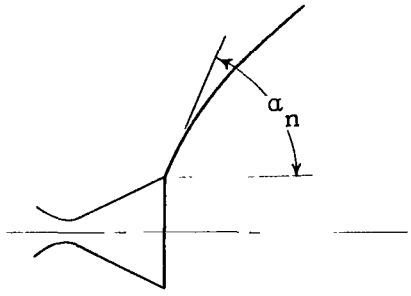

where

$$\alpha_n = \nu_1 - \nu_n + \theta_n \tag{1}$$

and

ν_1 Prandtl-Meyer expansion angle for jet-boundary Mach number

ν_n Prandtl-Meyer expansion angle for nozzle-exit Mach number

A more thorough discussion of this phase of free-jet expansion is presented in reference 1.

The boundary initial-turning angle at the nozzle lip α_n is presented in figure 4 as a function of the pressure ratio for each of the three different nozzles. The end points on the curves indicate the maximum pressure ratio for which theoretical boundaries have been computed and are indicative of turning angles that might be achieved during ground tests in large vacuum facilities. The curves for nozzles II and III also indicate a range of α_n which spans the pressure ratios over which these nozzles might operate. Nozzle I, however, designed for operation in the near-vacuum conditions of outer space will attain a smaller turning angle which approaches the maximum value of α_n for this configuration (approximately 81.5°). The maximum value of α_n for operation

in a near-perfect vacuum for each of the nozzles is indicated on the right-hand ordinate of figure 4.

A comparison of the values of α_n for nozzle I with those for nozzles II and III at a given pressure ratio illustrates the effects of M_j, γ, and θ_n on the initial turning angle. For a given nozzle the effect of θ_n is a constant factor regardless of the operating pressure ratio p_j/p_∞, M_j, or γ. (See eq. (1).) A more concrete illustration of these effects is obtained by comparing the values of α_n for nozzles I and III at $p_j/p_\infty = 10^5$. The difference between the two values of α_n is 54.2°, of which the θ_n accounts for 36 percent, the Mach number at the nozzle exit accounts for 44.8 percent, and the γ accounts for 19.2 percent. The figure indicates that either high Mach number nozzles or reflex nozzles (or both) are desirable to obtain low α_n values. However, consideration must be given to the weight penalty resulting from increase in nozzle thrust and other improvements in the operational characteristics when high Mach number nozzles and/or reflex nozzles are utilized.

Plume boundary contours.- Results of the calculations of jet plume boundaries are shown in figure 5 in which coordinates of the boundaries are presented in the nondimensional form x/r_j and r/r_j. Computations were made for several pressure ratios p_j/p_∞ to obtain a reasonably complete coverage of the range of pressure ratios shown in table I and figure 2. These jet plumes become extremely large as is evidenced by the maximum boundary coordinates at the highest computed pressure ratios; $r/r_j = 900$ and $x/r_j = 3.7 \times 10^3$ for nozzle I at $p_j/p_\infty = 120.700 \times 10^3$ (fig. 5(a)); $r/r_j = 192$ and $x/r_j = 424$ for nozzle II at $p_j/p_\infty = 5.0 \times 10^3$ (fig. 5(c)); and $r/r_j = 7.5 \times 10^3$ and $x/r_j = 19.340 \times 10^3$ for nozzle III at $p_j/p_\infty = 2.38 \times 10^6$ (fig. 5(e)). Further evidence of the enormous size of exhaust plumes in an actual space environment is illustrated by the photographs shown in reference 11. Since primary interest in jet plumes is centered around the regions near the nozzle exit, the initial portions of the boundaries are shown by means of an expanded scale for the three different nozzles in figures 5(b), 5(d), and 5(f).

Construction of additional jet-boundary contours at any intermediate pressure ratio may be obtained by using figure 6 for any one of the three nozzles. This figure was constructed by plotting the results of figure 5 at constant values of x/r_j. All curves of constant x/r_j are noted to fair asymptotically into a single curve which is defined as the locus of points representing the variation of the maximum plume radius $\left(r/r_j\right)_{max}$ with pressure ratio. Also shown in this figure is the corresponding downstream location $\left(x/r_j\right)_{max}$ at which the maximum plume radius occurs. The essentially linear variation, on logarithmic paper, of the maximum boundary size with pressure ratio permits reasonably accurate extrapolations to much higher pressure ratios. The symbols

plotted in figure 6 indicate the pressure ratios for which theoretical calculations were performed. The results shown in figures 6(b) and 6(c) are similar to those of reference 1 in that the turning angle at the nozzle lip exceeded 90°. For nozzles II and III the turning angle reaches 90° at $p_j/p_\infty = 1.13 \times 10^3$ and $p_j/p_\infty = 2.275 \times 10^3$, respectively.

Internal Mach number distribution.- The center-line Mach number distributions within the exhaust plume are shown in figure 7 as a function of distance downstream of the nozzle exit. The point designated L.C. represents the point of intersection of the leading characteristic line with the nozzle axial center line. The ticks on the curves indicate the center-line Mach number at the downstream location of the maximum plume diameter corresponding to the indicated pressure ratios. Since the Mach number distributions were obtained from the characteristic-network computations with isentropic flow assumed, the static pressure distribution may be determined directly from the nozzle total pressure and center-line Mach numbers up to the location of the first normal shock. The method-of-characteristic program that was used to obtain the theoretical plume characteristics had no provisions for calculating the location of the first normal shock; however, a prediction of this shock may be obtained from references 12 to 14. The approximate method of reference 12, for example, indicates the occurrence of a normal shock when the static pressure behind the shock is equal to the ambient pressure; this method was found to produce good agreement with experimental data for the $M_j = 1.0$ nozzle of reference 1.

The plume internal characteristics obtained from the theoretical computations are presented in the form of internal mappings of constant Mach number contours within the plume. This mapping in turn permits a direct construction of contours of constant density and temperature ratios by use of well-known density- and temperature-ratio equations expressed in terms of specific heats and Mach number. (See eqs. (45) and (43), respectively, of ref. 15.) The Mach number contours are presented in figures 8, 9, and 10 for the three different nozzles. The outside curve in each figure represents the jet-plume boundary which is a line of constant Mach number corresponding to the ratio of the total nozzle pressure to the ambient pressure. Two or more plots are presented for some pressure ratios to clarify details near the nozzle exit. The internal-shock location is omitted in all figures; however, the location may easily be approximated as a line formed by the intersections of the constant Mach number contour lines originating at the nozzle center line with the contours which are essentially parallel to the jet boundary. Also, any contour which can be traced from the nozzle-exit plane to the plume center line for a given pressure ratio is not influenced by a further increase in p_j/p_∞. Therefore, to eliminate congestion in the mapping at the higher pressure ratios some of the low Mach number contours have not been presented.

In planes perpendicular to the nozzle center line, local Mach number values increase continually with increases in radial distance out to the location of the internal shock, where a sharp Mach number decrease occurs and a subsequent gradual decrease out to the plume boundary. As stated previously, the computer program does not make any provision for an entropy gain as the flow proceeds across the internal shock toward the plume boundary. Thus,

contours of the flow parameters located outside the internal shock would be expected to be in slight error, particularly at large distances from the nozzle exit. Also, if the methods of references 12 to 14 indicate the occurrence of a normal shock before the maximum boundary diameter is reached, the internal mapping contours shown downstream of the normal-shock location should be disregarded.

Density and temperature distributions within the plume.- Since both density and temperature are functions of the ratio of the specific heats of the gas γ and of Mach number, the lines of constant Mach number shown in figures 8 to 10 may also be considered as lines of constant density and temperature. The conversion from Mach number to density and temperatures in ratio form may be easily accomplished by using table II (obtained through use of ref. 16). Typical curves showing the variation of density with radial distance from the axis r/r_j are presented in figure 11 at specific distances downstream of the nozzle exit. (The curves are for nozzle II.) The symbols on the curves indicate the boundary values at the stated pressure ratios. The density is noted to decrease continually from the axis out to the internal shock location where an abrupt increase occurs, followed by a more gradual increase out to the boundary. At a given station downstream of the nozzle exit the internal shock moves away from the center line as the pressure ratio is increased. Also, the density contours (same as Mach number contours) which are bounded by the internal shock for one ratio of nozzle-exit pressure to ambient pressure are not influenced by further pressure ratio increases. Therefore, density values bounded by the internal shock at one pressure ratio are merely repeated for a higher pressure ratio, which accounts for the smooth portion of the curves in figure 11.

Typical variations of temperature ratio within exhaust plumes are presented in figure 12. (Again values for nozzle II are used.) The temperature variations at constant distances downstream of the nozzle exit are very similar to the density profiles of figure 11.

Exhaust interference with communication signals.- The occurrence of radio-frequency signal attenuation has been experienced during various missile launchings. One such vehicle is the Scout which experiences attenuation during the final portion of the second-stage burning period as reported in references 3 to 6. The signal attenuation usually began when the vehicle had attained an altitude of approximately 180.0×10^3 feet $\left(p_j/p_\infty \approx 674\right)$. The signals were received by two different stations; the firing-range station experienced a large amount of attenuation whereas the other station experienced a signal enhancement. (Further discussion of signal attenuation and enhancement may be found in ref. 6.) Since the nozzle of the Scout second stage is comparable to the nozzle II configuration reported herein, a comparison of plume size with the beginning of signal attenuation yields some significant information. The actual Scout vehicle experiences effects from the free-stream flow whereas nozzle II is exhausting into quiescent air. For convenience, figure 2 includes notations of the burning and attenuation period relative to the Scout second stage. The firing-range station signal "look" path for an aspect angle of approximately 10° (ref. 6), superimposed on the curves of figures 5(d) and 9, shows that the path does pass through the plume at $p_j/p_\infty = 1.0 \times 10^3$

(altitude $\approx 190.0 \times 10^3$ ft). If values from figure 6(b) at $p_j/p_\infty = 680$ (altitude $\approx 180.0 \times 10^3$ ft) are used, it can be seen that the "look" path is just beginning to pass through the exhaust plume. The onset of attenuation therefore appears to correspond to the time that the signal "look" path is intercepted by the theoretical exhaust plume. This suggests that the onset of attenuation may be predicted by theoretical data obtained for quiescent air conditions.

Analysis of Exhaust Effects on a Typical Spacecraft

A comparison of the results from a brief study of exhaust-plume effects on a typical spacecraft made in conjunction with the analytical calculations performed in this investigation suggests several possible problem areas which warrant consideration. The magnitude of these problems is such that additional experimental work may be required. Figure 13 shows a typical spacecraft and indicates the location of two of the three vernier engines in relation to a retro-rocket nozzle with attached jettisonable altitude marking antenna. Exhaust-plume boundaries, including the approximate boundary for outer-space operation, are shown for the vernier engines (nozzle I) at four pressure ratios. An estimated normal shock produced by impingement of the exhaust jet on the retro-rocket nozzle is also indicated. One area of prime concern is the heating problem produced by jet impingement on the nozzle. The estimated normal shock adjacent to the retro-rocket nozzle is shown again in figure 14 together with the line of intersection of the three vernier exhaust jets beneath the nozzle and a turbulent dead-gas region of high temperature beneath the radar antenna. Impingement of the vernier exhaust plumes on the retro-rocket nozzle will probably result in a region behind the normal shock of relatively high pressure and temperature. The possibility of a midcourse maneuver lasting several minutes may therefore subject the retro-rocket nozzle and antenna to high-temperature flow and overheating. Reference 17 indicates that for a particular spacecraft the allowable temperature variation for satisfactory operation of the various components is relatively small.

Additional problem areas are indicated in figure 15 in terms of the possible intersection of the vernier exhaust jet with a radar antenna and the landing pads. Here again, the impingements may produce shocks which will result in high local gas temperatures. At an angle of about 80°, each occurrence of jet impingement with equipment or structure and the resultant complex shock of the system increases the amount of backflow of the exhaust gases. In this instance the blocked-base area is about 95 percent, as shown in figure 16; however, this blockage may not always occur in a single plane. With this situation the backflow of hot exhaust gases will follow a circuitous route and will come in contact with various pieces of equipment including the aluminum support structure and the fuel and oxidizer tanks.

Finally, the possibility of radar antennas located near the zones of intersection of the jet exhaust boundaries may be another area of concern. (See fig. 17.) The intersection of these boundaries will result in considerable molecular bombardment and the creation of a zone of high temperature and,

consequently, of high ionization. Much uncertainty exists as to the magnitude of the signal attenuation expected for plume interactions such as this. (See ref. 18.)

CONCLUDING REMARKS

Internal characteristics of exhaust plumes have been computed out to the plume maximum diameter for three different nozzles at ratios of nozzle-exit pressure to ambient pressure ranging from 10 to 2.38×10^6. Exhaust plume boundaries are shown for several pressure ratios and figures are presented that allow the size and shape of the exhaust plumes to be determined at intermediate pressure ratios. Internal contours of constant Mach number are shown for several pressure ratios from which density and temperature within the exhaust plume may be obtained. It was noted that the plume internal Mach number (also density and temperature) at points within the internal shock for one ratio of nozzle-exit pressure to ambient pressure was not influenced by a further increase in pressure ratio.

A brief study of the exhaust-plume effects on a typical spacecraft has led to the conclusion that several problem areas can exist which may require further consideration.

Langley Research Center,
National Aeronautics and Space Administration,
Langley Station, Hampton, Va., November 3, 1964.

APPENDIX

COMPUTER PROGRAM

The method-of-characteristics computer program of reference 1 yields boundary coordinates and several additional internal-flow parameters, one of which is the local Mach number. Plots of constant Mach number contours within the exhaust plumes are desired; however, in order to obtain these plots, it is necessary to interpolate between consecutive points in the characteristic net. For this reason a program has been set up to have the interpolation performed by a computer which yields output cards that are used directly in machine plotting of Mach number contours. The program obtains the point values by second-order interpolation of the program-output tape of reference 1.

The only input required for the interpolation program is the coordinate-scale ranges for the plot and the Mach numbers for which contour lines are desired. The coordinate ranges and Mach numbers are selected from the output listing of the characteristic program of reference 1. Care should be taken in the selection of the Mach numbers so as not to have the constant Mach number lines too dense near the nozzle exit; figure 10(b) is an example of dense Mach number lines. The results of the machine plotting are presented in figures 8 to 10.

The interpolating program for an IBM 7090 electronic data processing system, written in FORTRAN II language, is reproduced in the following pages.

APPENDIX

```
CP5431
C
C     READS TAPE WRITTEN BY P-5430,
C     INTERPRETS FOR SPECIFIC MACH NUMBERS IN THE NETWORK,
C     PUNCHES CARDS FOR MACHINE PLOTTING
C
C
C              INPUT FOR A CASE
C
C     1ST CARD  IDENTIFICATION, COL.1-80
C     2ND CARD  ID FOR CARD OUTPUT, COL.1-6
C     3RD CARD  MACH NO., COL.1-7
C               INCREMENT FOR MACH NO., COL.8-14
C               X SCALE FACTOR (CANT BE 0), COL.15-21
C               Y SCALE FACTOR (CANT BE 0), COL.22-28
C               SET X ORIGIN, COL.29-35
C               SET Y ORIGIN, COL.36-42
C               SQUARED ACCEPTABLE DISTANCE BETWEEN POINTS, COL.43-49
C               LIMITS SIZE OF X, COL.50-56
C               LIMITS SIZE OF Y, COL.57-63
C     4TH CARD  NO, OF INCREMENTED MACH NOS, TO BE USED, COL.1-4
C               =1 INITIAL RUN (COMPUTES NB AND PICKS BND PTS) OR
C               =2 PICKUP (EXPECTS NB VALUE AND IGNORES BND PTS),COL.5-8
C               =0 INITIAL RUN OR
C               =NB VALUE (NO. X,Y COORDINATES FOR BND PTS), COL.9-12
C               =0 EXIT AFTER THIS CASE OR
C               =1 READ MORE INPUT, COL.13-16
C
      DIMENSION FILE(10,1000),BPTS(2000),BP(2000),
     1XYPTS(4000),XY(4000),CASID(14)
      COMMON FILE
C
C          COM TO OPER
C
      PRINT 1
    1 FORMAT (38HOGIVEN TAPE ON B5, SAVE B5, START, CBC)
      PAUSE
      REWIND 9
      WRITE OUTPUT TAPE 6,2
   20FORMAT (1H1CHARLOTTE CRAIDON/
     11H1////28HOSETUP FOR PLOTTING   P-5431///)
      IF DIVIDE CHECK 3,3
C
C          INPUT AND RETURN FOR NEW CASE
C
    3 READ INPUT TAPE 5,4,CASID,RUN,FINDV,FINCR,XSCAL,
     1YSCAL,XMIN,YMIN,DTEST,XBIG,YBIG,
     2NIND,NBND,NB,NCASE
    4 FORMAT(13A6,A2/A6/9F7.0/4I4)
C
C          SET J FOR MACH
C
      J=9
C
C          PRINT CASE ID
C
    9 WRITE OUTPUT TAPE 6,10,CASID
   10 FORMAT(1H ,13A6,A2///)
C
C          USE OR IGNORE BOUNDARY PTS
C
   11 IF (NBND-2) 12,35,920
C
C
C          BOUNDARY POINT SECTION
C
C
   12 NSIG=1
      LTST=1
C
C          RETURN FOR NEW FILE
C
   13 CALL XTPRD(NUSE,NSIG)
C
C          TEST FOR MORE FILES
C
   14 IF(NSIG)930,20,15
   15 N=NUSE
      NB=NB+2
      BPTS(NB-1)=FILE(8,N)
C
C          SET Y+
C
      BPTS(NB)=ABSF(FILE(7,N))
   16 GO TO(17,18),LTST
   17 LTST=2
      GO TO 13
C
C          TEST FOR ABS Y DECREASING
C
   18 IF (BPTS(NB)-BPTS(NB-2)) 20,13,13
   20 REWIND 9
      NBND=2
C
C          SETUP FOR PLOT
C
C          PUNCH OFFSET CARD
      WRITE OUTPUT TAPE 7,22,RUN
   22 FORMAT (6H$$$$$N,6X2H0,6X2H0,1X1H-42X
     .11HCBC5431 OFFSET .A61
```

APPENDIX

```
C
C          PRINT HEADINGS
C
      WRITE OUTPUT TAPE 6,23,NB,RUN
   23 FORMAT (23H0BOUNDARY POINTS    NB=I5,4X,A6//
     17X4HPLOT14X4HREAL//4X1HX7X1HY8X1HX9X1HY///)
C
C          SCALE AND SET 0 PT. FOR BOUNDARY
C
      DO 24 I=1,NB,2
      BP(I)=BPTS(I)*XSCAL-XMIN
      BP(I+1)=BPTS(I+1)*YSCAL-YMIN
   24 CONTINUE
C
C          PUNCH AND PRINT
C
      BPX=BP(1)
      BPY=BP(2)
C
C          OMIT POINT IF OUTSIDE RANGE
C
      IF(XBIG-BPX) 245,240,240
  240 IF(YBIG-BPY) 245,242,242
  242 WRITE OUTPUT TAPE 7,28,BPX,BPY,BPTS(1),BPTS(2),RUN
      WRITE OUTPUT TAPE 6,29,BPX,BPY,BPTS(1),BPTS(2)
  245 DO 30 I=3,NB,2
C
C          CHECK DISTANCE BETWEEN POINTS
C
      D2=(BPX-BP(I))**2+(BPY-BP(I+1))**2
      IF(D2-DTEST)30,25,25
   25 BPX=BP(I)
      BPY=BP(I+1)
C
C          OMIT POINTS IF OUTSIDE RANGE
C
      IF (XBIG-BPX) 30,26,26
   26 IF (YBIG-BPY) 30,27,27
   27 WRITE OUTPUT TAPE 7,28,BPX,BPY,BPTS(I),BPTS(I+1),RUN
   28 FORMAT(6H$$$$$N,2F8.0,2F10.2,24X14HCBC5431  BND  ,A6)
      WRITE OUTPUT TAPE 6,29,BPX,BPY,BPTS(I),BPTS(I+1)
   29 FORMAT(2F8.0,2F10.2)
   30 CONTINUE
      WRITE OUTPUT TAPE 6,33
   33 FORMAT (1H1)
C
C
C          SEARCH AND INTERPOLATION SECTION
C
C
   35 FIV=FINDV
C
C          RETURN FOR INCREMENTED VARIABLE
C
   40 NSIG=1
      IGN=NB
      NXY=0
C
C          NXY COUNTS COORDINATES
C
C
C          RETURN FOR NEW FILE
C
   45 CALL XTPRD(NUSE,NSIG)
C
C          TEST FOR MORE FILES
C
   46 IF (NSIG)930,84,47
   47 IGN=IGN-2
      IF(IGN)48,50,50
   48 N=NUSE
      GO TO 51
   50 N=NUSE+1
   51 IF(N-998)52,65,45
C
C          SEARCH FILE
C          SET Y+
C
   52 DO 63 I=N,997
      IF(FILE(J,I)-FIV)53,53,60
   53 IF(FIV-FILE(J,I+1))54,54,60
   54 IF(FILE(J,I+1)-FILE(J,I+2))55,55,60
   55 IF(FILE(J,I+2)-FILE(J,I+3))56,56,58
   56 NXY=NXY+2
   57 XYPTS(NXY-1)=TERP2 (FIV,FILE(J,I),FILE(J,I+1),
     1FILE(J,I+2),FILE(8,I),FILE(8,I+1),FILE(8,I+2))
      XYPTS(NXY)=ABSF(TERP2 (FIV,FILE(J,I),FILE(J,I+1),
     1FILE(J,I+2),FILE(7,I),FILE(7,I+1),FILE(7,I+2)))
      GO TO 63
   58 IF(I-(N+1))63,59,59
   59 NXY=NXY+2
      XYPTS(NXY-1)=TERP2 (FIV,FILE(J,I-1),FILE(J,I),
     1FILE(J,I+1),FILE(8,I-1),FILE(8,I),FILE(8,I+1))
      XYPTS(NXY)=ABSF(TERP2 (FIV,FILE(J,I-1),FILE(J,I),
     1FILE(J,I+1),FILE(7,I-1),FILE(7,I),FILE(7,I+1)))
      GO TO 63
   60 IF(FILE(J,I+1)-FIV)61,61,63
   61 IF(FIV-FILE(J,I))56,56,63
   63 CONTINUE
C
C          TEST FOR LAST 3 PTS OR ONLY 3 PTS
$
```

APPENDIX

```
   65 IF(FILE(J,998)-FIV)66,66,68
   66 IF(FIV-FILE(J,999))67,67,70
   67 IF(FILE(J,999)-FILE(J,1000))75,75,70
   68 IF(FIV-FILE(J,999))70,70,69
   69 IF(FILE(J,999)-FILE(J,1000)) 70,70,75
   70 IF(FILE(J,998)-FILE(J,999))71,71,73
   71 IF(FILE(J,999)-FIV)72,72,45
   72 IF(FIV-FILE(J,1000))75,75,45
   73 IF(FILE(J,999)-FIV)45,45,74
   74 IF(FIV-FILE(J,1000))45,45,75
   75 NXY=NXY+2
   78 XYPTS(NXY-1)=TERP2 (FIV,FILE(J,998),FILE(J,999),
     1FILE(J,1000),FILE(8,998),FILE(8,999),FILE(8,1000))
      XYPTS(NXY)=ABSF(TERP2 (FIV,FILE(J,998),FILE(J,999),
     1FILE(J,1000),FILE(7,998),FILE(7,999),FILE(7,1000)))
C
C          READ ANOTHER FILE
C
   80 GO TO 45
   84 IF(NXY)920,105,85
C
C          PRINT HEADINGS
C
   85 WRITE OUTPUT TAPE 6,86,FIV,RUN
   86 FORMAT(15HOMACH NUMBER = ,F6.2,4X,A6//
     17X4HPLOT14X4HREAL//4X1HX7X1HY8X1HX9X1HY///)
C
C          SCALE AND SET 0 PT.
C
      DO 87 I=1,NXY,2
      XY(I)=XYPTS(I)*XSCAL-XMIN
      XY(I+1)=XYPTS(I+1)*YSCAL-YMIN
   87 CONTINUE
C
C          PUNCH AND PRINT
C
      XSAV=XY(1)
      YSAV=XY(2)
C
C          OMIT POINT IF OUTSIDE RANGE
C
      IF (XBIG-XSAV) 90,88,88
   88 IF(YBIG-YSAV) 90,89,89
   89 WRITE OUTPUT TAPE 7,98,XSAV,YSAV,XYPTS(1),XYPTS(2),FIV,RUN
      WRITE OUTPUT TAPE 6,99,XSAV,YSAV,XYPTS(1),XYPTS(2)
   90 IF(NXY-2)920,101,91
   91 DO 100 I=3,NXY,2
C
C          CHECK DISTANCE BETWEEN POINTS
C
      D2=(XSAV-XY(I))**2+(YSAV-XY(I+1))**2
      IF(D2-DTEST)100,92,92
   92 XSAV=XY(I)
      YSAV=XY(I+1)
C
C          OMIT POINTS IF OUTSIDE RANGE
C
      IF (XBIG-XSAV) 100,94,94
   94 IF (YBIG-YSAV) 100,97,97
   97 WRITE OUTPUT TAPE 7,98,XSAV,YSAV,XYPTS(I),XYPTS(I+1),FIV,RUN
   98 FORMAT(6H$$$$$$N,2F8.0,2F10.2,24X7HCBC5431,F6.2,1X,A6)
      WRITE OUTPUT TAPE 6,99,XSAV,YSAV,XYPTS(I),XYPTS(I+1)
   99 FORMAT(2F8.0,2F10.2)
  100 CONTINUE
  101 WRITE OUTPUT TAPE 6,33
C
C          TEST FOR VARIABLE INCREMENT
C
  105 IF(NIND)107,107,106
  106 NIND=NIND-1
      FIV=FIV+FINCR
      GO TO 40
C
C          EXIT TEST
C
  107 IF(NCASE)108,108,3
  108 REWIND 9
      END FILE 7
      CALL EXIT
C
C        ERR RETURN
C
  920 REWIND 9
      END FILE 7
      WRITE OUTPUT TAPE 6,921
  921 FORMAT(14HOPROGRAM ERROR/1H1)
      CALL DUMP
C
C          REDUNDANCY CHECK RETURN
C
  930 WRITE OUTPUT TAPE 6,931
  931 FORMAT(43HOREDUNDANCY CHECK AFTER 10 ATTEMPTS TO READ/1H1)
      REWIND 9
      END FILE 7
      CALL EXIT
      END
```

APPENDIX

```
C              SECOND ORDER INTERPOLATION
C
C
C
      FUNCTION TERP2(X,X0,X1,X2,F0,F1,F2)
    1 F11=(F0*(X1-X)-F1*(X0-X))/(X1-X0)
    2 F21=(F0*(X2-X)-F2*(X0-X))/(X2-X0)
    3 TERP2=(F11*(X2-X)-F21*(X1-X))/(X2-X1)
      IFDIVIDECHECK6,8
    6 WRITE OUTPUT TAPE6,7
    7 FORMAT(30HODIVIDE CHECK IN INTERP, SUBR,/1H1)
      CALL DUMP
    8 RETURN
      END
```

```
*       FAP
        COUNT   55
        LBL     XTPRD,X
        ENTRY   XTPRD
*
*  XTPRD (N,NSIG)    SUBR, TO READ A FILE ON B5 FOR P-5431
*       N = BEGINNING RECORD FOR FORTRAN PROGRAM
*       NSIG = -  REDUNDANCY CHECK AFTER 10 TRIES
*            = 0  END OF TAPE
*            = +  MORE FILES TO BE READ
*
 XTPRD  CLA     1,4
        STA     ANS
        CLA     2,4
        STA     OUT+1
        STA     REDUN+3
        SXA     AC,1
        SXA     AC+1,2
        SXA     AC+2,4
        AXT     10,1
 IN     TEFB    *+1             EOF LIGHT OFF
        RTBB    5
        RCHB    IO
        TCOB    *
        TEFB    OUT             EOF,END TAPE
        RTBB    5
        RCHB    IO1
        TCOB    *
        TRCB    REDUN
        SCHB    BADD
        CLA     BADD
        ANA     MASK
        SUB     FX1
        CHS
        ADD     LFILE
        LRS     35
        DVP     FX10
        XCA
        ADD     FX1
        ALS     18
 ANS    STO     **
 AC     AXT     **,1
        AXT     **,2
        AXT     **,4
        TRA     3,4
 IO     IOCD    FILE-9999,0,10
 IO1    IOCD    FILE-9989,0,9991
 REDUN  BSFB    5
        TIX     IN,1,1
        CLA     MASK1
        STO     **
        TRA     AC
 OUT    REWB    5
        STZ     **
        TRA     AC
 LFILE  PZE     FILE
 BADD   BSS     1
 FX1    DEC     1
 FX10   DEC     10
 MASK   OCT     77777
 MASK1  OCT     400001000000
 FILE   COMMON  10000
        END
```

REFERENCES

1. Vick, Allen R.; Andrews, Earl H., Jr.; Dennard, John S.; and Craidon, Charlotte B.: Comparisons of Experimental Free-Jet Boundaries With Theoretical Results Obtained With the Method of Characteristics. NASA TN D-2327, 1964.

2. Vick, Allen R.; Cubbage, James M.; and Andrews, Earl H., Jr.: Rocket Exhaust Plume Problems and Some Recent Related Research. Presented at a Specialists' Meeting on "The Fluid Dynamic Aspects of Space Flight" (Marseille, France), AGARD, April 20-24, 1964.

3. Mayhue, Robert J., compiler: NASA Scout ST-1 Flight-Test Results and Analyses, Launch Operations, and Test Vehicle Description. NASA TN D-1240, 1962.

4. Sims, Theo E.; and Jones, Robert F.: Rocket Exhaust Effects on Radio Frequency Propagation From a Scout Vehicle and Signal Recovery During the Injection of Decomposed Hydrogen Peroxide. NASA TM X-529, 1961.

5. Sims, Theo E.; and Jones, Robert F.: Flight Measurements of VHF Signal Attenuation and Antenna Impedance for the RAM A1 Slender Probe at Velocities Up to 17,800 Feet per Second. NASA TM X-760, 1963.

6. McIver, Duncan E., Jr.: Study of the Effects of a Rocket Exhaust on Radio Frequency Signal Attenuation by the Use of a Recoverable Camera on the NASA Scout Vehicle. NASA TM X-888, 1963.

7. Balwanz, W. W.; and Weston, J. P.: The Prediction of Rocket Exhaust Interference With Radio Signals. [Preprint] 2591-62, American Rocket Soc., Oct. 1962.

8. Anon.: Rocket Testing in Simulated Space and High Altitude Environments. Vol. I. AEDC-TR-61-14(Contract No. AF 40(600)-800 S/A 24(61-73)), Arnold Eng. Develop. Center, Oct. 1961.

9. Margolin, E. L.; and Welch, Eugene: Final Report - Single Nozzle Jet Plume Test in the Rocket Nozzle Test Facility. SID 63-426, North American Aviation, Inc., May 6, 1963.

10. Love, Eugene S.; Grigsby, Carl E.; Lee, Louise P.; and Woodling, Mildred J.: Experimental and Theoretical Studies of Axisymmetric Free Jets. NASA TR R-6, 1959. (Supersedes NACA RM L54L31 by Love and Grigsby, RM L55J14 by Love, RM L56G18 by Love, Woodling, and Lee, and TN 4195 by Love and Lee.)

11. Anon.: South African Station's Photo Sequence. Aviation Week and Space Technol., vol. 79, no. 8, Aug. 19, 1963, pp. 30-31.

12. Adamson, Thomas C., Jr.: The Structure of the Rocket Exhaust Plume Without Reaction at Various Altitudes. 4613-45-T(Contract SD-91), Inst. Sci. and Technol., Univ. of Michigan, June 1963.

13. Eastman, Donald W.; and Radtke, Leonard P.: Location of the Normal Shock Wave in the Exhaust Plume of a Jet. AIAA J., (Tech. Notes and Comments), vol. 1, no. 4, Apr. 1963, pp. 918-919.

14. D'Attorre, L.; and Harshbarger, F.: Experimental and Theoretical Studies of Underexpanded Jets Near the Mach Disc. GDA-DBE 64-008(Contract No. AF 19(628)-3269, Gen. Dyn./Astronaut., Feb. 19, 1964.

15. Ames Research Staff: Equations, Tables, and Charts for Compressible Flow. NACA Rept. 1135, 1953. (Supersedes NACA TN 1428.)

16. Wang, C. J.; Peterson, J. B.; and Anderson, R.: Gas Flow Tables. GM-TR-154, Space Technol. Labs., Inc., Mar. 14, 1957. (Available from ASTIA as AD No. 221012.)

17. Anon.: The Lunar Program. Space Programs Sum. No. 37-15, Vol. 1 (Contract No. NAS 7-100), Jet Propulsion Lab., C.I.T., May 31, 1962.

18. Anon.: Landing Problem. Aviation Week and Space Technol., vol. 77, no. 15, Oct. 8, 1962, p. 81.

TABLE I.- NOZZLE EXIT GEOMETRY AND OPERATING CONDITIONS FOR CALCULATIONS

	Nozzle I (circular arc)	Nozzle II (conical)	Nozzle III (conical)
M_j	5.35	3.41	3.39
θ_n, deg	0	20.66	19.5
γ	1.24	1.15	1.18
p_t, psia	70 to 240	520	500
p_j, mm Hg	1.65 to 5.64	219.8	246
r_j, in.	2.545	19.25	0.415
Values of p_j/p_∞ used for theoretical calculations	9.88	15	15
	31.9	100	2.38×10^2
	188.1	500	2.38×10^3
	1.359×10^3	1.0×10^3	2.38×10^4
	5.410×10^3	3.0×10^3	2.38×10^5
	13.756×10^3	5.0×10^3	2.38×10^6
	120.700×10^3	7.0×10^3	----------

TABLE II.- GAS FLOW TABLES

[Numbers to right of tabulated values indicate power of 10 by which the number should be multiplied]

Nozzle I, $\gamma = 1.24$

M	$\frac{\rho}{\rho_t}$	$\frac{T}{T_t}$
5.35	0.2017 -2	0.2255
6.0	.9449 -3	.1880
6.5	.5454 -3	.1647
7.0	.3236 -3	.1453
7.5	.1970 -3	.1290
8.0	.1229 -3	.1152
8.5	.7835 -4	.1034
9.0	.5099 -4	.9328 -1
9.5	.3382 -4	.8453 -1
10.0	.2283 -4	.7692 -1
10.5	.1567 -4	.7027 -1
11.0	.1091 -4	.6443 -1
11.5	.7709 -5	.5928 -1
12.0	.5518 -5	.5470 -1
12.5	.3998 -5	.5063 -1
13.0	.2929 -5	.4699 -1
13.5	.2170 -5	.4373 -1
14.0	.1623 -5	.4078 -1
14.5	.1226 -5	.3812 -1
15.0	.9336 -6	.3571 -1
16.5	.4330 -6	.2970 -1
17.0	.3401 -6	.2803 -1
17.5	.2689 -6	.2649 -1
18.0	.2139 -6	.2508 -1
18.5	.1712 -6	.2377 -1
19.0	.1378 -6	.2256 -1
20.0	.9068 -7	.2041 -1
20.5	.7419 -7	.1945 -1
21.0	.6087 -7	.1855 -1
21.5	.5025 -7	.1771 -1
22.0	.4159 -7	.1693 -1
22.5	.3462 -7	.1620 -1
23.0	.2889 -7	.1551 -1
23.5	.2423 -7	.1487 -1
24.0	.2037 -7	.1426 -1
24.5	.1721 -7	.1369 -1
25.0	.1456 -7	.1316 -1
25.5	.1238 -7	.1266 -1
26.0	.1055 -7	.1218 -1
26.5	.9021 -8	.1173 -1
27.0	.7729 -8	.1130 -1
27.5	.6648 -8	.1090 -1
28.0	.5727 -8	.1052 -1
28.5	.4952 -8	.1016 -1
29.0	.4288 -8	.9812 -2
29.5	.3726 -8	.9486 -2
30.0	.3241 -8	.9174 -2
30.5	0.2829 -8	0.8879 -2
31.5	.2167 -8	.8329 -2
32.0	.1902 -8	.8072 -2
32.5	.1674 -8	.7828 -2
33.5	.1303 -8	.7371 -2
34.0	.1152 -8	.7157 -2
34.5	.9992 -9	.6953 -2
35.5	.8061 -9	.6569 -2
36.0	.7177 -9	.6389 -2
36.5	.6405 -9	.6216 -2
37.5	.5120 -9	.5891 -2
38.0	.4586 -9	.3738 -2
Jet boundary		
7.018	0.3178 -3	0.1447
7.995	.1235 -3	.1154
9.67	.2954 -4	.8183 -1
11.875	.5992 -5	.5580 -1
13.667	.1967 -5	.4271 -1
15.014	.9267 -6	.3565 -1
18.643	.1608 -6	.2341 -1

Nozzle II, $\gamma = 1.15$

M	$\frac{\rho}{\rho_t}$	$\frac{T}{T_t}$
3.41	0.1529 -1	0.5342
4.0	.5214 -2	.4545
4.5	.2116 -2	.3970
5.0	.8758 -3	.3478
5.25	.5689 -3	.3260
5.5	.3722 -3	.3059
5.75	.2453 -3	.2874
6.0	.1629 -3	.2703
6.25	.1090 -3	.2545
6.5	.7356 -4	.2399
6.75	.5001 -4	.2264
7.0	.3426 -4	.2139
7.25	.2365 -4	.2023
7.5	.1645 -4	.1916
7.75	.1153 -4	.1817
8.0	.8137 -5	.1724
8.25	.5784 -5	.1638
8.5	.4140 -5	.1558
8.75	.2983 -5	.1483
9.0	.2163 -5	.1413
9.25	.1579 -5	.1348
9.5	.1160 -5	.1287
9.75	.8567 -6	.1230
10.0	.6366 -6	.1176
10.25	.4758 -6	.1126
10.5	.3574 -6	.1079
10.75	.2700 -6	.1035
11.0	.2050 -6	.9926 -1
11.25	.1564 -6	.9531 -1
11.5	.1199 -6	.9159 -1
11.75	.9237 -7	.8807 -1
12.0	.7147 -7	.8475 -1
Jet boundary		
5.677	0.2769 -3	0.2926
6.544	.6869 -4	.2374
6.944	.3727 -4	.2166
7.907	.9256 -5	.1758

Nozzle III, $\gamma = 1.18$

M	$\frac{\rho}{\rho_t}$	$\frac{T}{T_t}$
3.39	0.1935 -1	0.4916
4.0	.7044 -2	.4098
4.25	.4687 -2	.3809
4.5	.3137 -2	.3543
4.75	.2113 -2	.3300
5.0	.1433 -2	.3077
5.25	.9790 -3	.2873
5.5	.6741 -3	.2686
5.75	.4677 -3	.2515
6.0	.3271 -3	.2358
6.25	.2305 -3	.2215
6.5	.1637 -3	.2082
6.75	.1172 -3	.1961
7.0	.8447 -4	.1848
7.25	.6134 -4	.1745
7.5	.4487 -4	.1649
7.75	.3304 -4	.1561
8.0	.2450 -4	.1479
8.25	.1828 -4	.1403
8.5	.1373 -4	.1335
8.75	.1038 -4	.1267
9.0	.7887 -5	.1206
9.25	.6029 -5	.1149
9.5	.4635 -5	.1096
9.75	.3582 -5	.1047
10.0	.2783 -5	.1000
10.25	.2173 -5	.9564 -1
10.5	.1704 -5	.9155 -1
10.75	.1344 -5	.8772 -1
11.0	.1064 -5	.8410 -1
11.25	.8458 -6	.8071 -1
11.5	.6754 -6	.7750 -1
11.75	.5417 -6	.7449 -1
12.0	.4360 -6	.7163 -1
12.25	.3524 -6	.6894 -1
12.5	.2858 -6	.6639 -1
13.0	.1901 -6	.6169 -1
13.25	.1559 -6	.5953 -1
13.5	.1281 -6	.5746 -1
13.75	.1057 -6	.5551 -1
14.0	.8749 -7	.5365 -1
14.25	.7263 -7	.5188 -1
14.5	.6045 -7	.5019 -1
14.75	.5047 -7	.4859 -1
15.0	.4225 -7	.4706 -1
15.25	.3546 -7	.4560 -1
15.5	.2984 -7	.4420 -1
15.75	0.2517 -7	0.4287 -1
16.0	.2129 -7	.4160 -1
16.25	.1800 -7	.4038 -1
16.5	.1533 -7	.3921 -1
17.0	.1115 -7	.3702 -1
17.5	.8170 -8	.3501 -1
18.0	.6039 -8	.3316 -1
18.25	.5207 -8	.3229 -1
18.5	.4498 -8	.3144 -1
18.75	.3893 -8	.3064 -1
19.0	.3375 -8	.2986 -1
19.25	.2932 -8	.2911 -1
19.5	.2550 -8	.2839 -1
19.75	.2223 -8	.2767 -1
20.0	.1940 -8	.2703 -1
20.25	.1698 -8	.2638 -1
20.5	.1488 -8	.2576 -1
20.75	.1304 -8	.2516 -1
21.0	.1144 -8	.2458 -1
21.5	.8876 -9	.2348 -1
22.0	.6905 -9	.2244 -1
22.5	.5317 -9	.2148 -1
23.0	.4259 -9	.2057 -1
23.5	.3374 -9	.1973 -1
24.0	.2679 -9	.1893 -1
24.5	.2142 -9	.1818 -1
25.0	.1716 -9	.1747 -1
25.25	.1541 -9	.1713 -1
25.5	.1384 -9	.1680 -1
25.75	.1244 -9	.1648 -1
26.0	.1118 -9	.1617 -1
26.25	.9887 -10	.1587 -1
26.5	.9088 -10	.1558 -1
26.75	.8199 -10	.1529 -1
27.0	.7400 -10	.1501 -1
27.25	.6695 -10	.1475 -1
27.5	.6059 -10	.1448 -1
Jet boundary		
6.414	0.1840 -3	0.2127
7.946	.2612 -4	.1496
9.728	.3663 -5	.1050
11.779	.5281 -6	.7414 -1
14.194	.7570 -7	.5227 -1

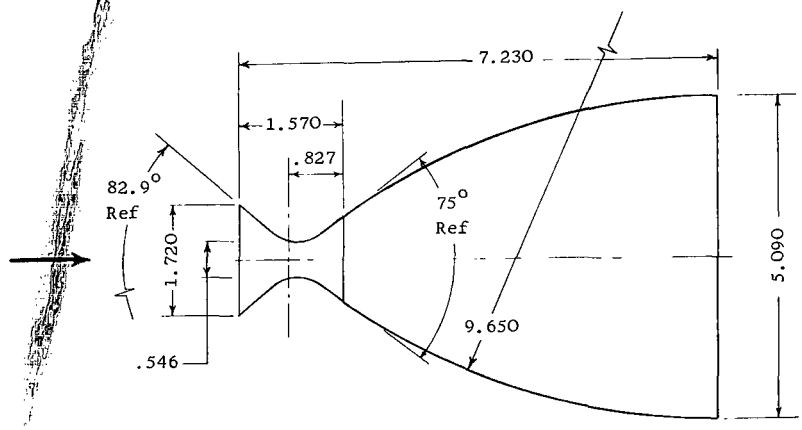

Nozzle I

$M_j = 5.35$
$\gamma = 1.24$
$\theta_n = 0°$

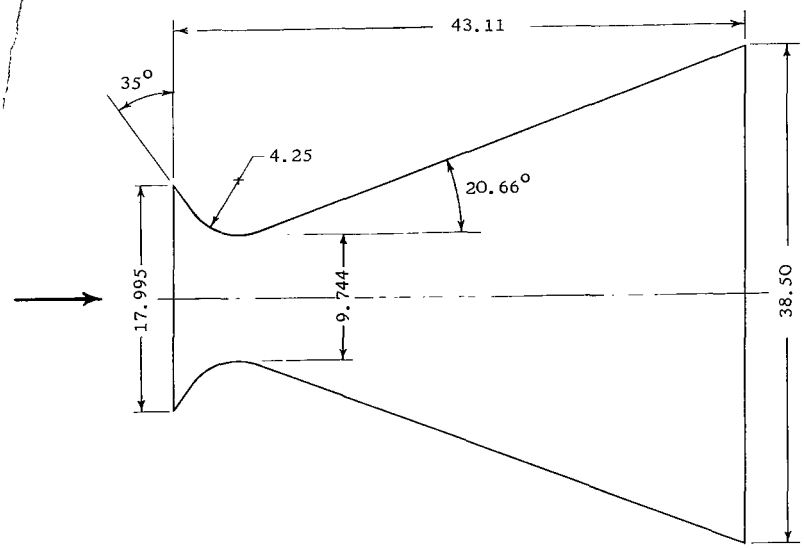

Nozzle II

$M_j = 3.41$
$\gamma = 1.15$
$\theta_n = 20.66°$

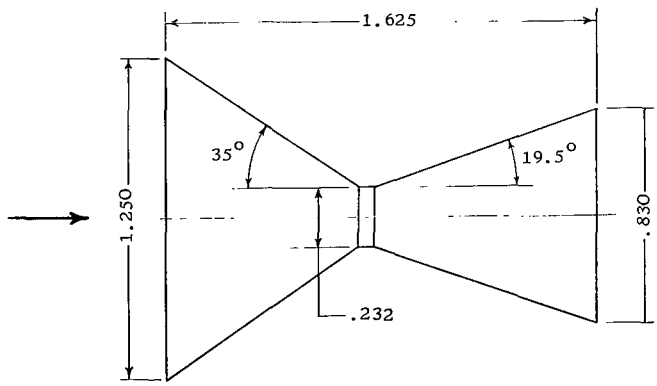

Nozzle III

$M_j = 3.39$
$\gamma = 1.18$
$\theta_n = 19.5°$

Figure 1.- Sketches of nozzles having operating conditions that dictated the theoretical computations reported herein. All dimensions are in inches.

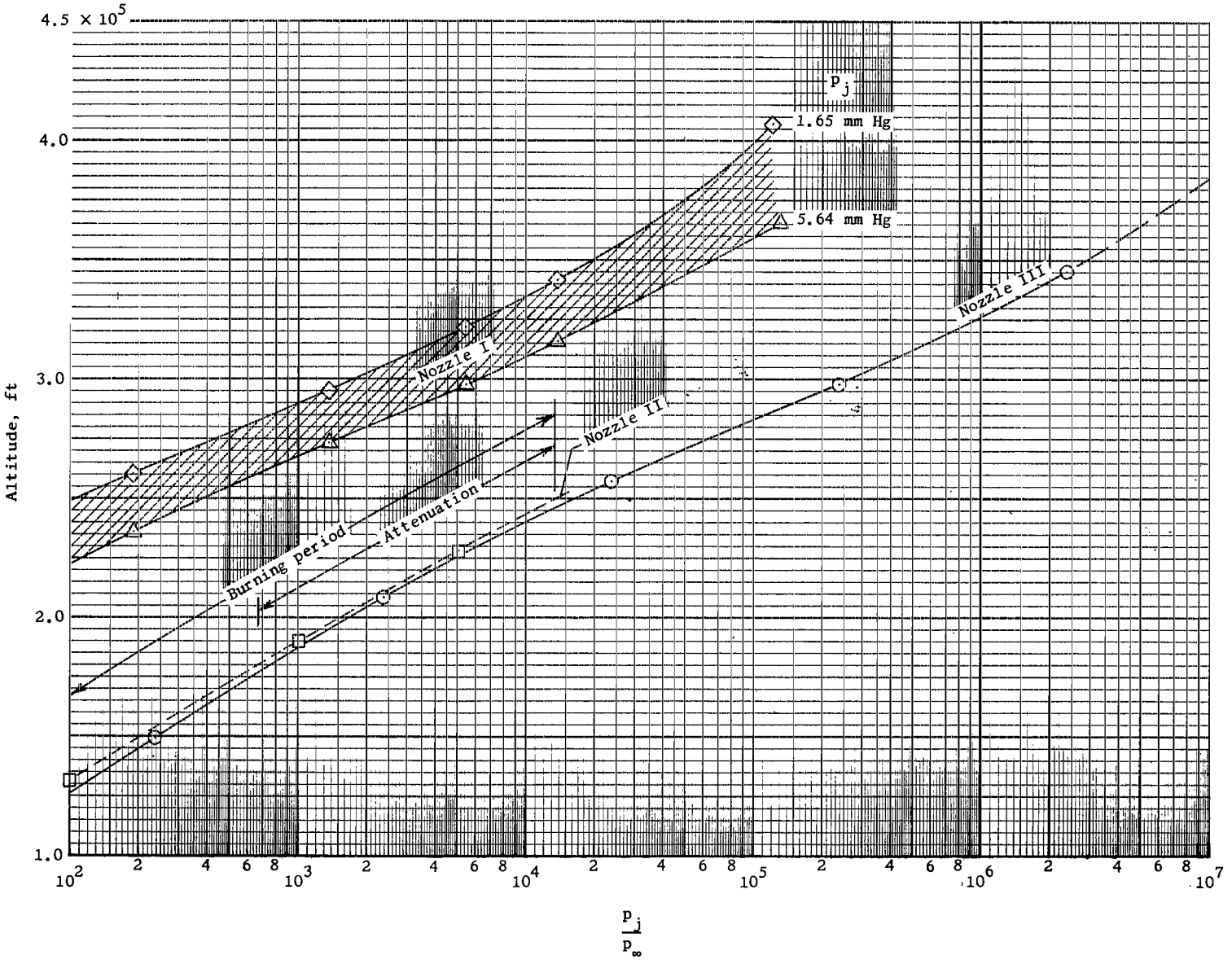

Figure 2.- Operational ranges of three different nozzles.

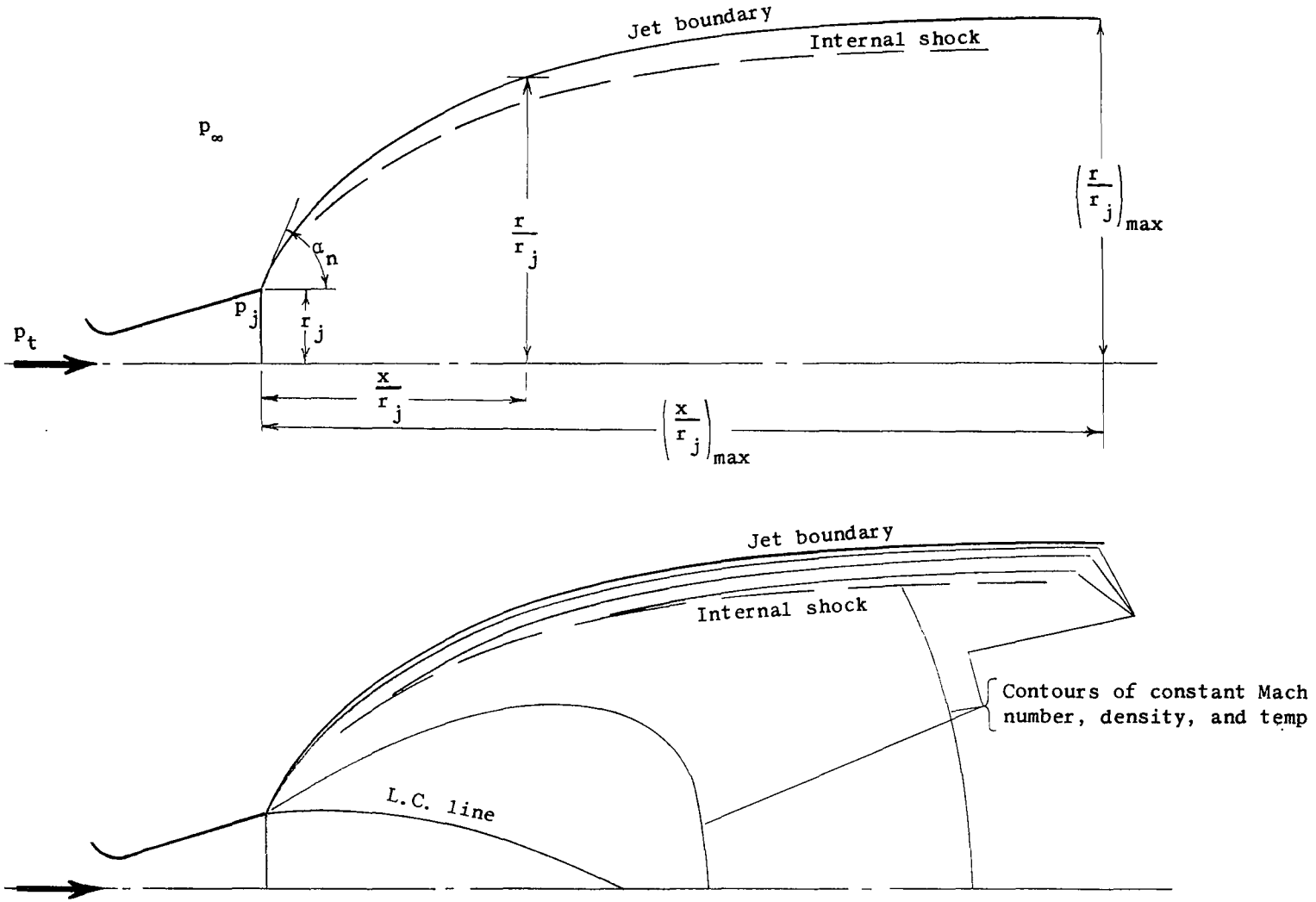

Figure 3.- General details of exhaust plume.

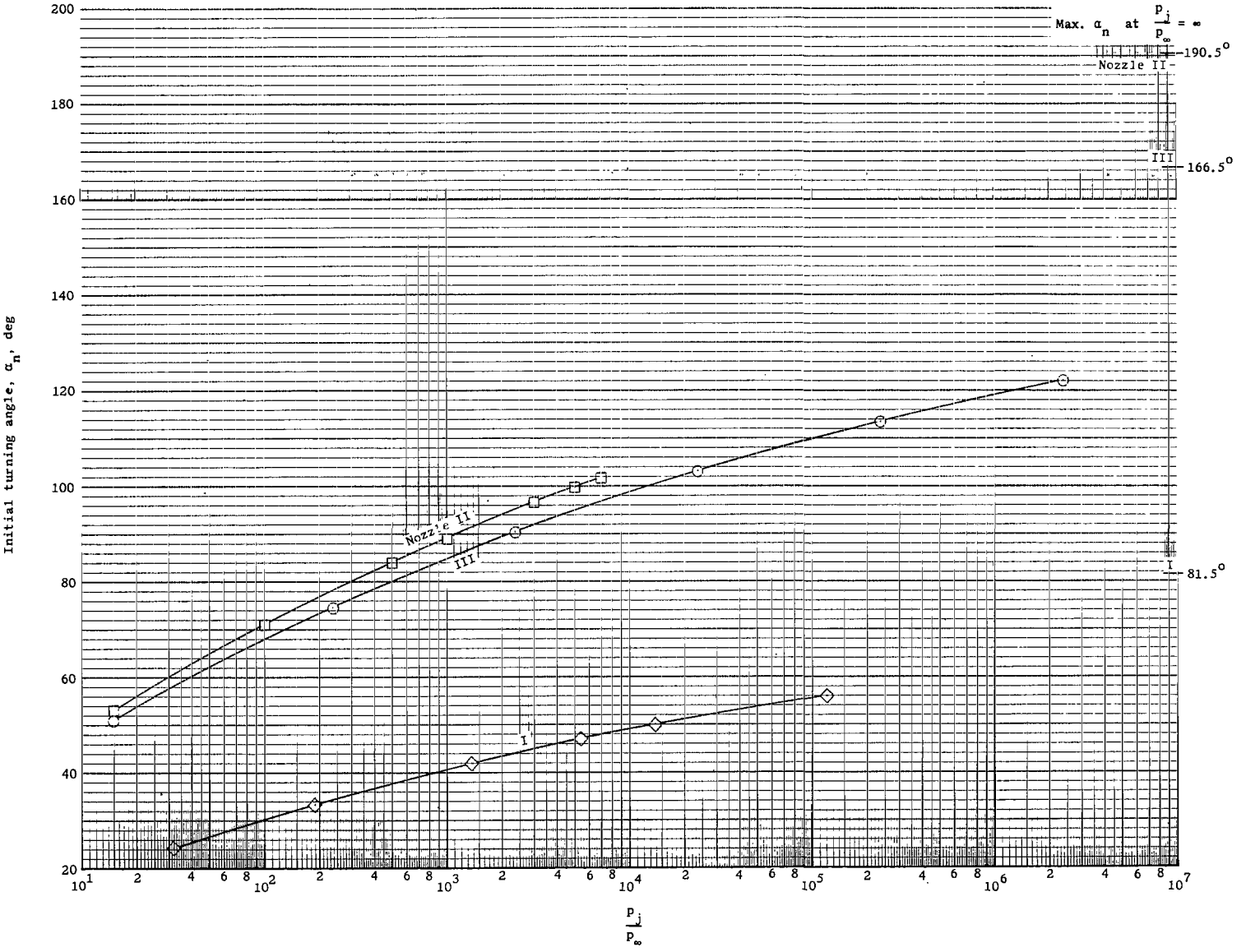

Figure 4.- Initial turning angle of plume boundary at nozzle lip.

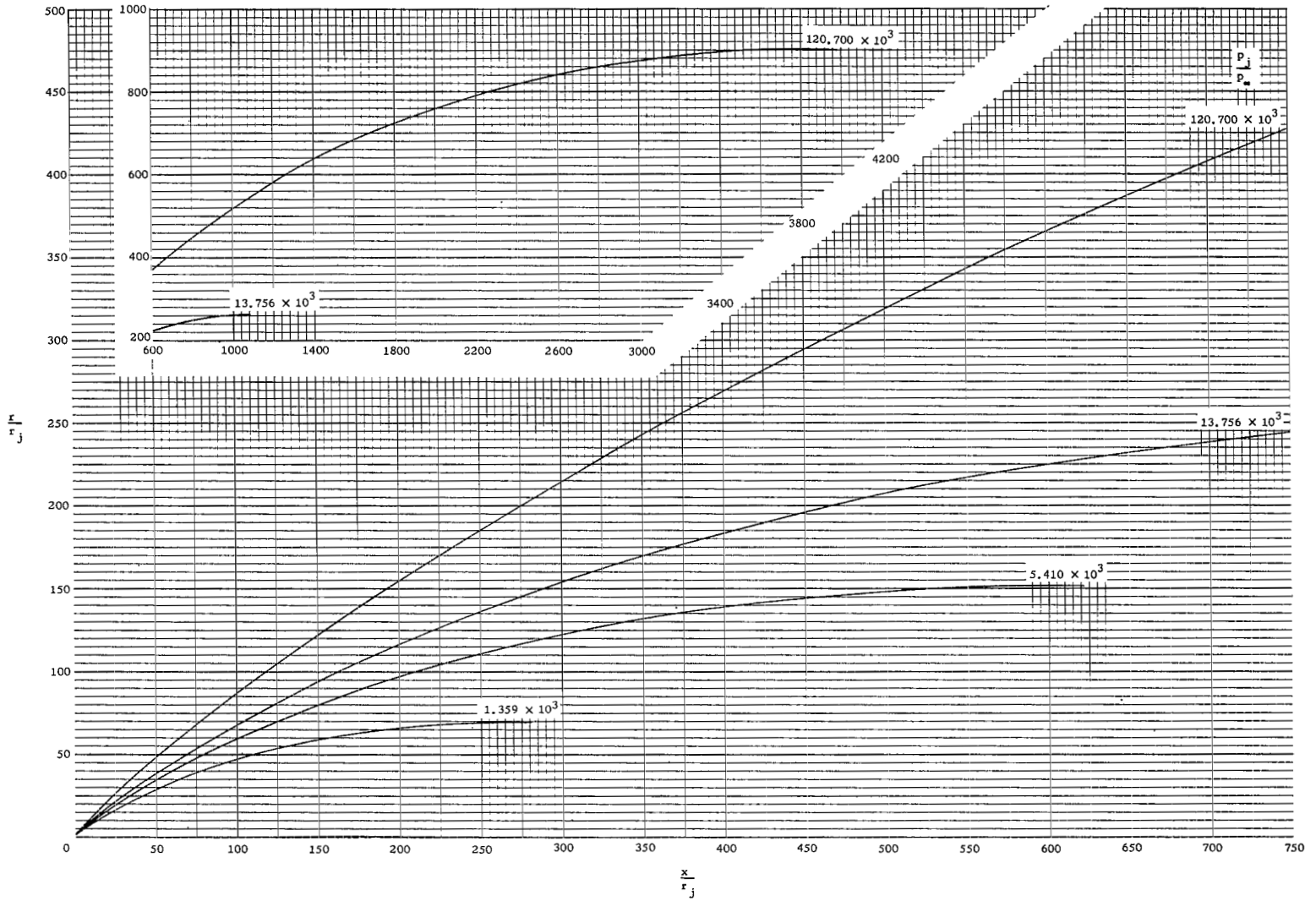

(a) Complete boundaries; nozzle I.

Figure 5.- Exhaust-plume-boundary coordinates for various pressure ratios.

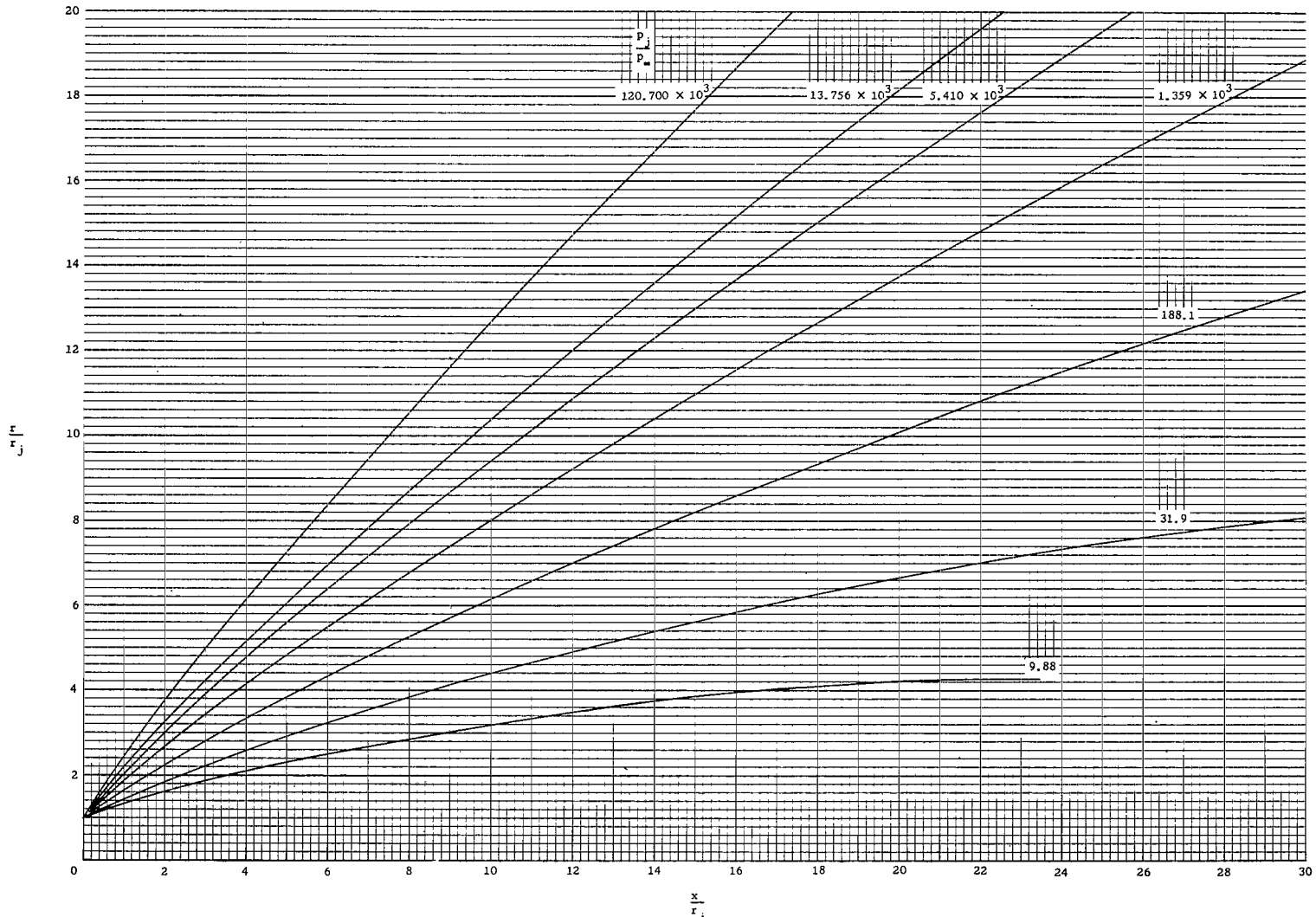

(b) Initial boundary portions, nozzle I.

Figure 5.- Continued.

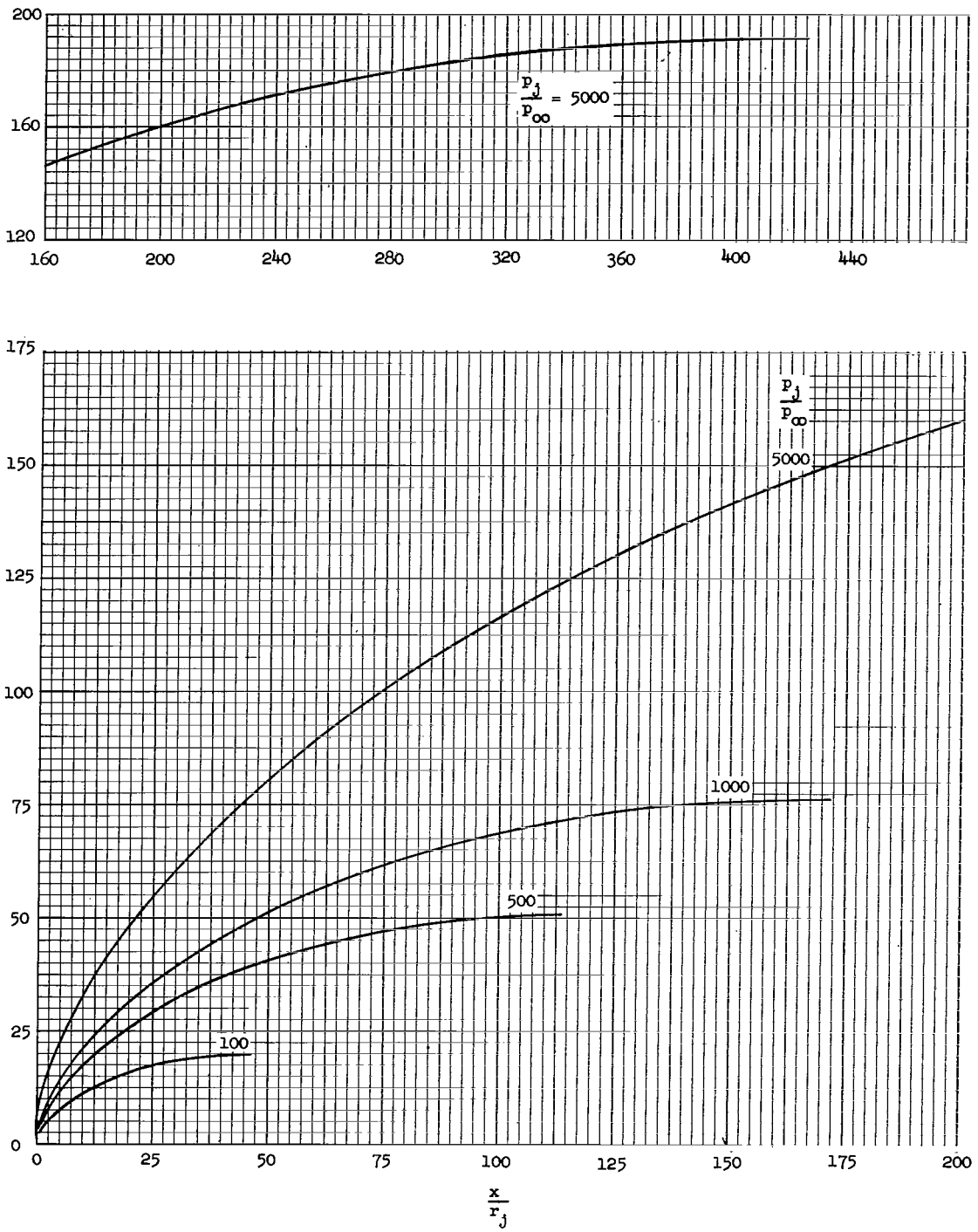

(c) Complete boundaries for nozzle II.

Figure 5.- Continued.

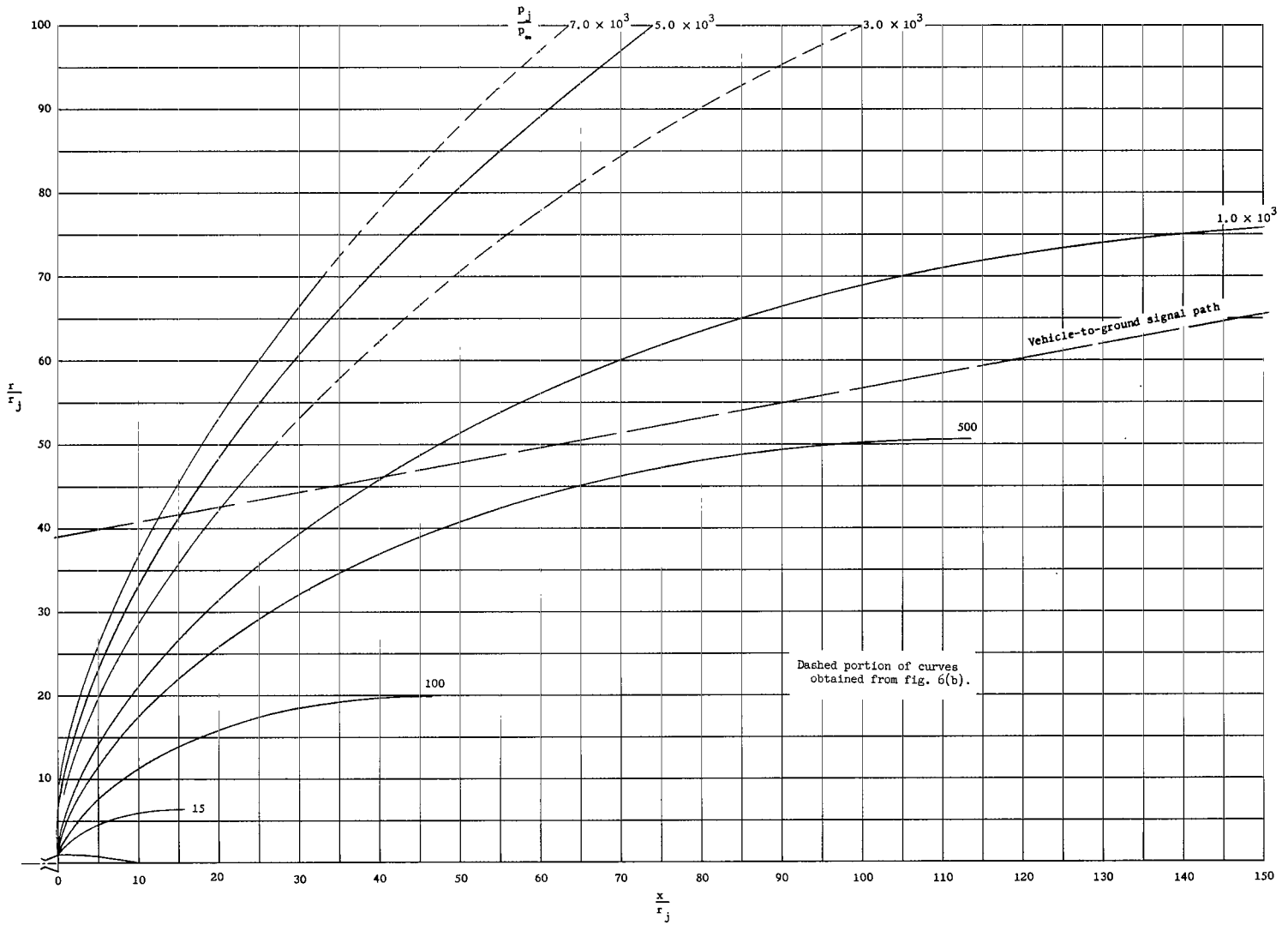

(d) Initial boundary portions; nozzle II.

Figure 5.- Continued.

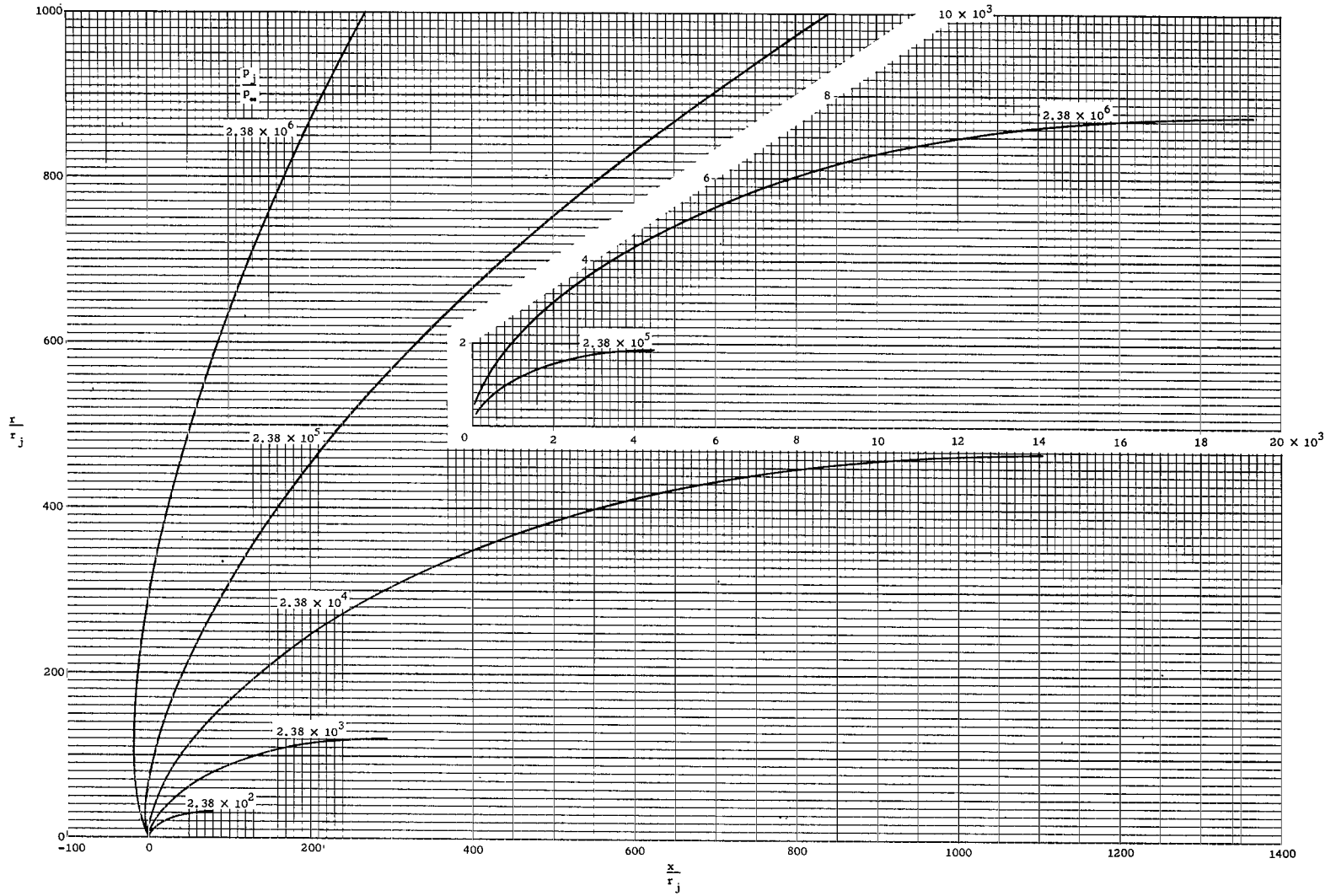

(e) Complete boundaries; nozzle III.

Figure 5.- Continued.

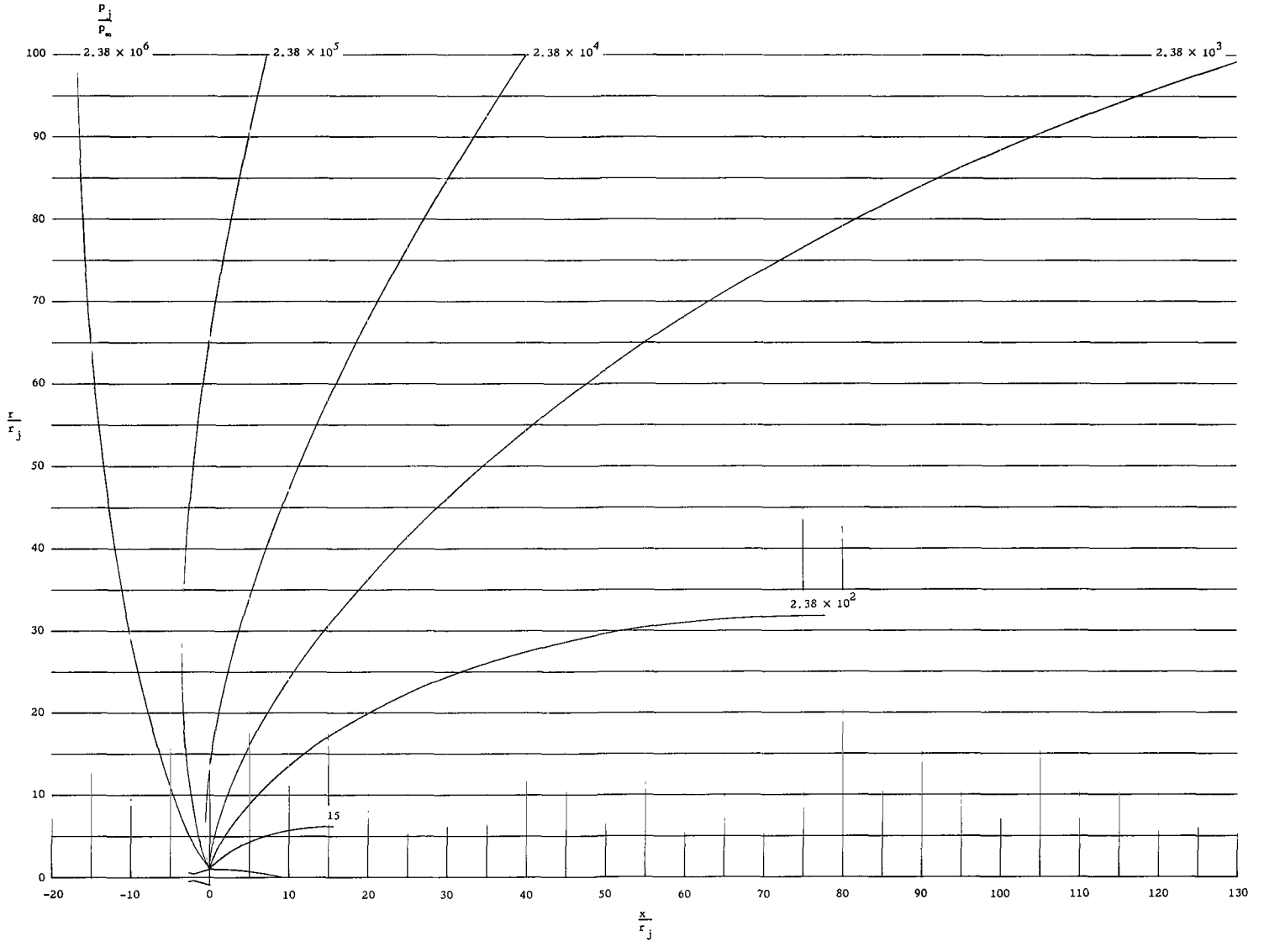

(f) Initial boundary portions; nozzle III.

Figure 5.- Concluded.

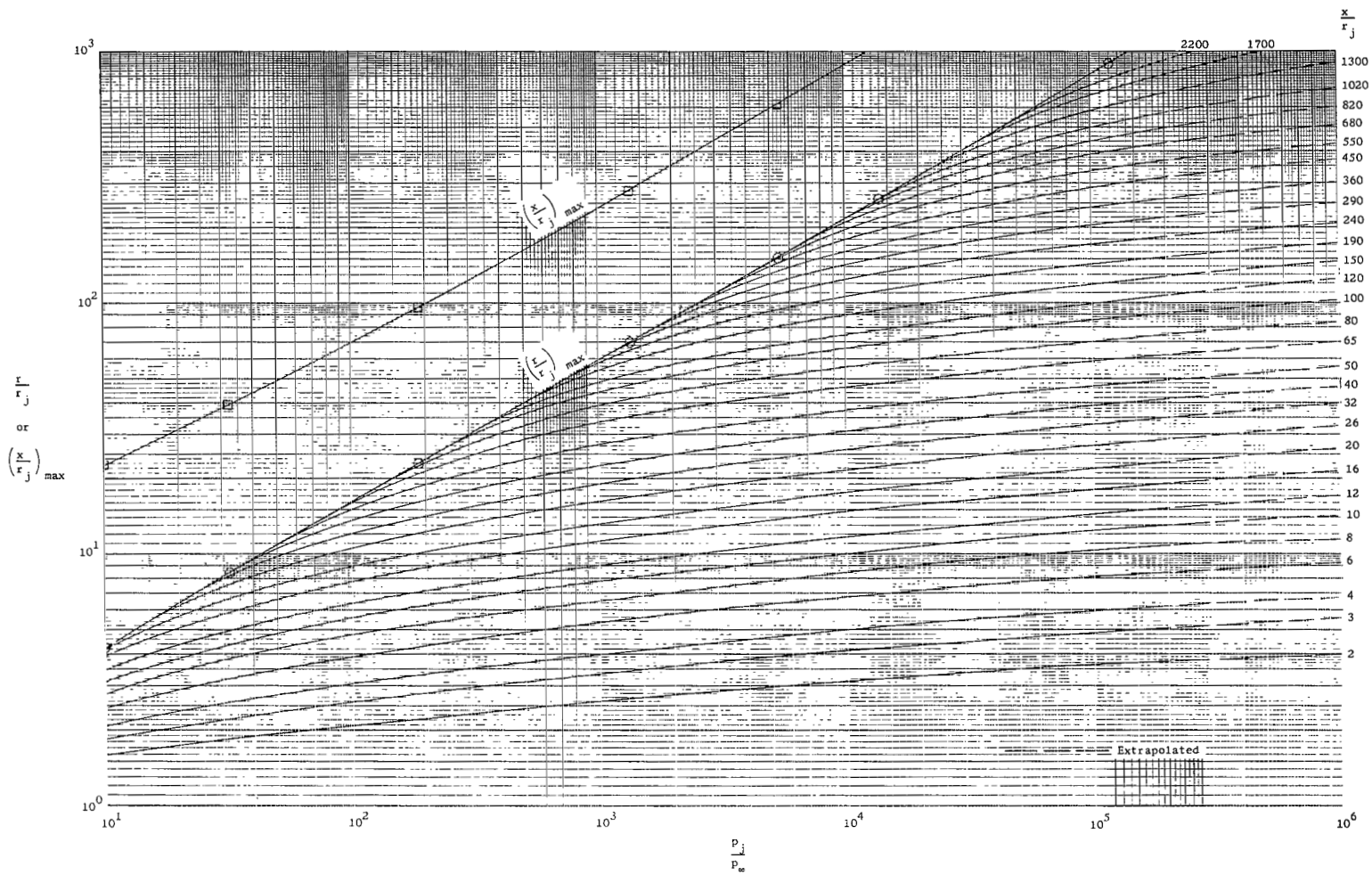

(a) Nozzle I.

Figure 6.- Variation of radial distance of plume boundary from the center line with pressure ratio for various distances downstream of nozzle exit.

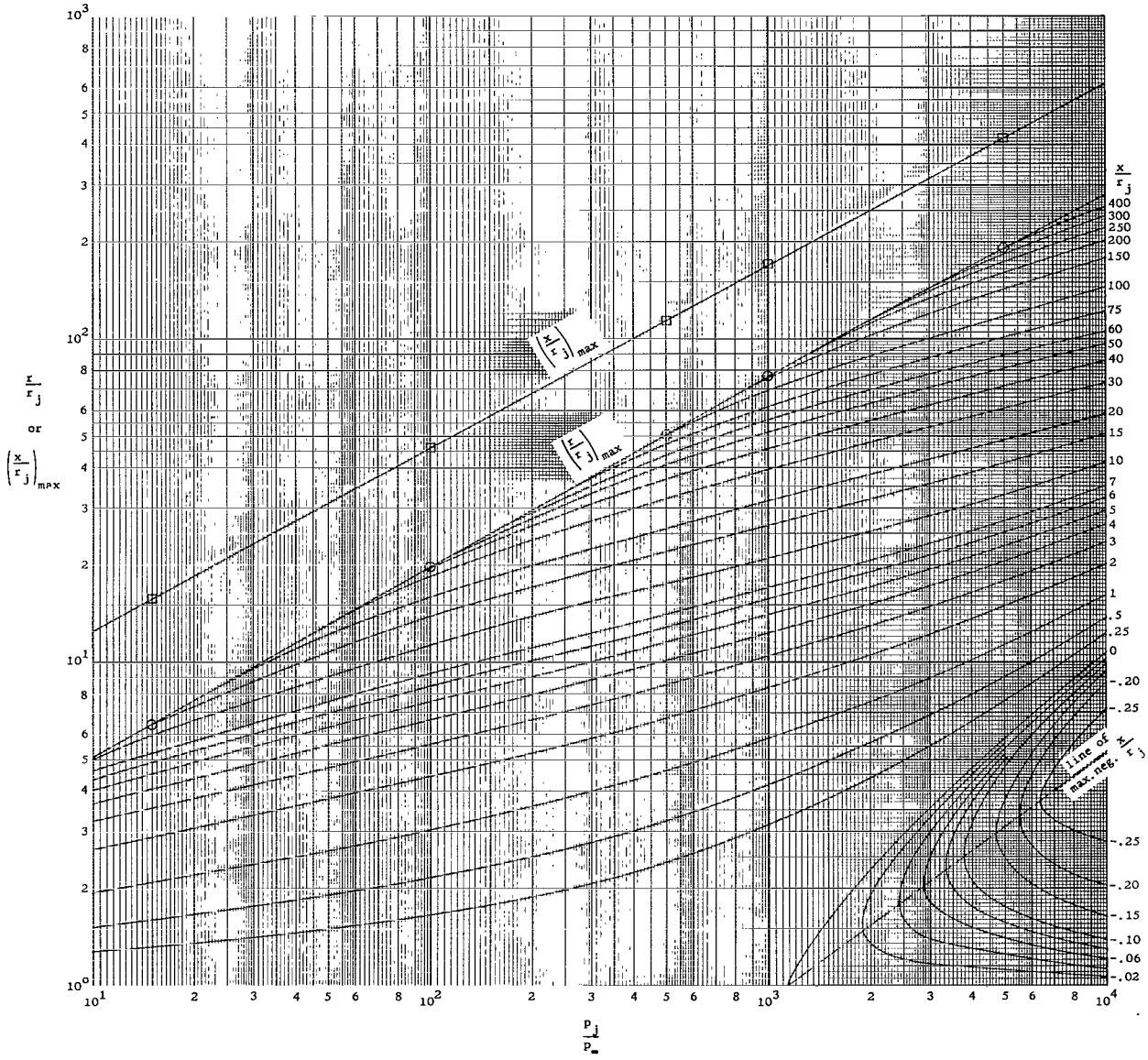

(b) Nozzle II.

Figure 6.- Continued.

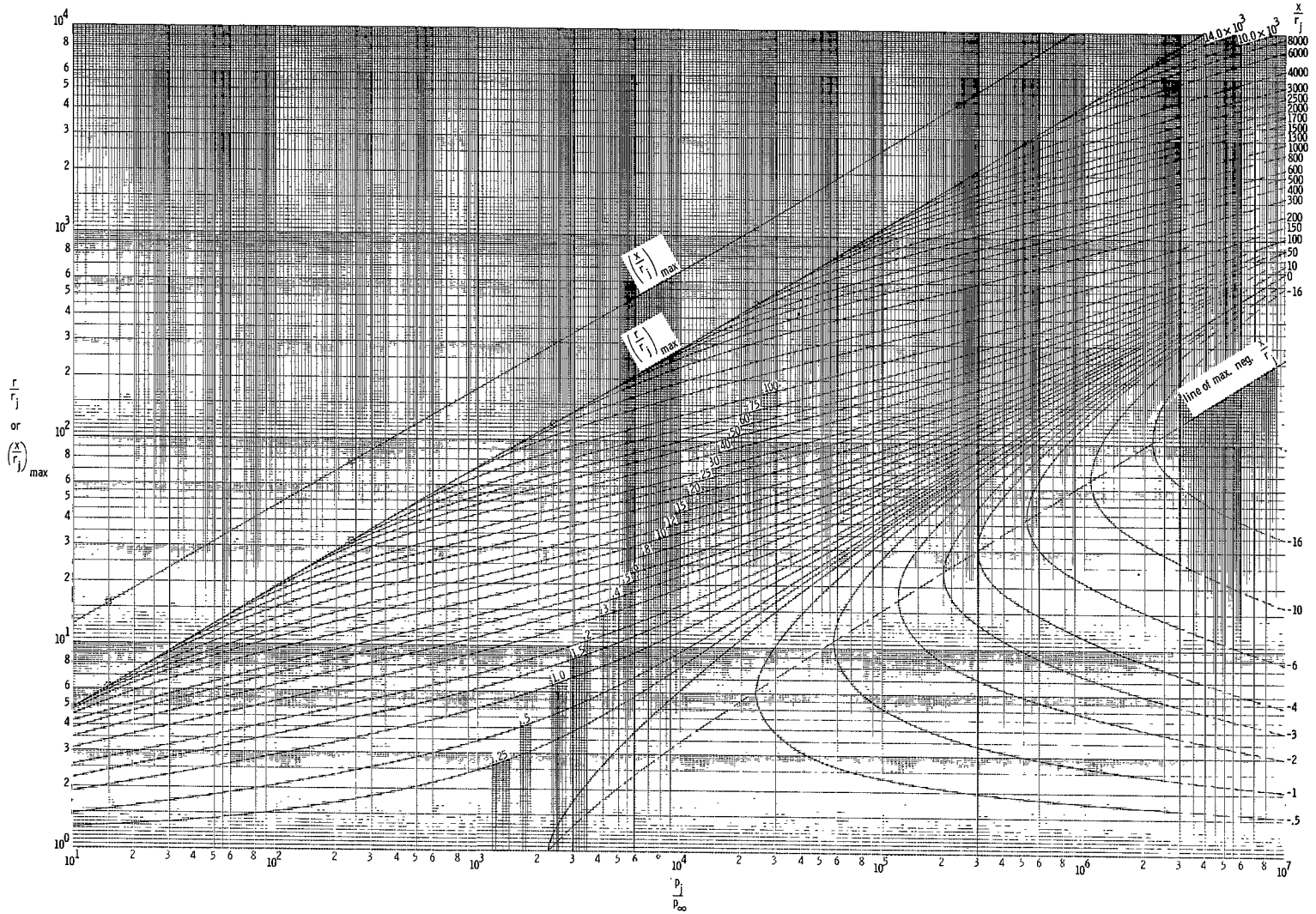

(c) Nozzle III.

Figure 6.- Concluded.

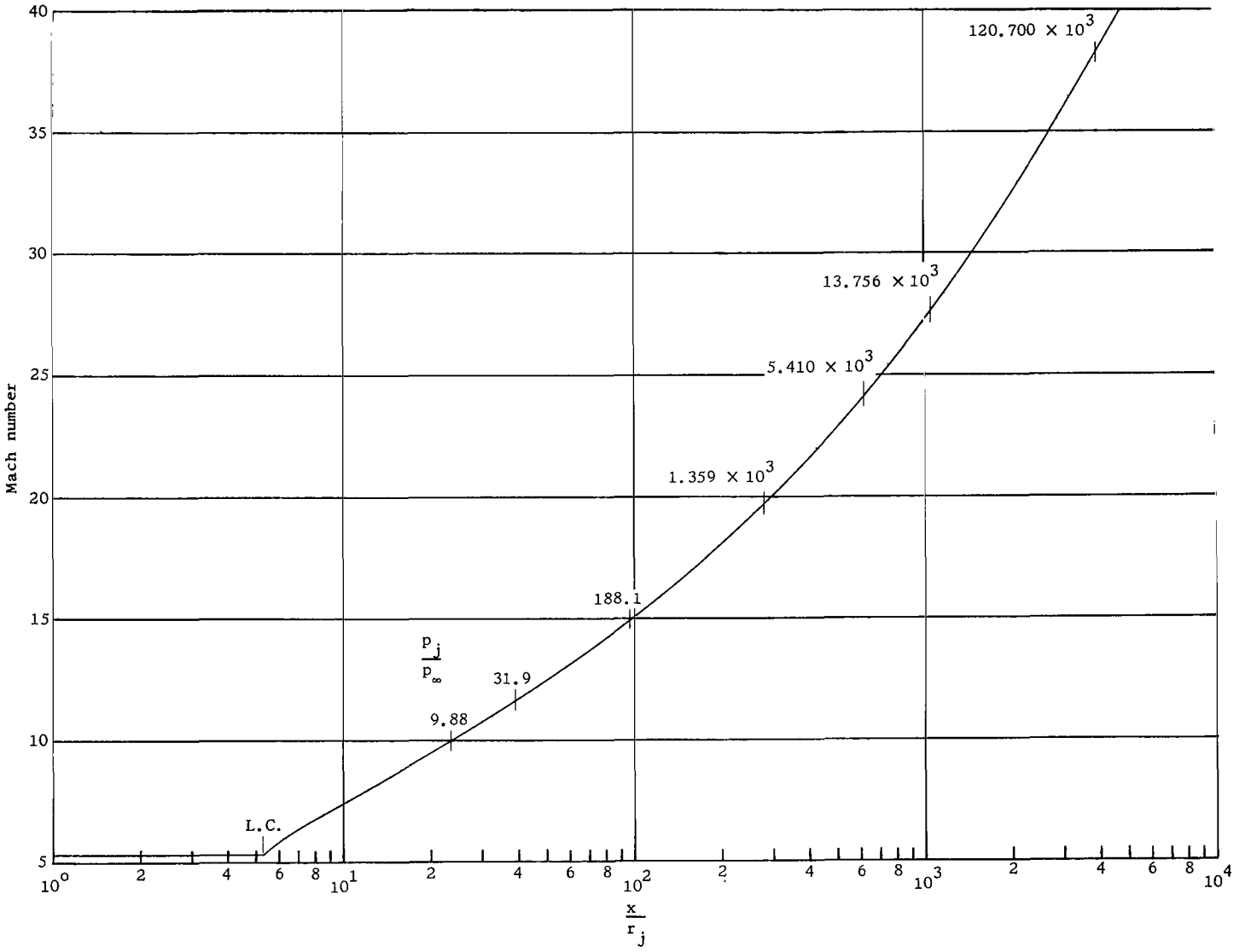

(a) Nozzle I.

Figure 7.- Mach number distribution along center line of exhaust plume.

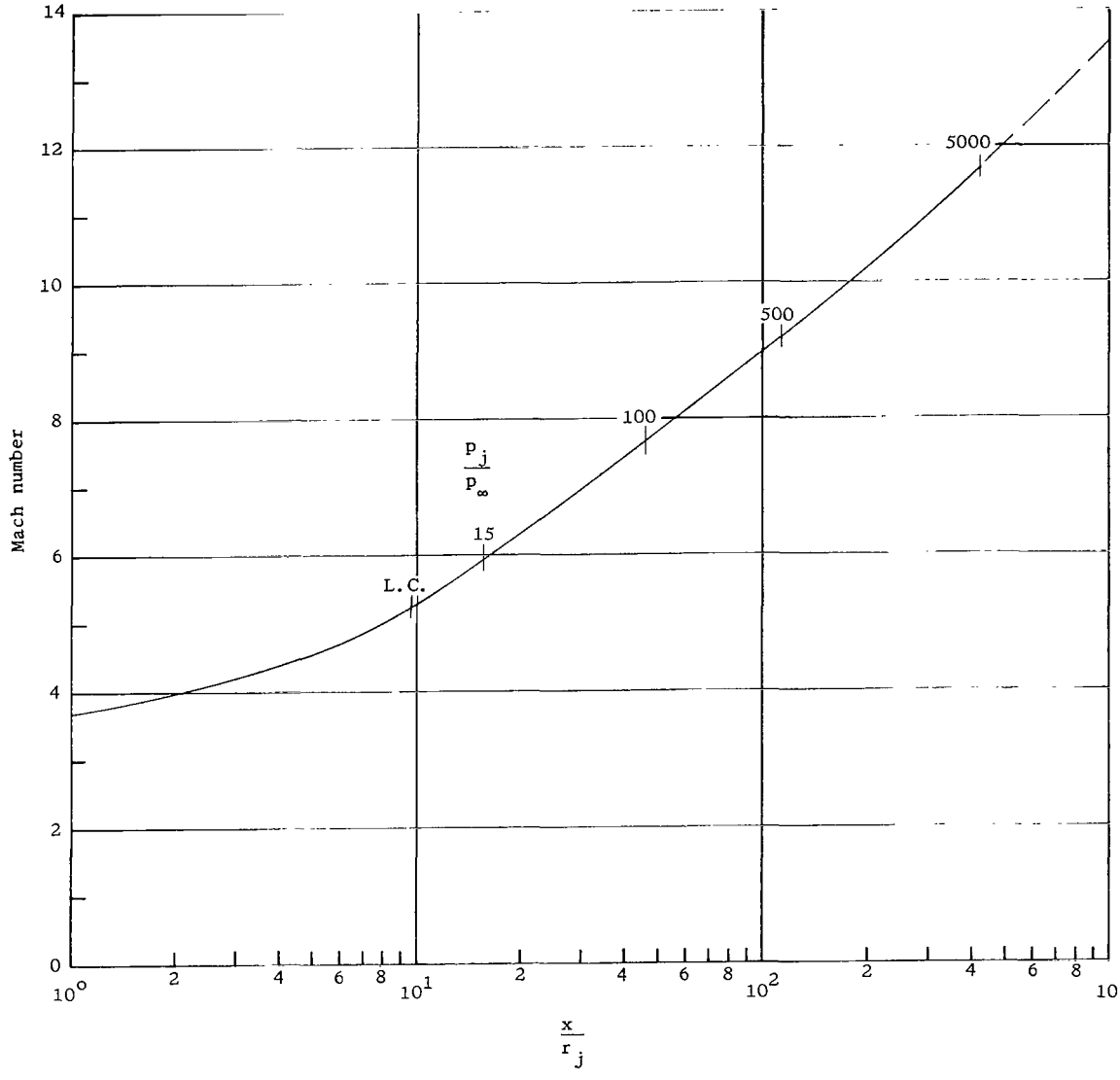

(b) Nozzle II.

Figure 7.- Continued.

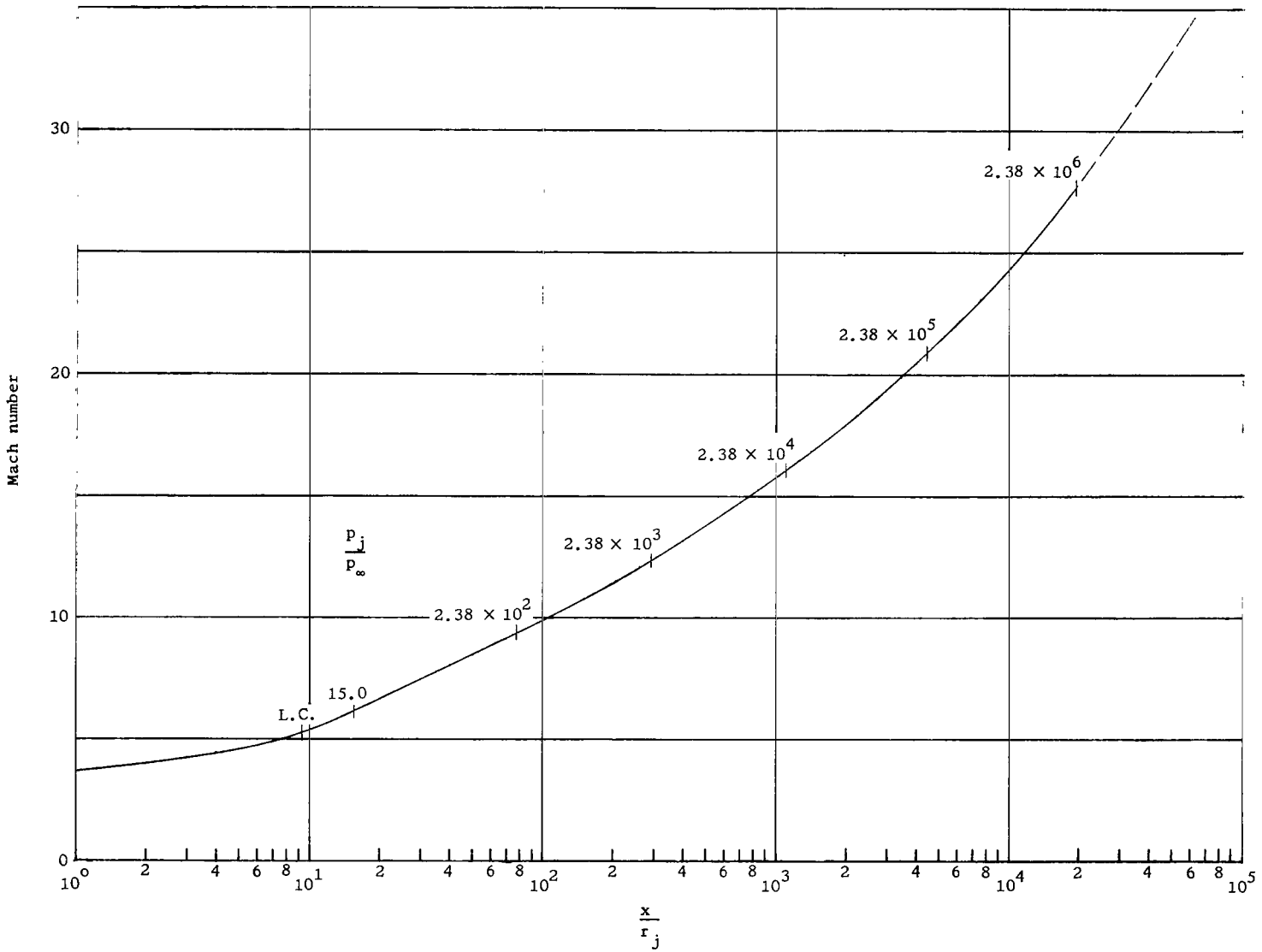

(c) Nozzle III.

Figure 7.- Concluded.

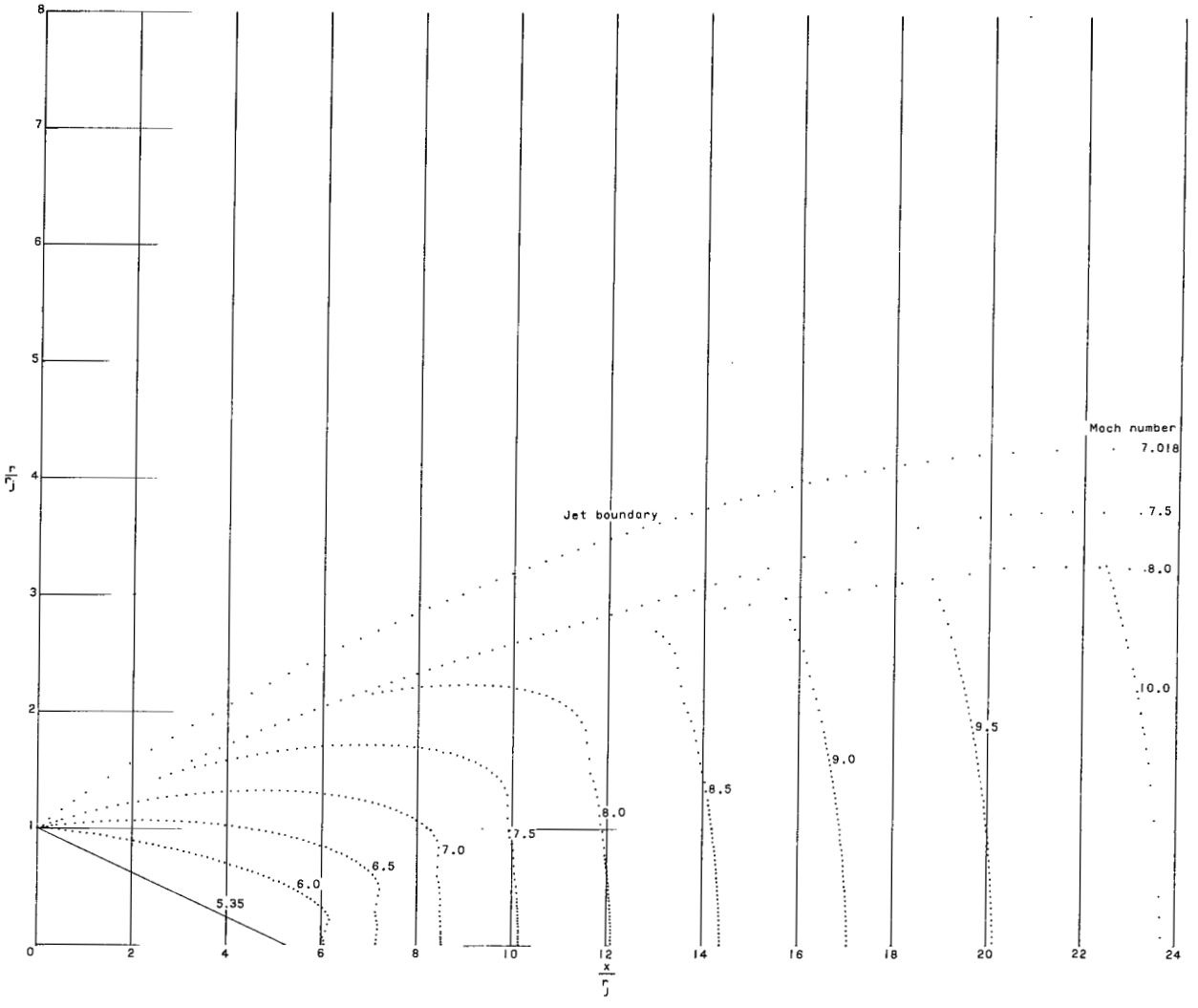

(a) $p_j/p_\infty = 9.88$; $\alpha_n = 17.125^\circ$.

Figure 8.- Contours of constant Mach number within the exhaust plume; nozzle I.

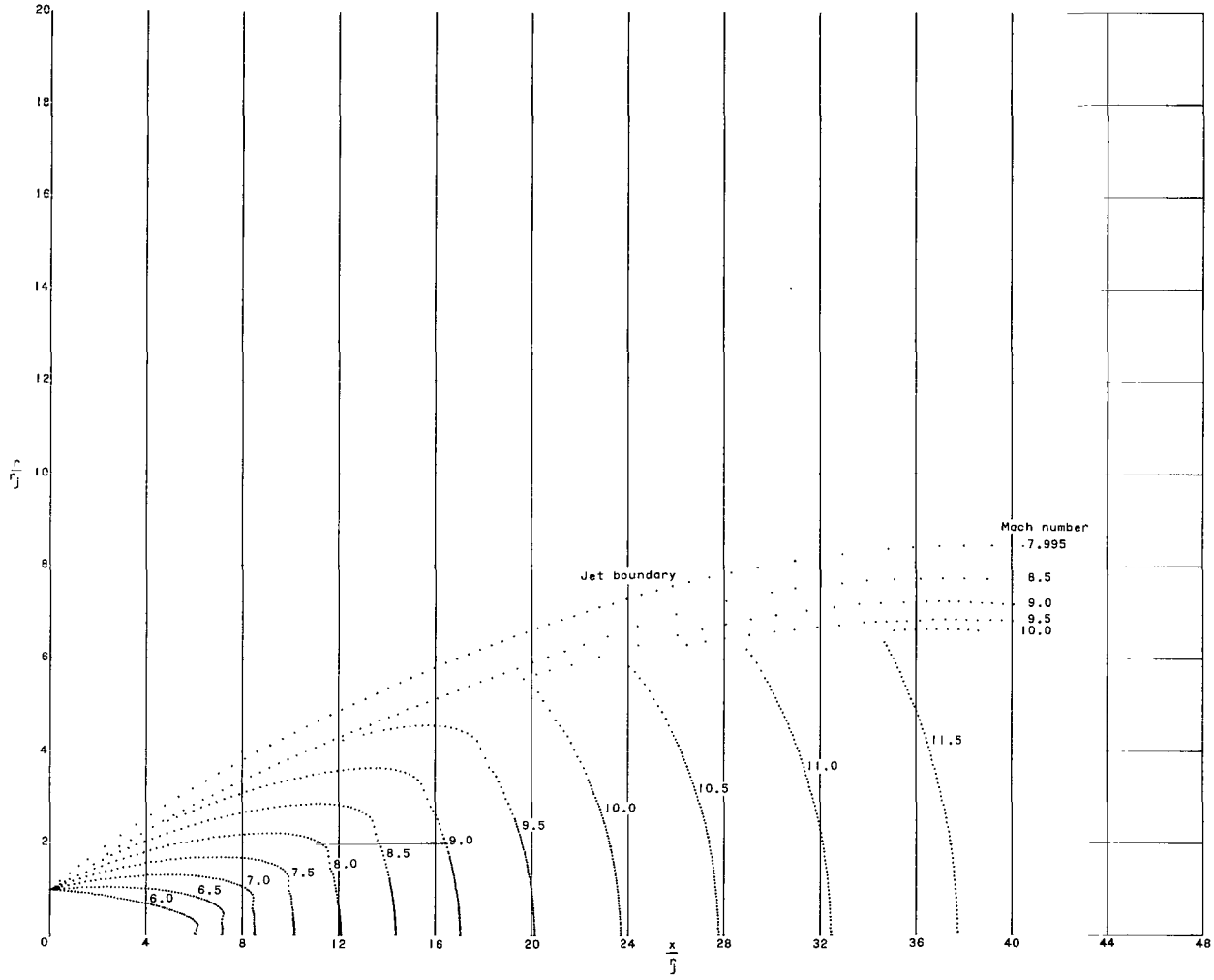

(b) $p_j/p_\infty = 31.9$; $\alpha_n = 24.25^\circ$.

Figure 8.- Continued.

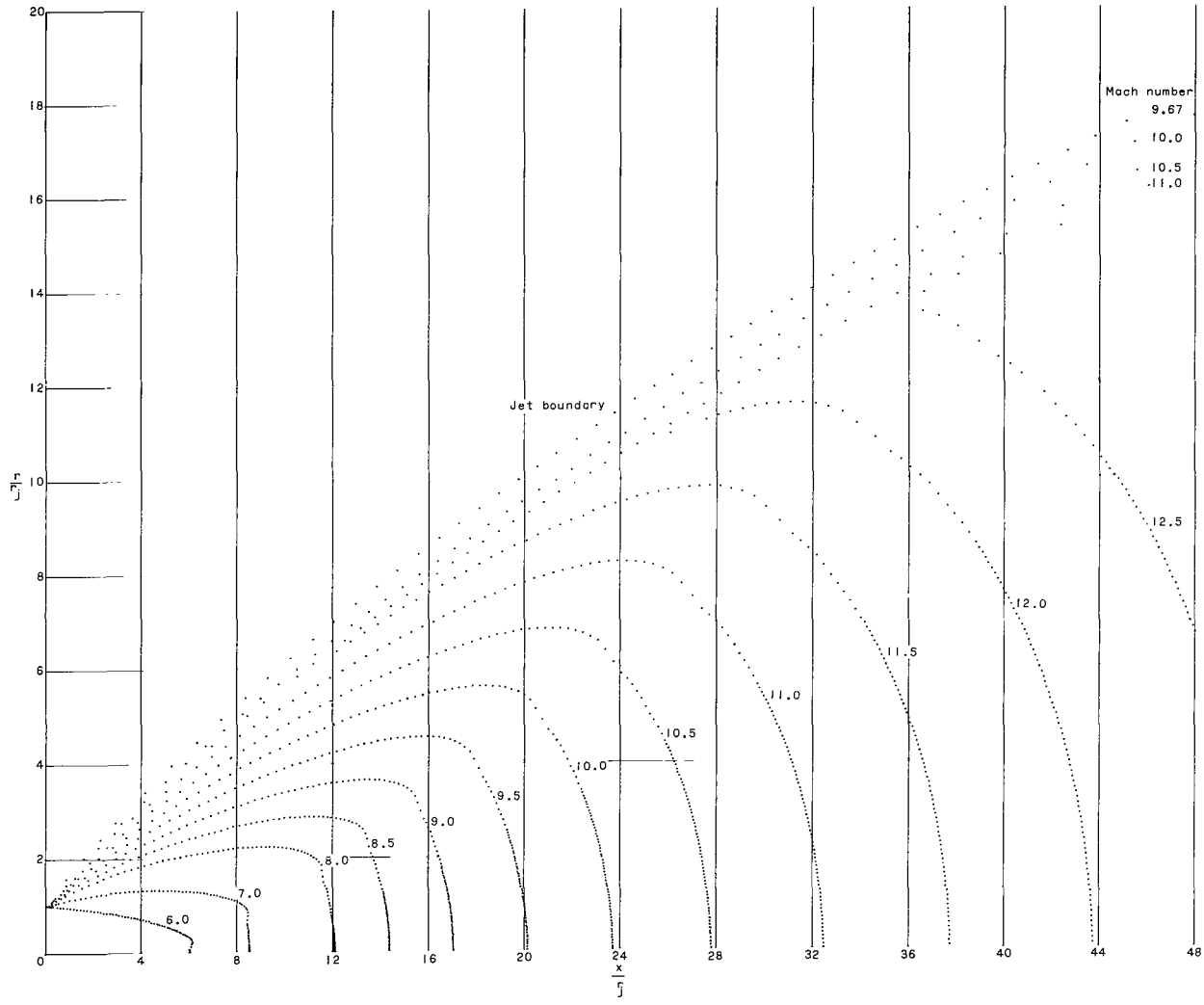

(c) $p_j/p_\infty = 188.1$; $\alpha_n = 33.5^\circ$.

Figure 8.- Continued.

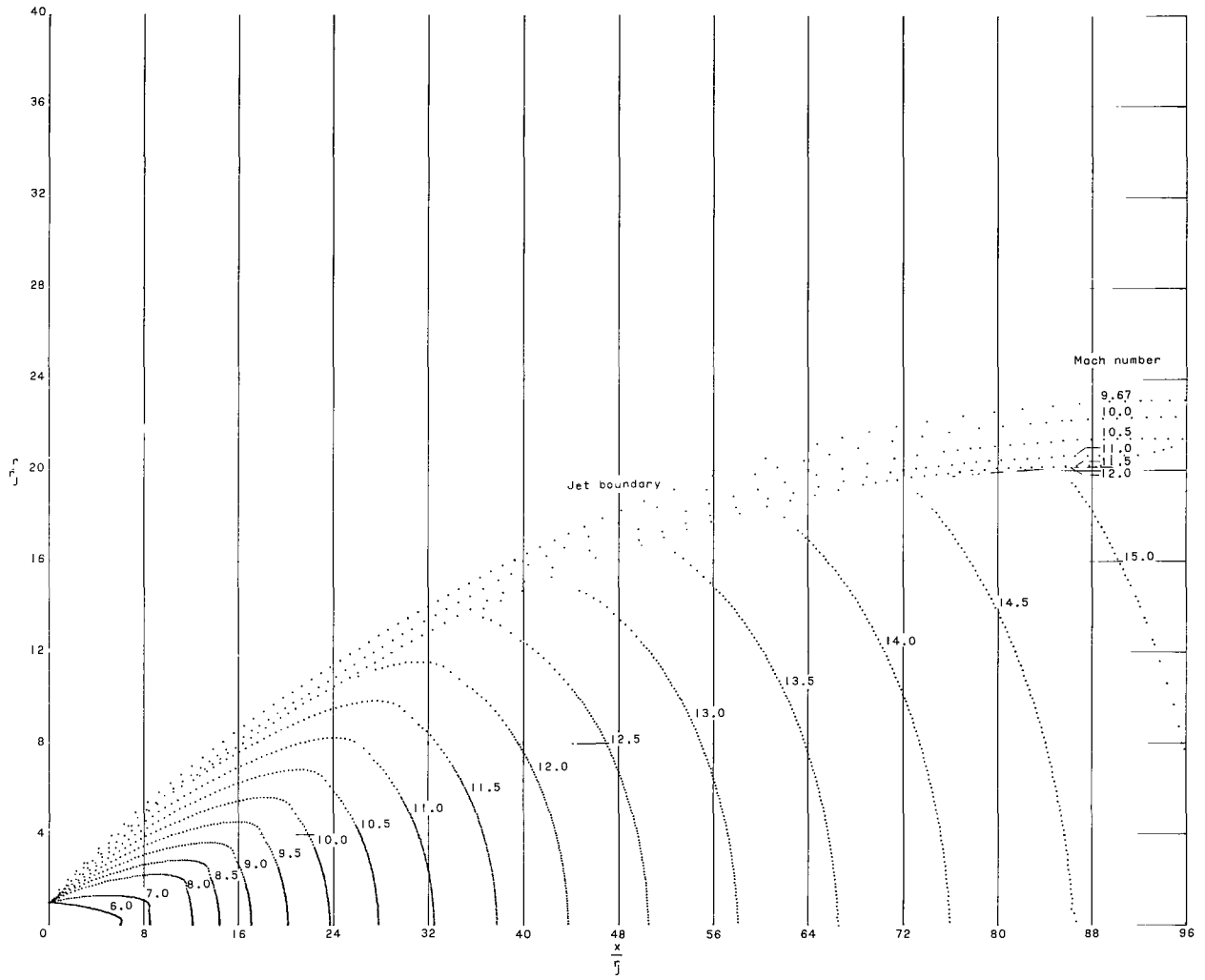

(c) $p_j/p_\infty = 188.1$; $\alpha_n = 33.5^\circ$. Concluded.

Figure 8.- Continued.

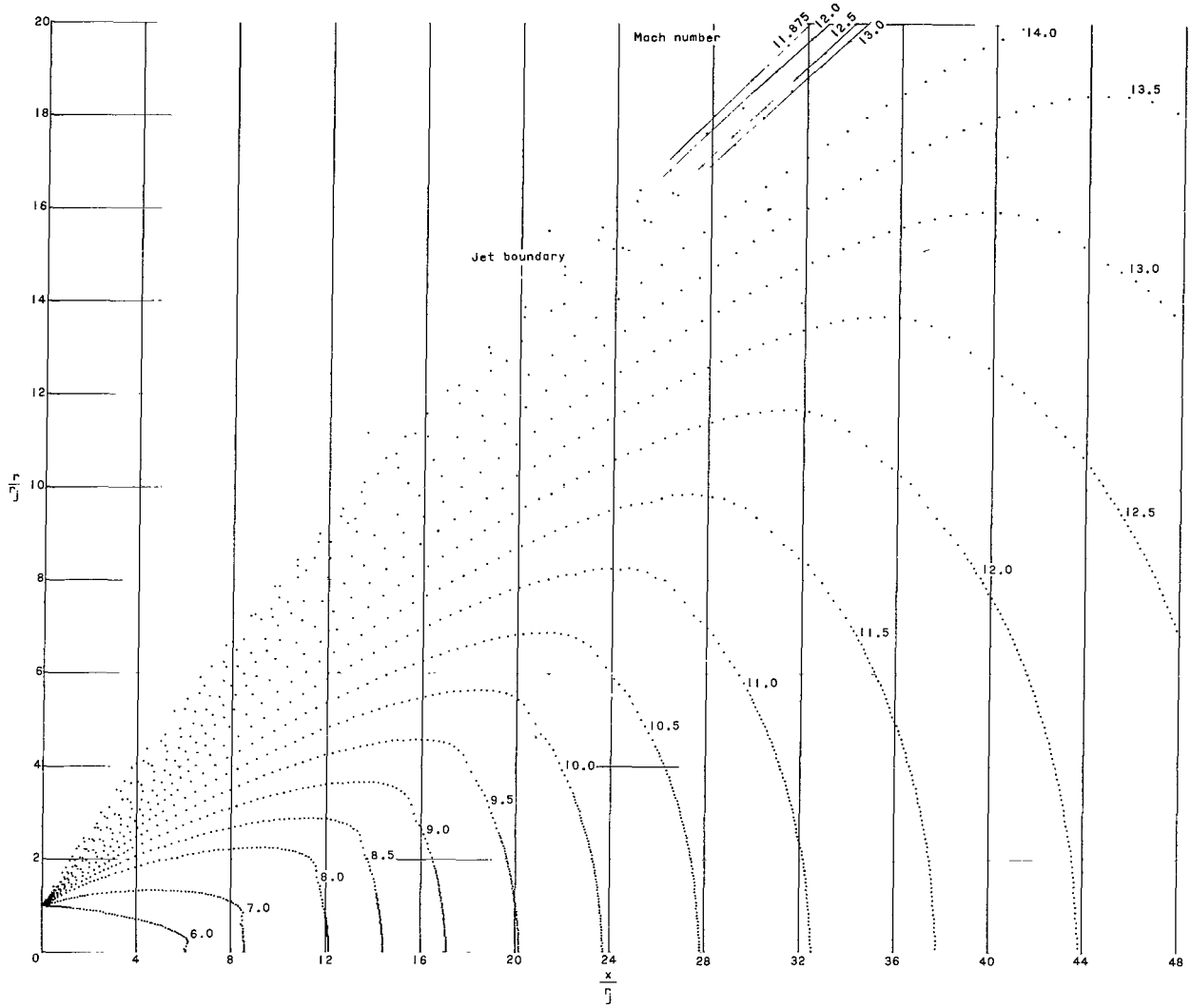

(d) $p_j/p_\infty = 1.359 \times 10^3$; $\alpha_n = 42^\circ$.

Figure 8.- Continued.

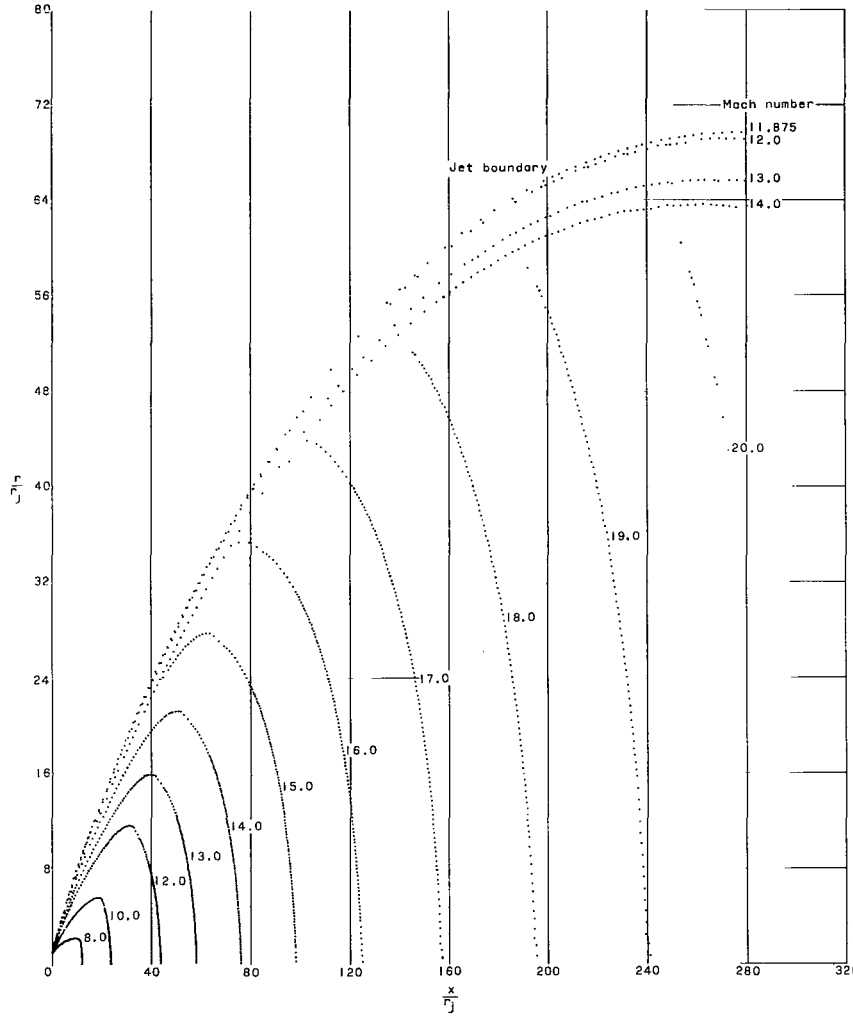

(d) $p_j/p_\infty = 1.359 \times 10^3$; $\alpha_n = 42^\circ$. Continued.

Figure 8.- Continued.

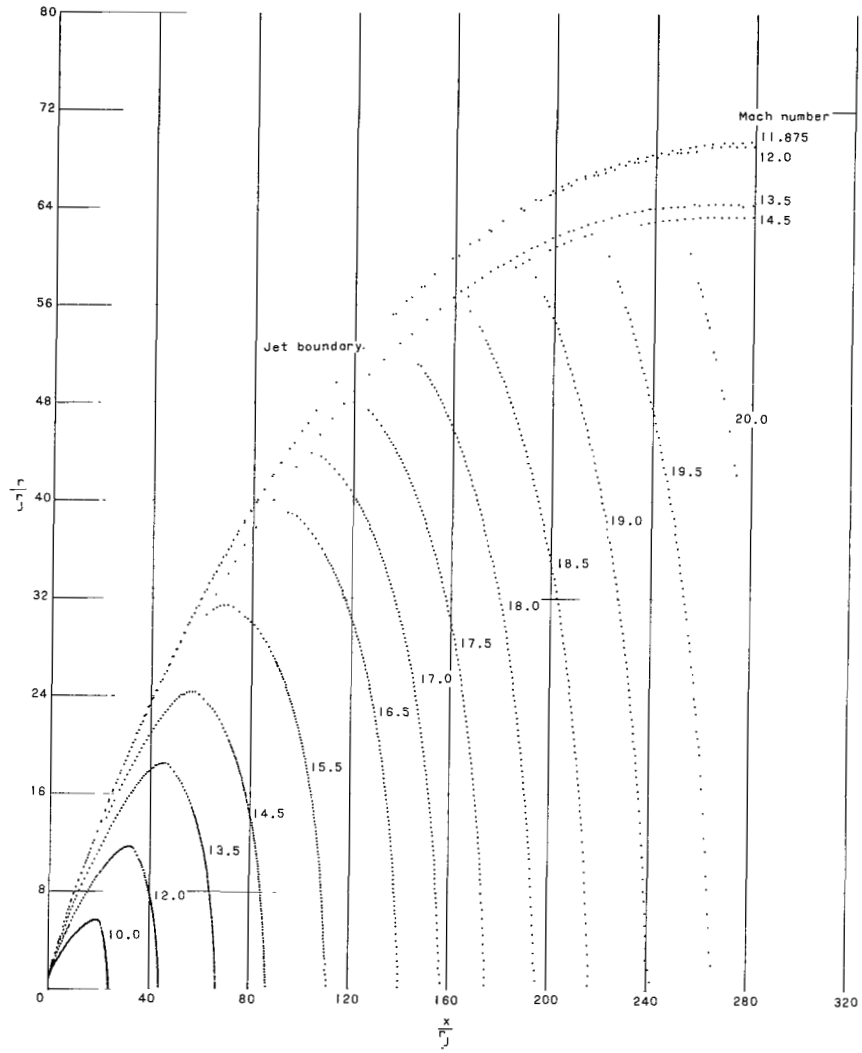

(d) $p_j/p_\infty = 1.359 \times 10^3$; $\alpha_n = 42^\circ$. Concluded.

Figure 8.- Continued.

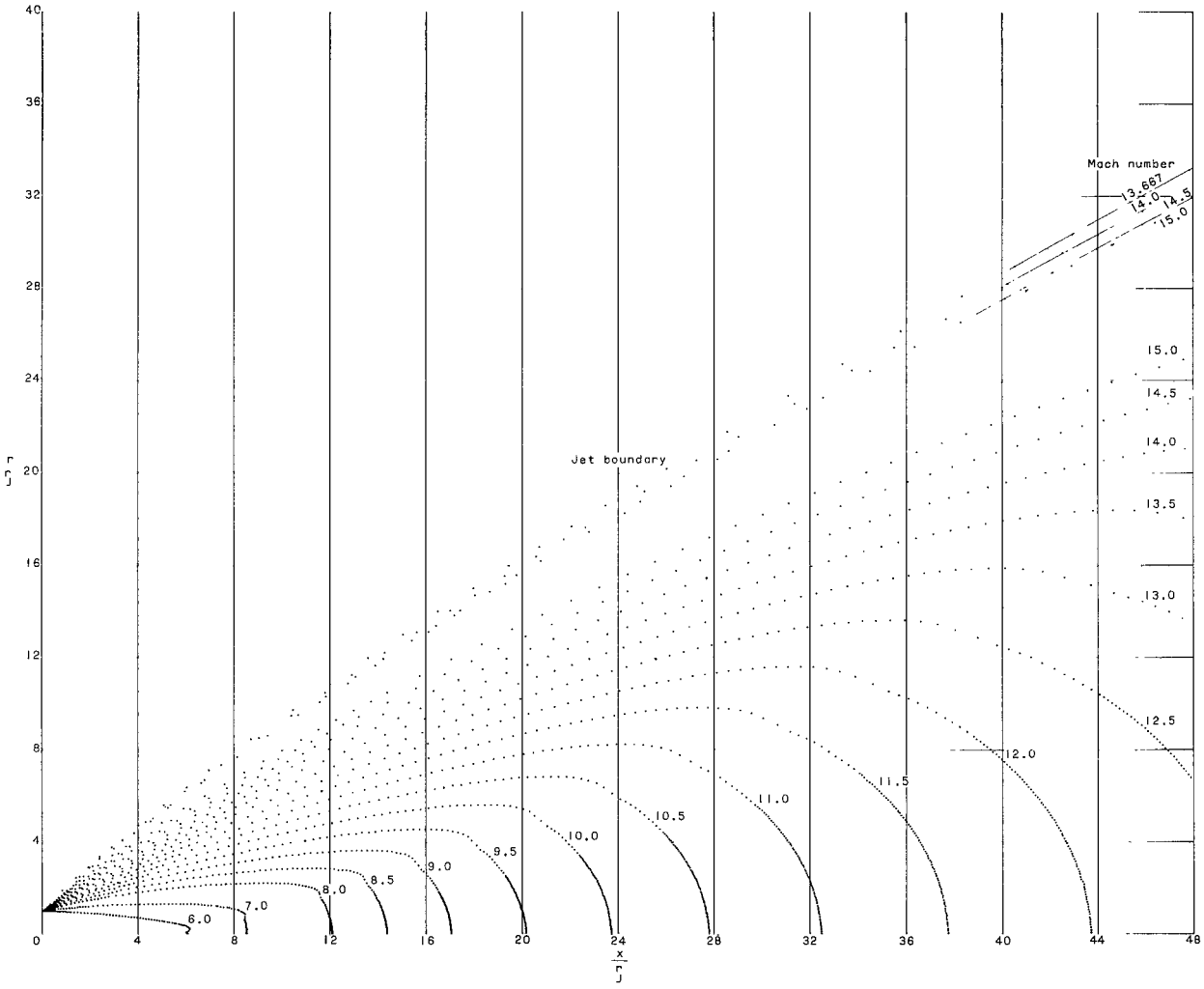

(e) $p_j/p_\infty = 5.410 \times 10^3$; $\alpha_n = 47^\circ$.

Figure 8.- Continued.

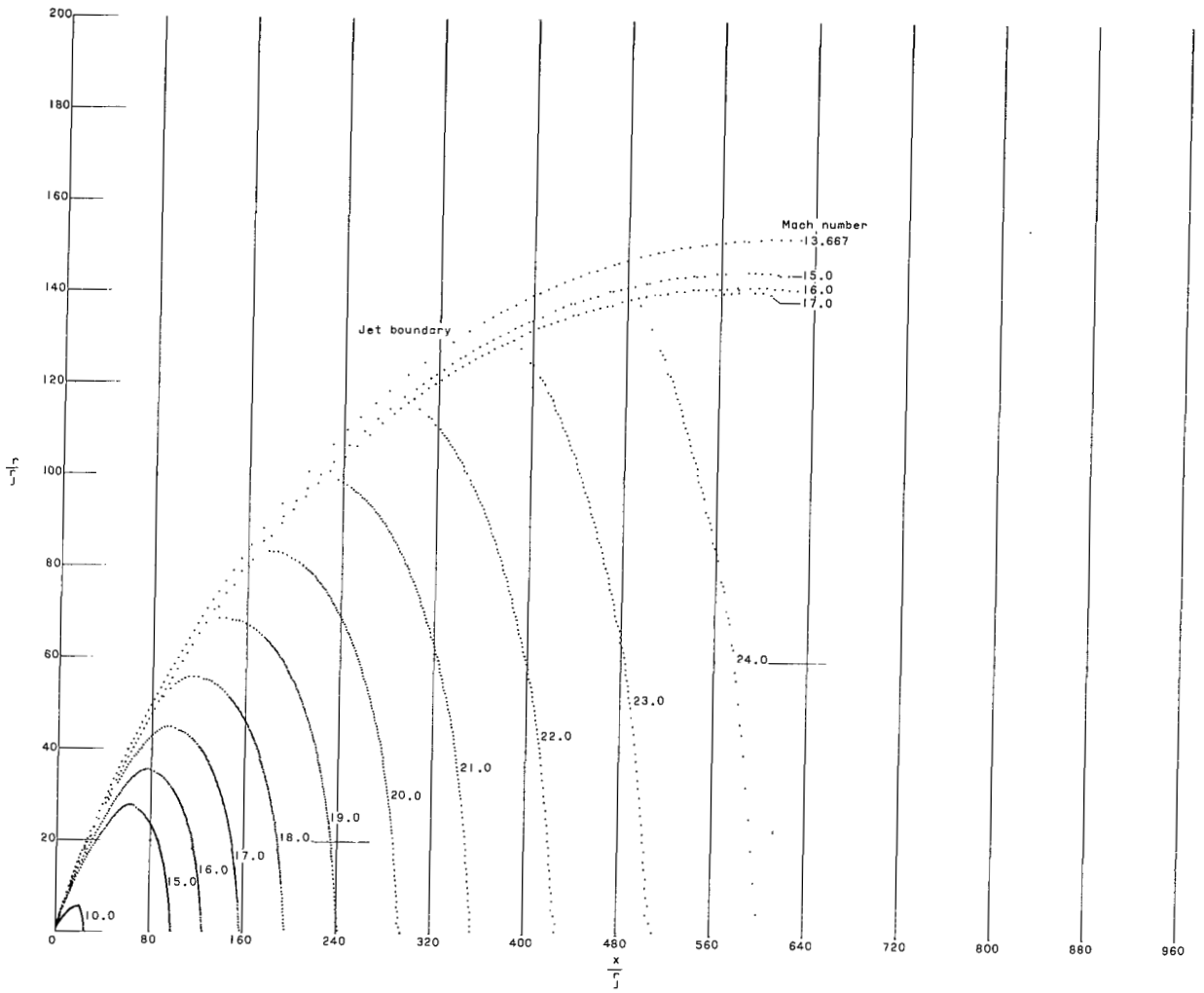

(e) $p_j/p_\infty = 5.410 \times 10^3$; $\alpha_n = 47^\circ$. Continued.

Figure 8.- Continued.

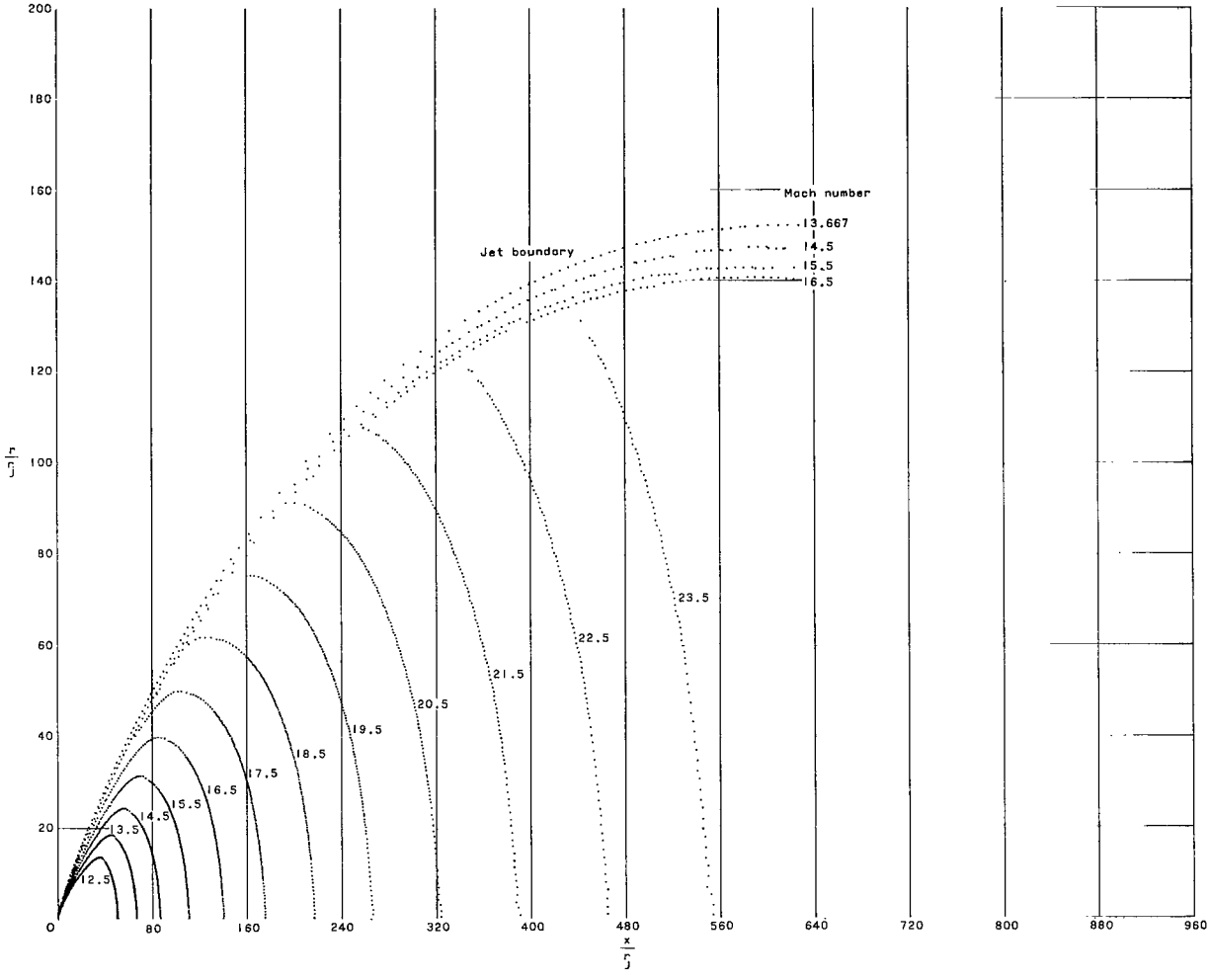

(e) $p_j/p_\infty = 5.410 \times 10^3$; $\alpha_n = 47^\circ$. Concluded.

Figure 8.- Continued.

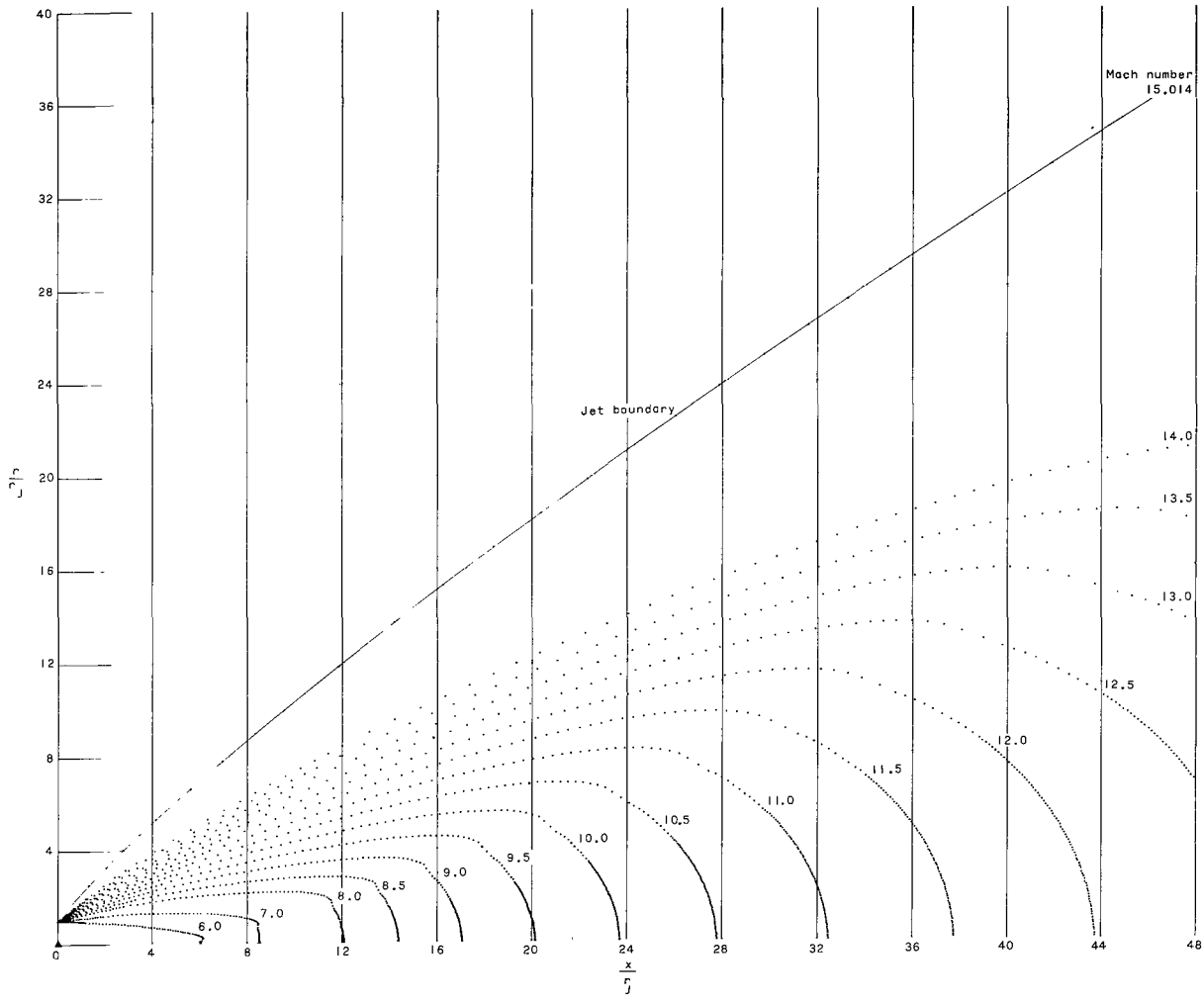

(f) $p_j/p_\infty = 13.756 \times 10^3$; $\alpha_n = 50^\circ$.

Figure 8.- Continued.

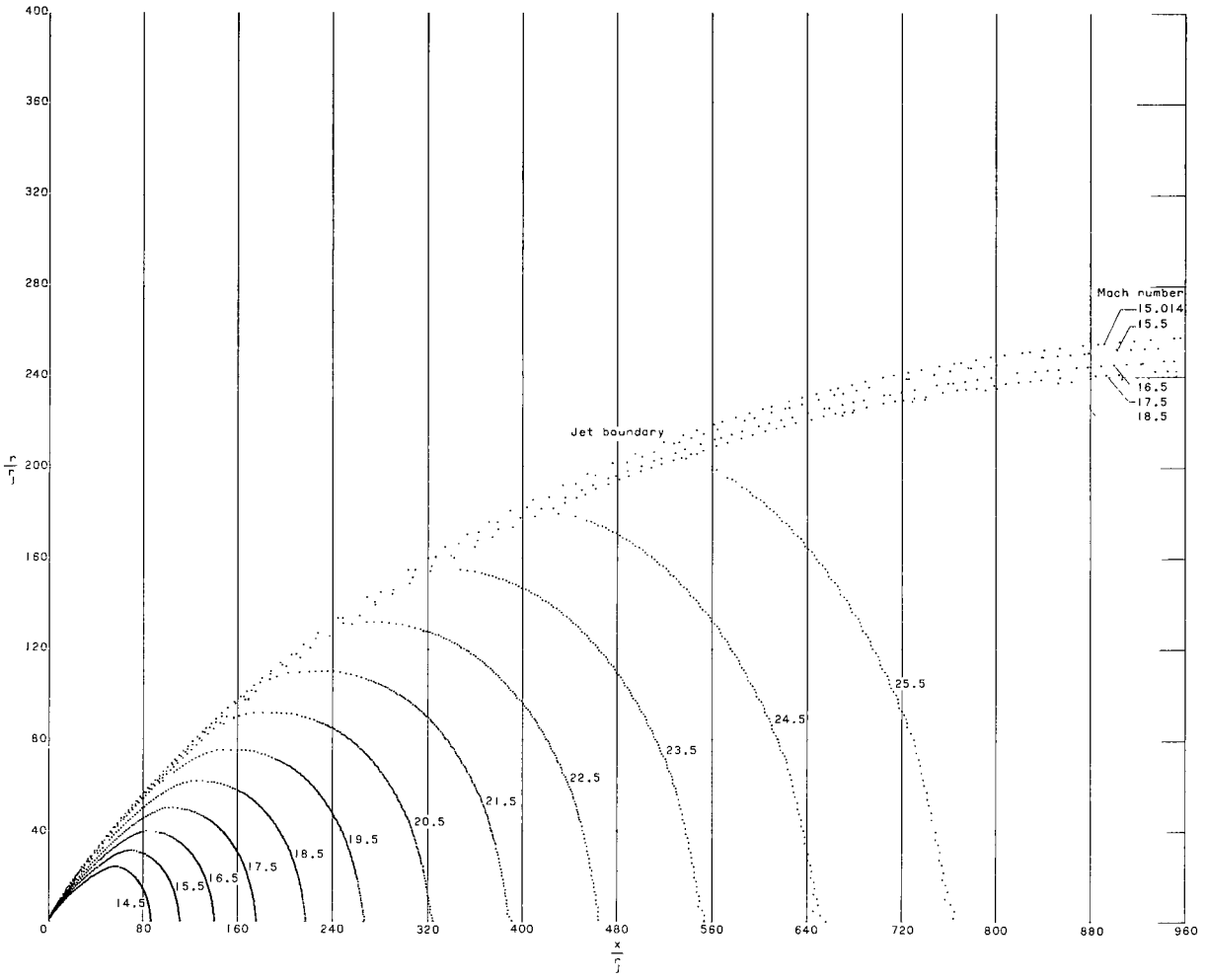

(f) $p_j/p_\infty = 13.756 \times 10^3$; $\alpha_n = 50^\circ$. Continued.

Figure 8.- Continued.

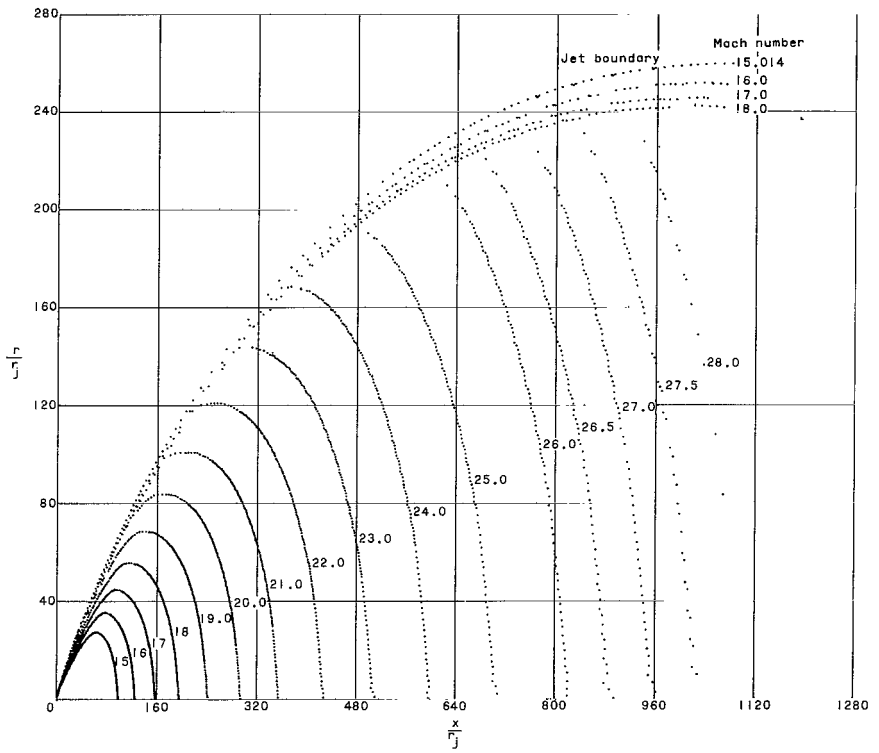

(f) $p_j/p_\infty = 13.756 \times 10^3$; $\alpha_n = 50^\circ$. Concluded.

Figure 8.- Continued.

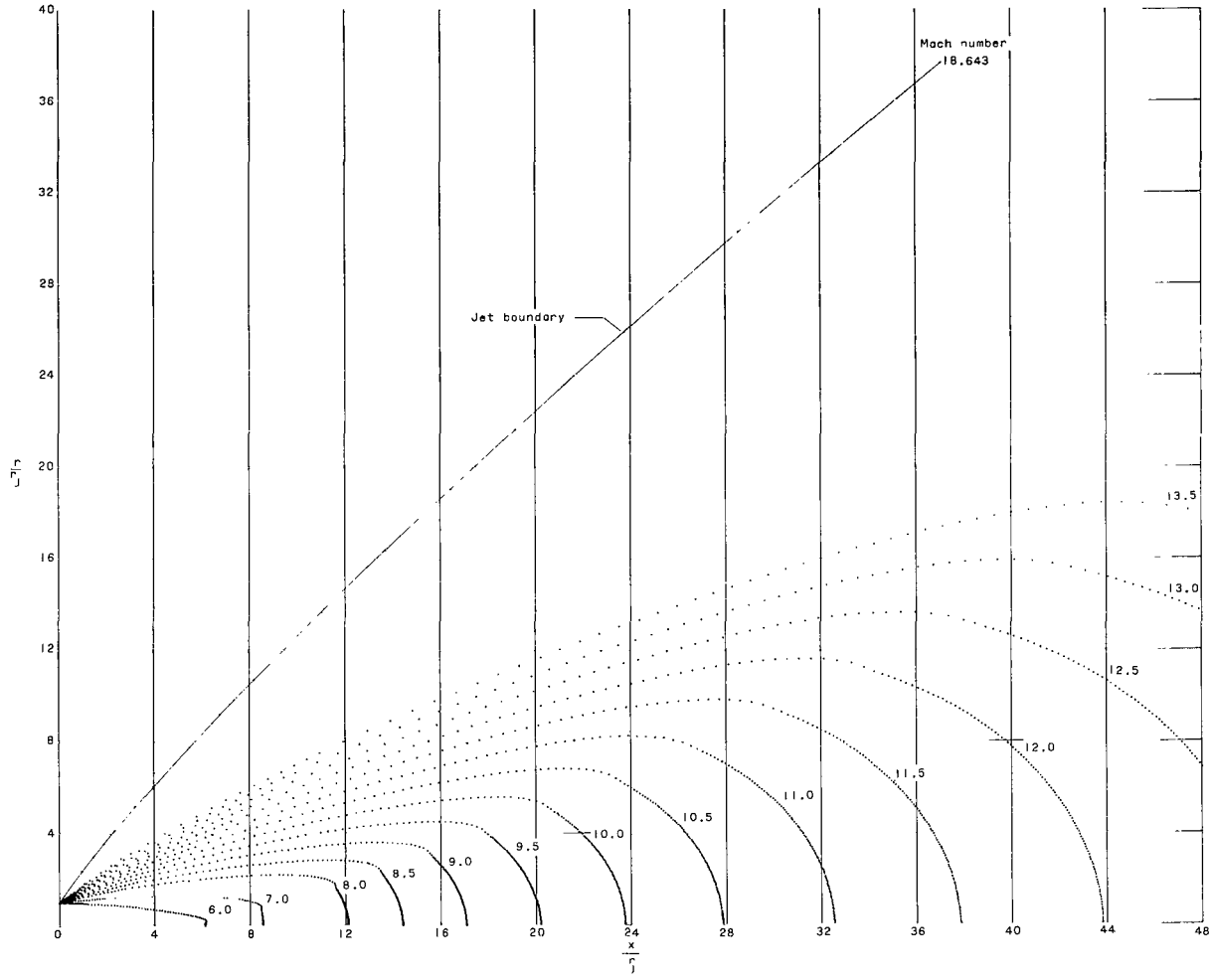

(g) $p_j/p_\infty = 120.700 \times 10^3$; $\alpha_n = 56^\circ$.

Figure 8.- Continued.

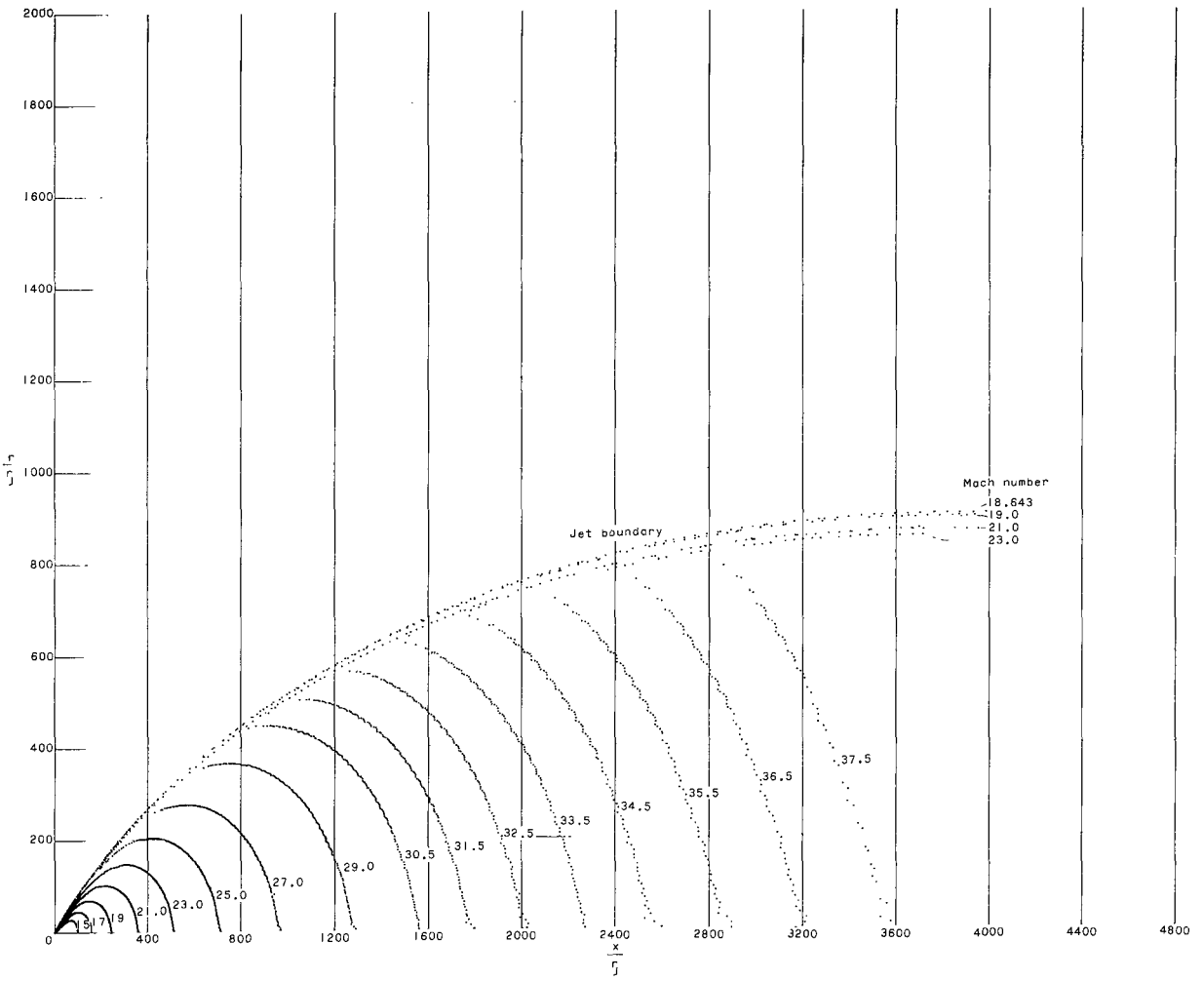

(g) $p_j/p_\infty = 120.700 \times 10^3$; $\alpha_n = 56^\circ$. Continued.

Figure 8.- Continued.

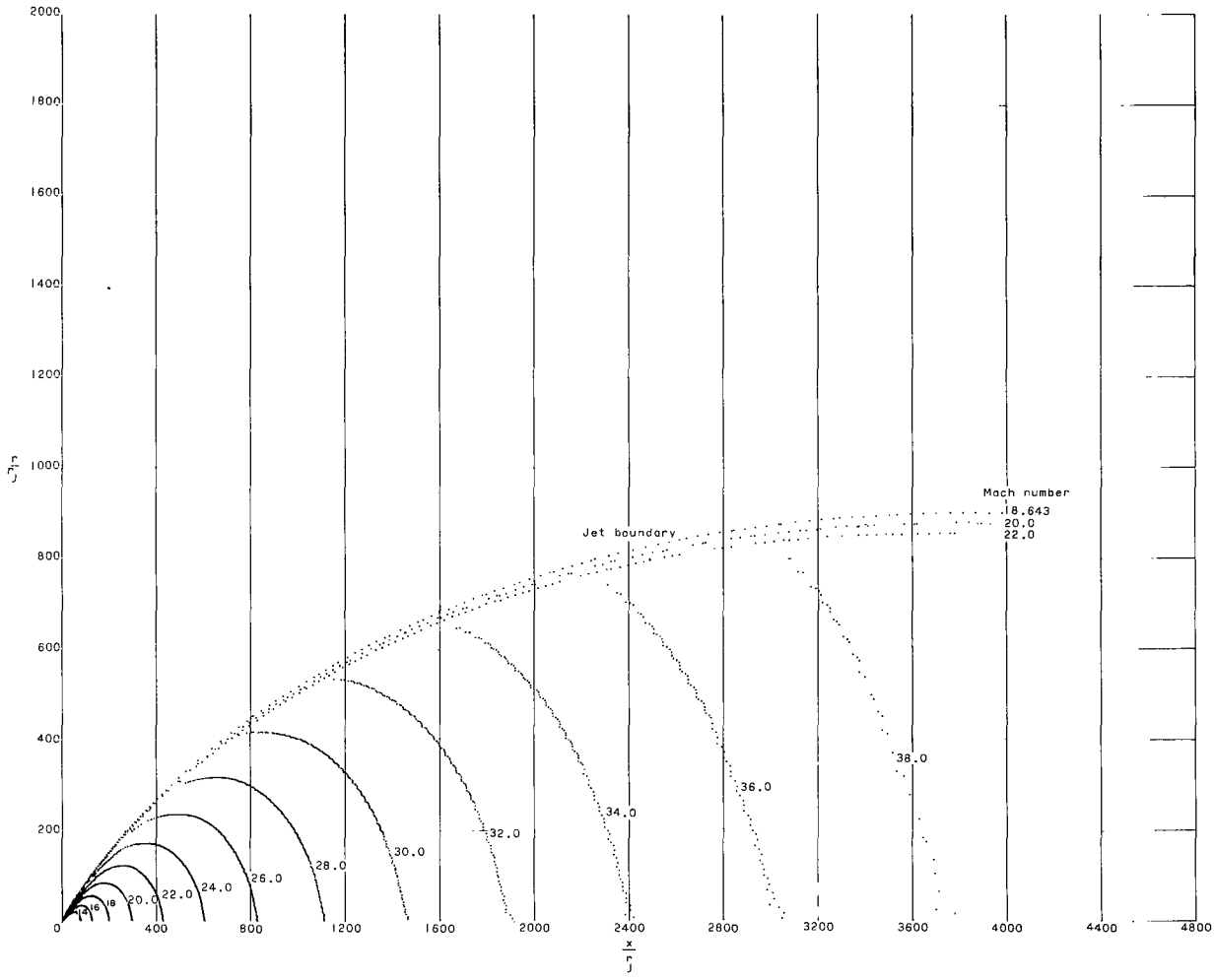

(g) $p_j/p_\infty = 120.700 \times 10^3$; $\alpha_n = 56^\circ$. Concluded.

Figure 8.- Concluded.

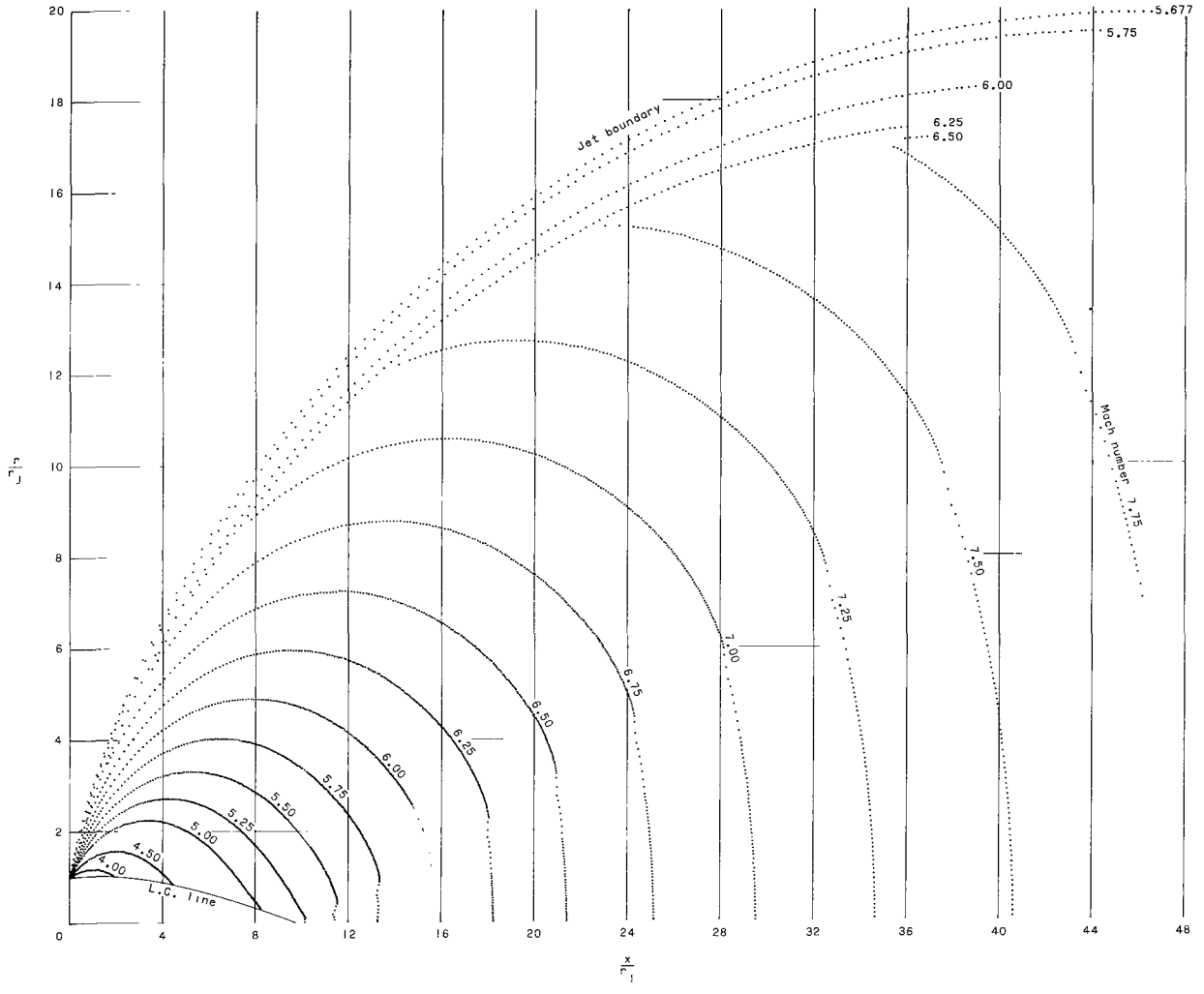

(a) $p_j/p_\infty = 100$; $\alpha_n = 71.043^\circ$.

Figure 9.- Contours of constant Mach number within the exhaust plume; nozzle II.

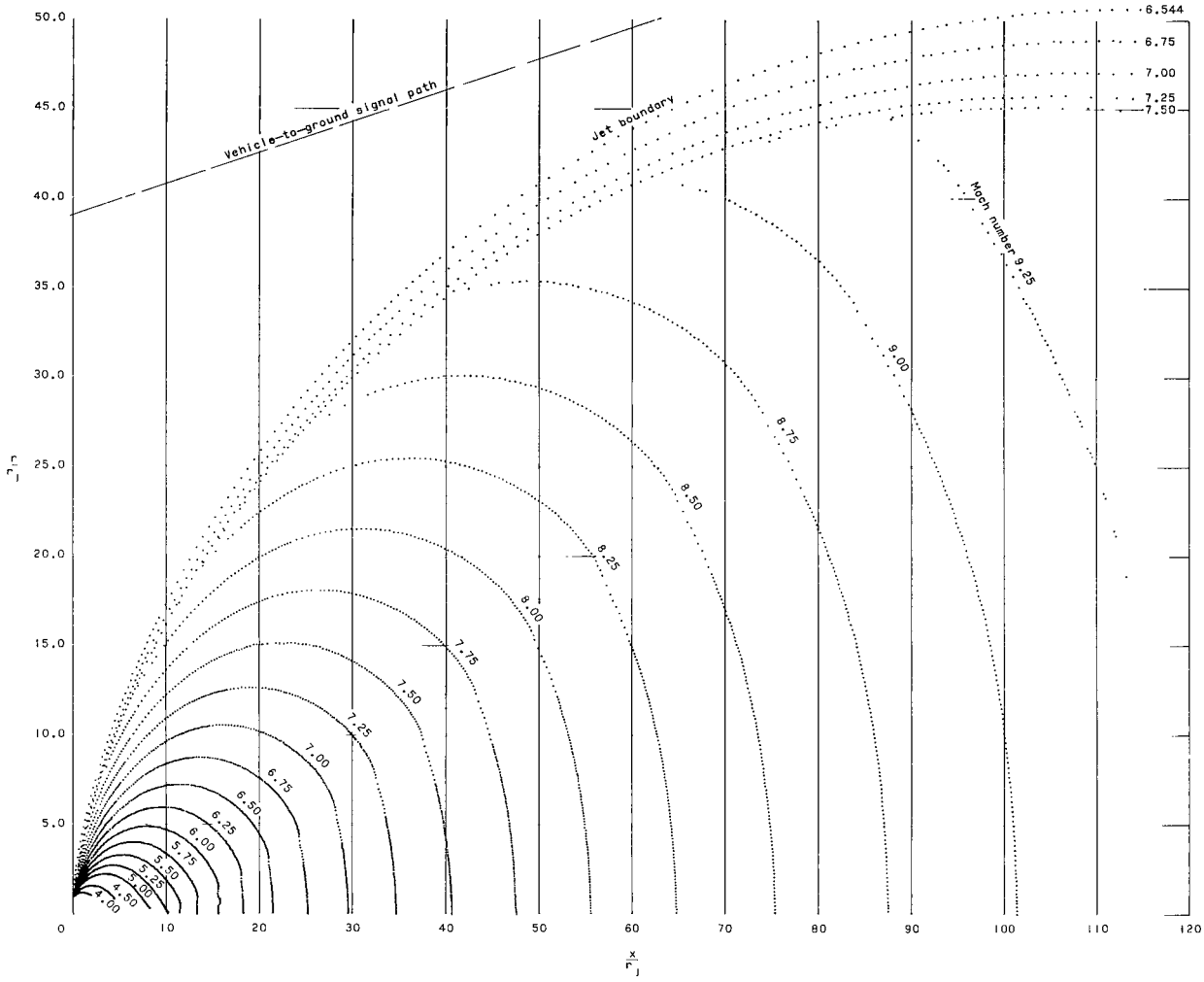

(b) $p_j/p_\infty = 500$; $\alpha_n = 84.029°$.

Figure 9.- Continued.

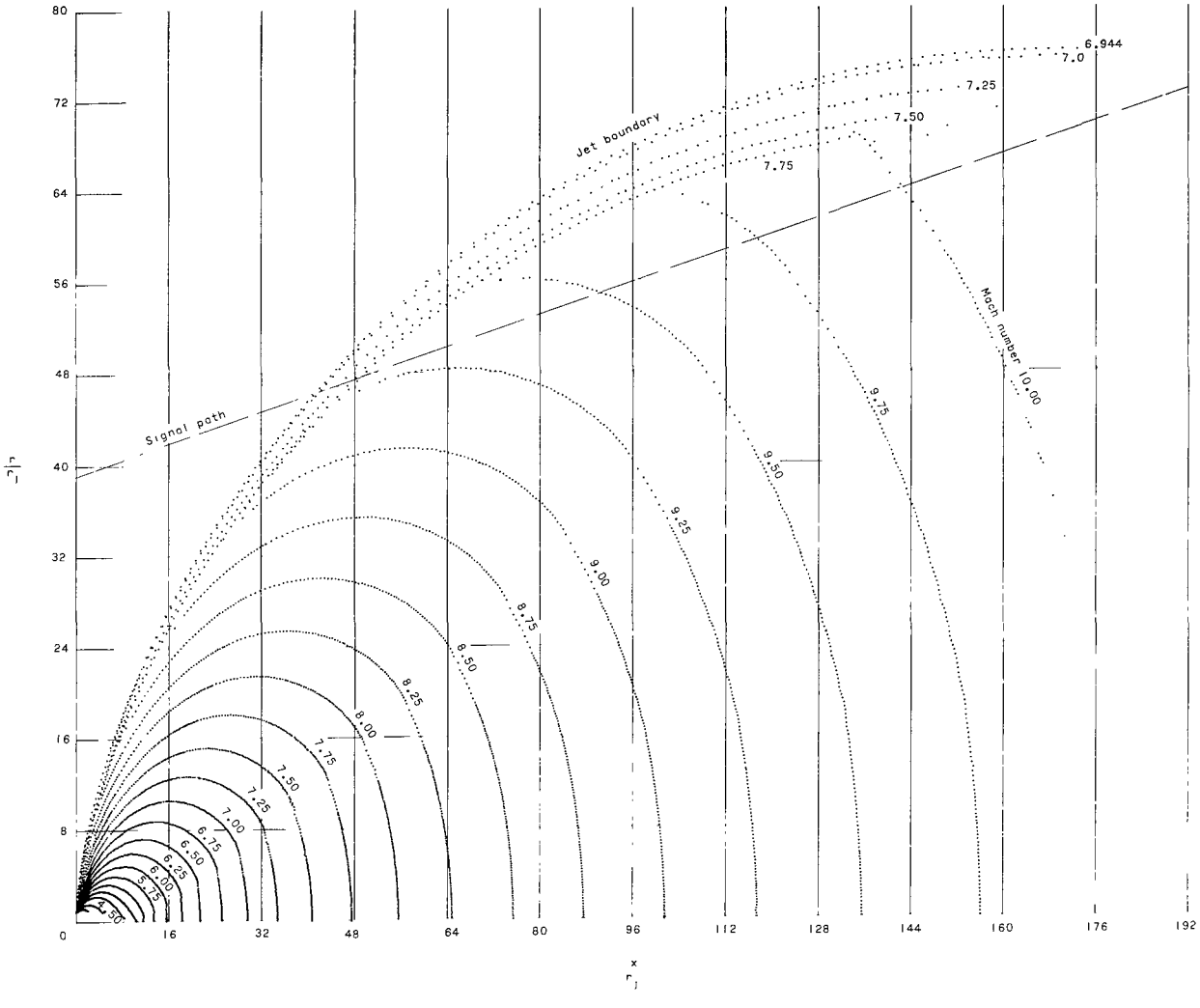

(c) $p_j/p_\infty = 1000$; $\alpha_n = 89.095^\circ$.

Figure 9.- Continued.

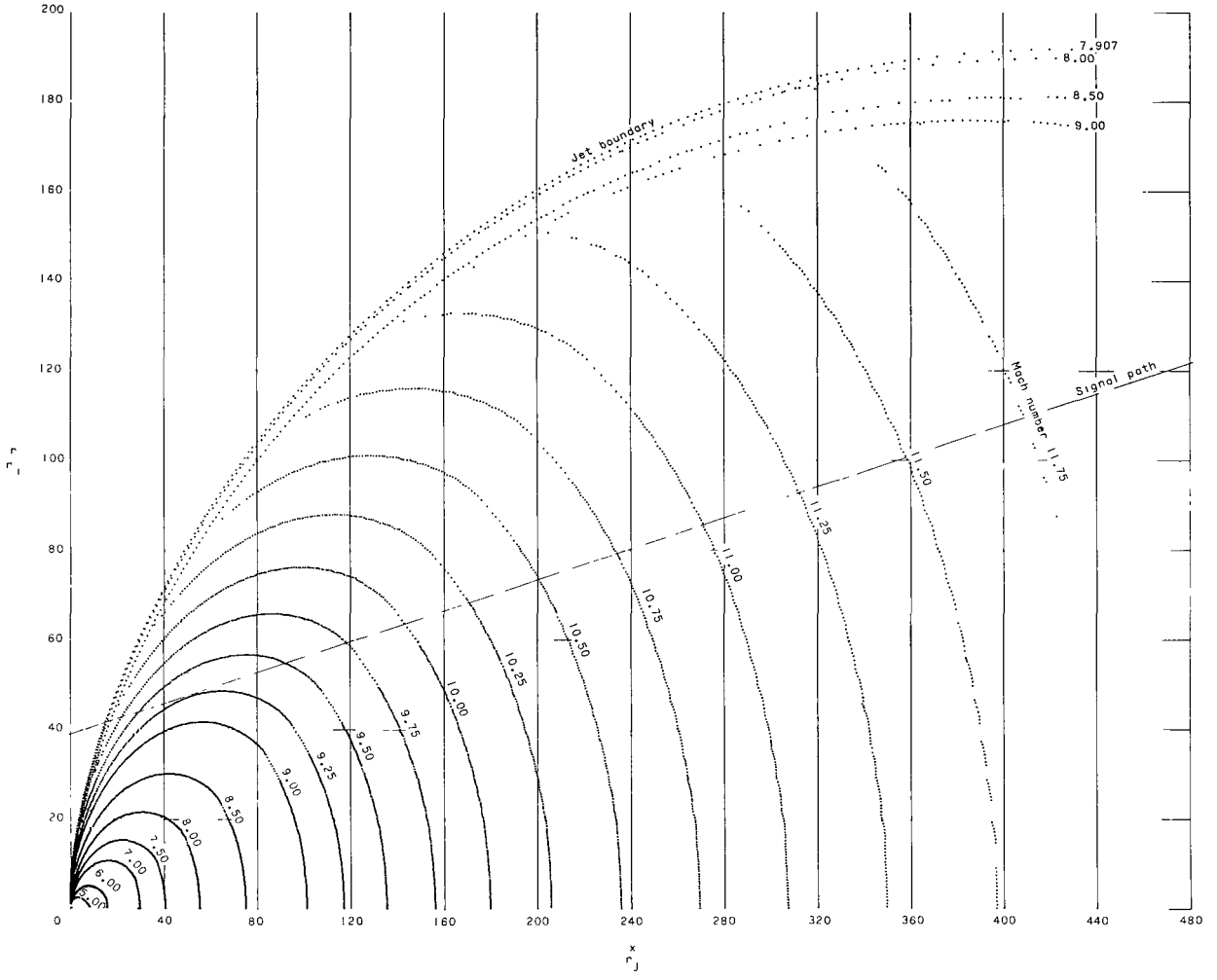

(d) $p_j/p_\infty = 5000$; $\alpha_n = 99.847°$.

Figure 9.- Concluded.

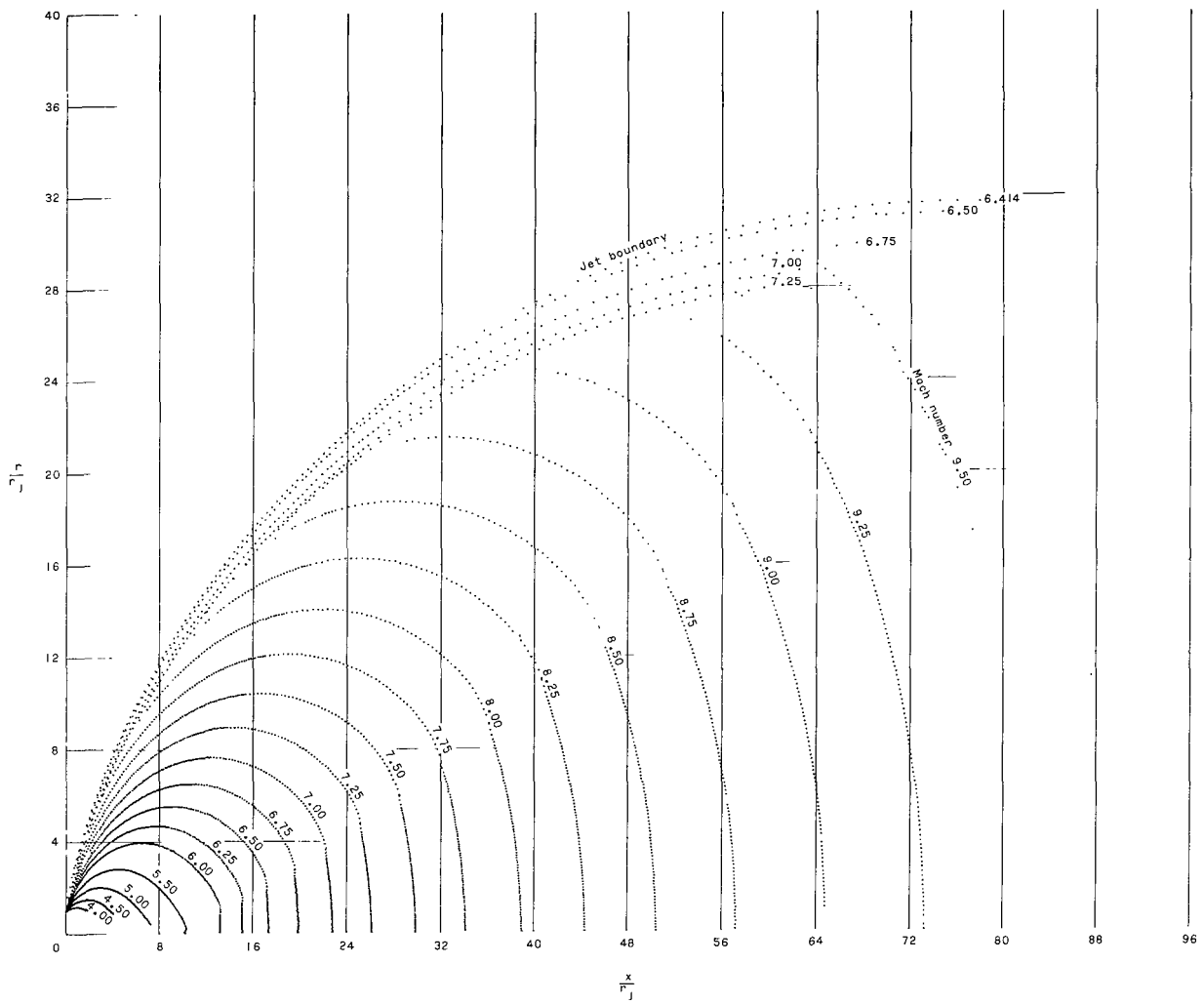

(a) $p_j/p_\infty = 2.38 \times 10^2$; $\alpha_n = 74.740^\circ$.

Figure 10.- Contours of constant Mach number within the exhaust plume; nozzle III.

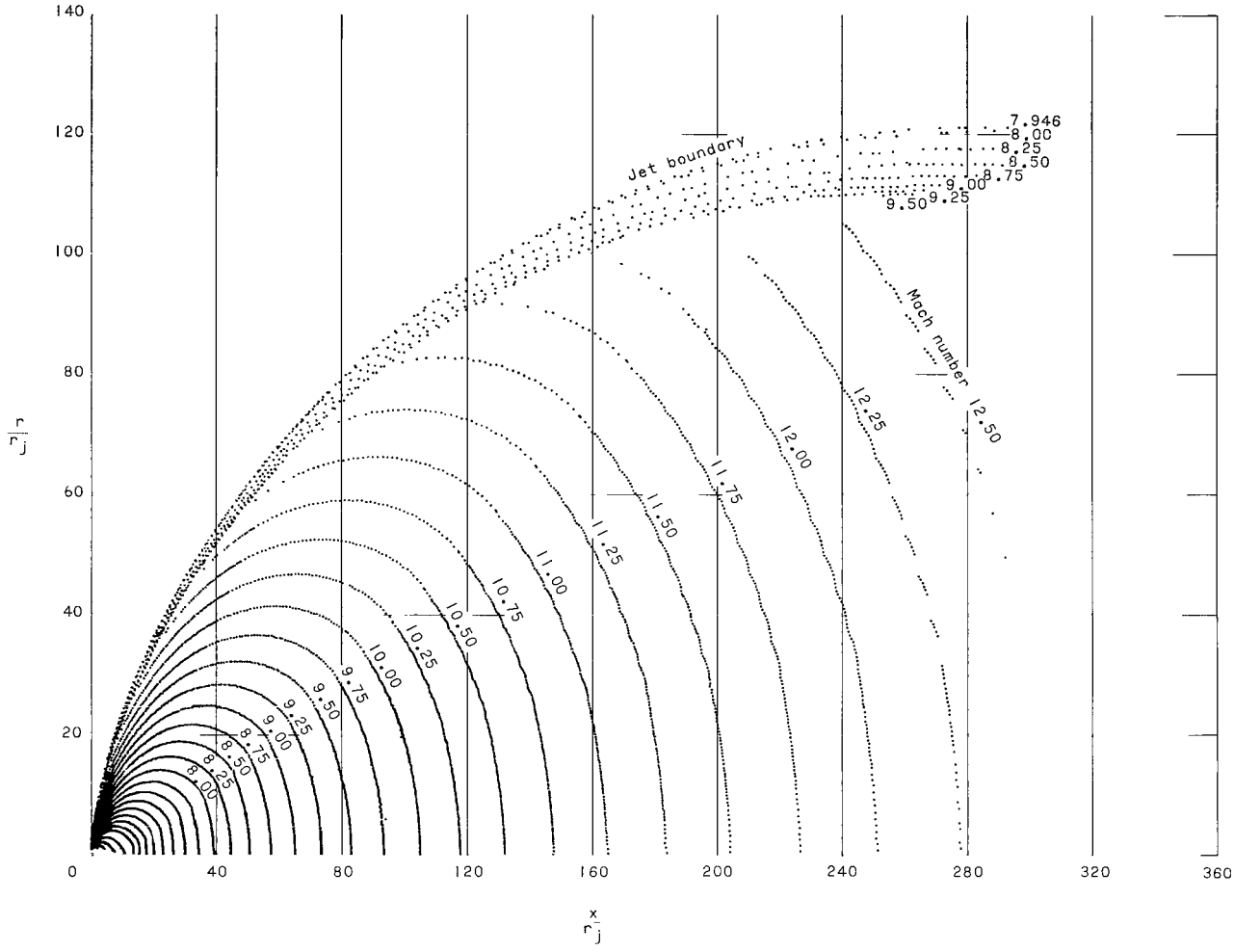

(b) $p_j/p_\infty = 2.38 \times 10^3$; $\alpha_n = 90.443^\circ$.

Figure 10.- Continued.

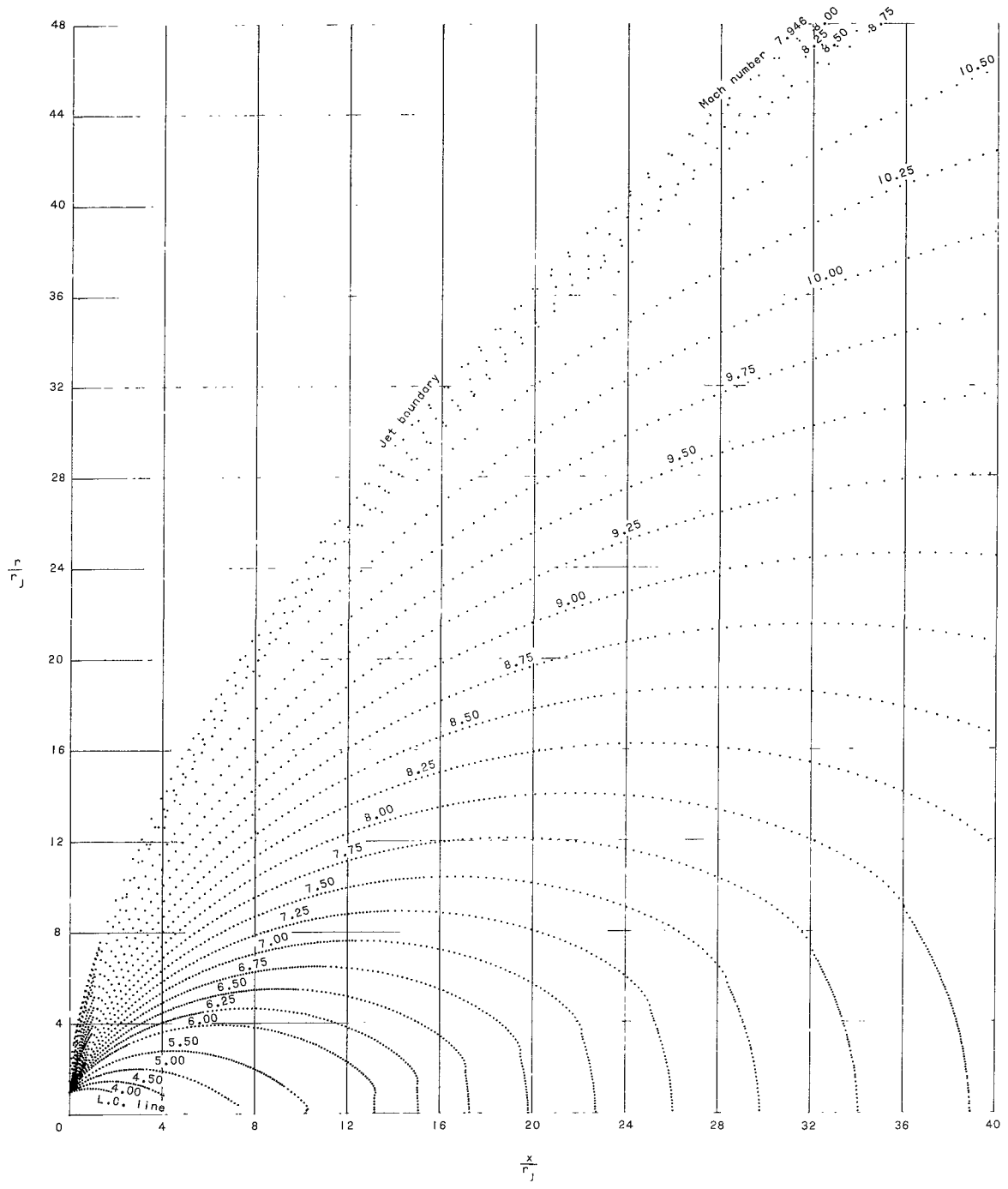

(b) $p_j/p_\infty = 2.38 \times 10^3$; $\alpha_n = 90.443^\circ$. Concluded.

Figure 10.- Continued.

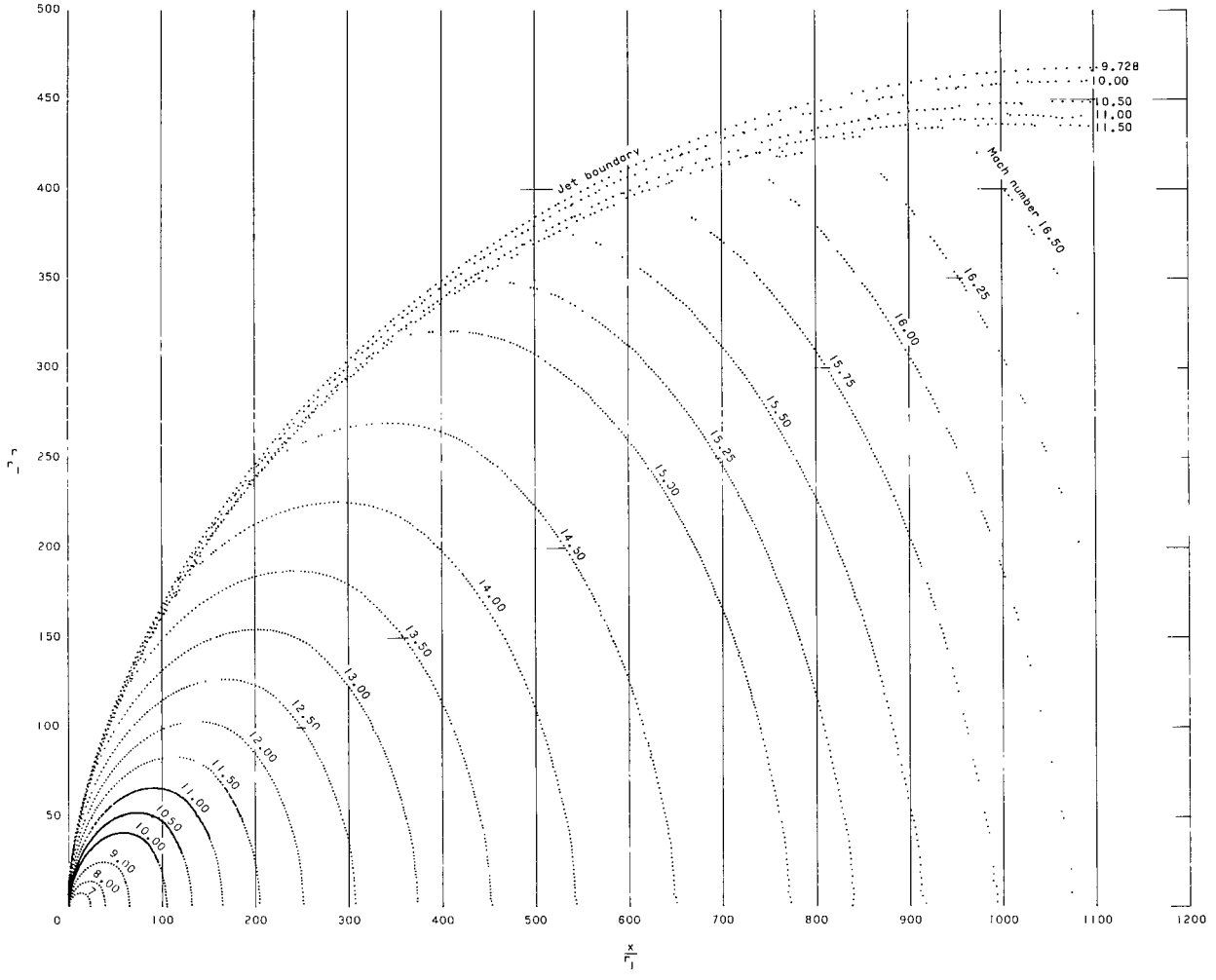

(c) $p_j/p_\infty = 2.38 \times 10^4$; $\alpha_n = 103.175^\circ$.

Figure 10.- Continued.

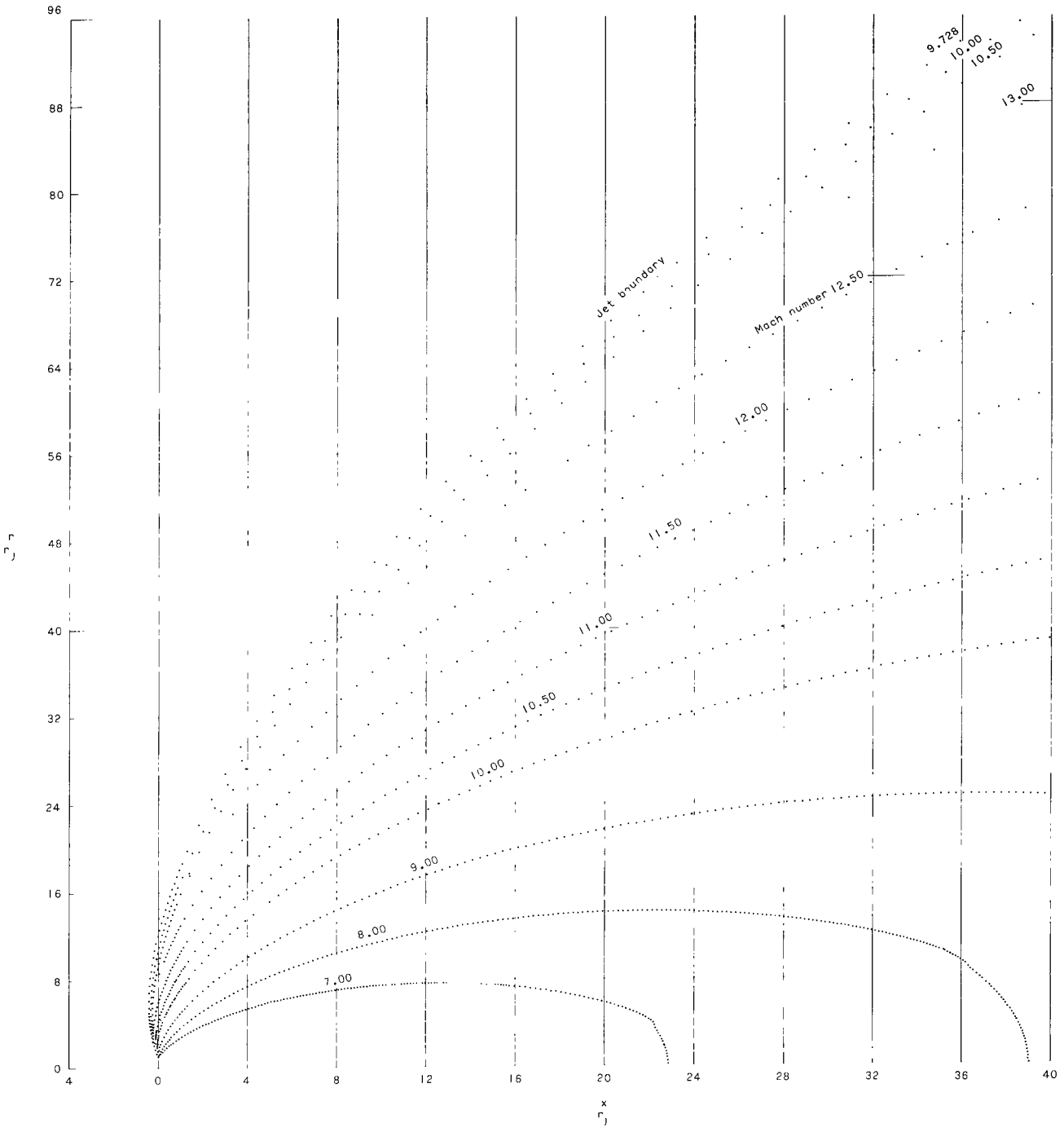

(c) $p_j/p_\infty = 2.38 \times 10^4$; $\alpha_n = 103.175^\circ$. Concluded.

Figure 10.- Continued.

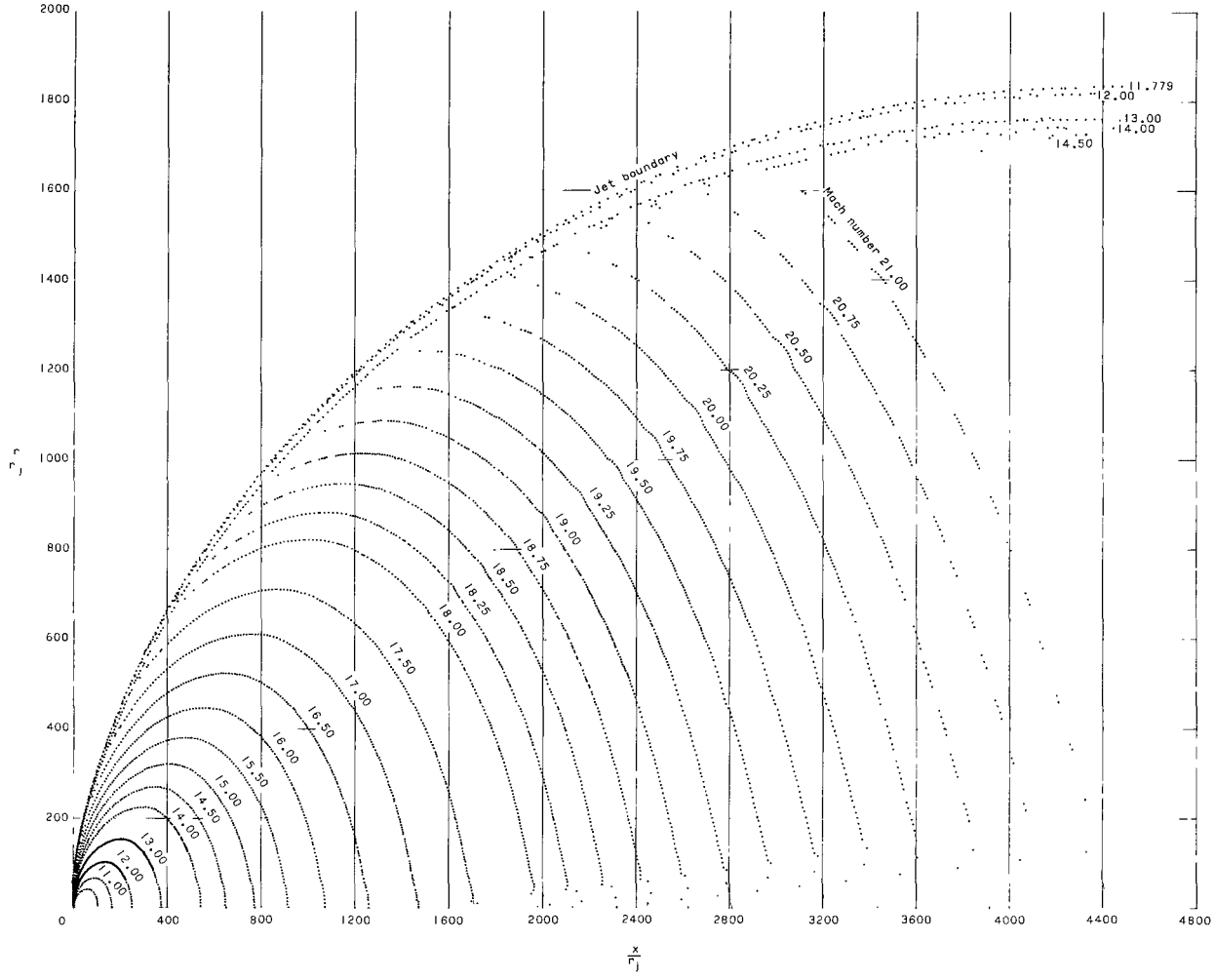

(d) $p_j/p_\infty = 2.38 \times 10^5$; $\alpha_n = 113.506^\circ$.

Figure 10.- Continued.

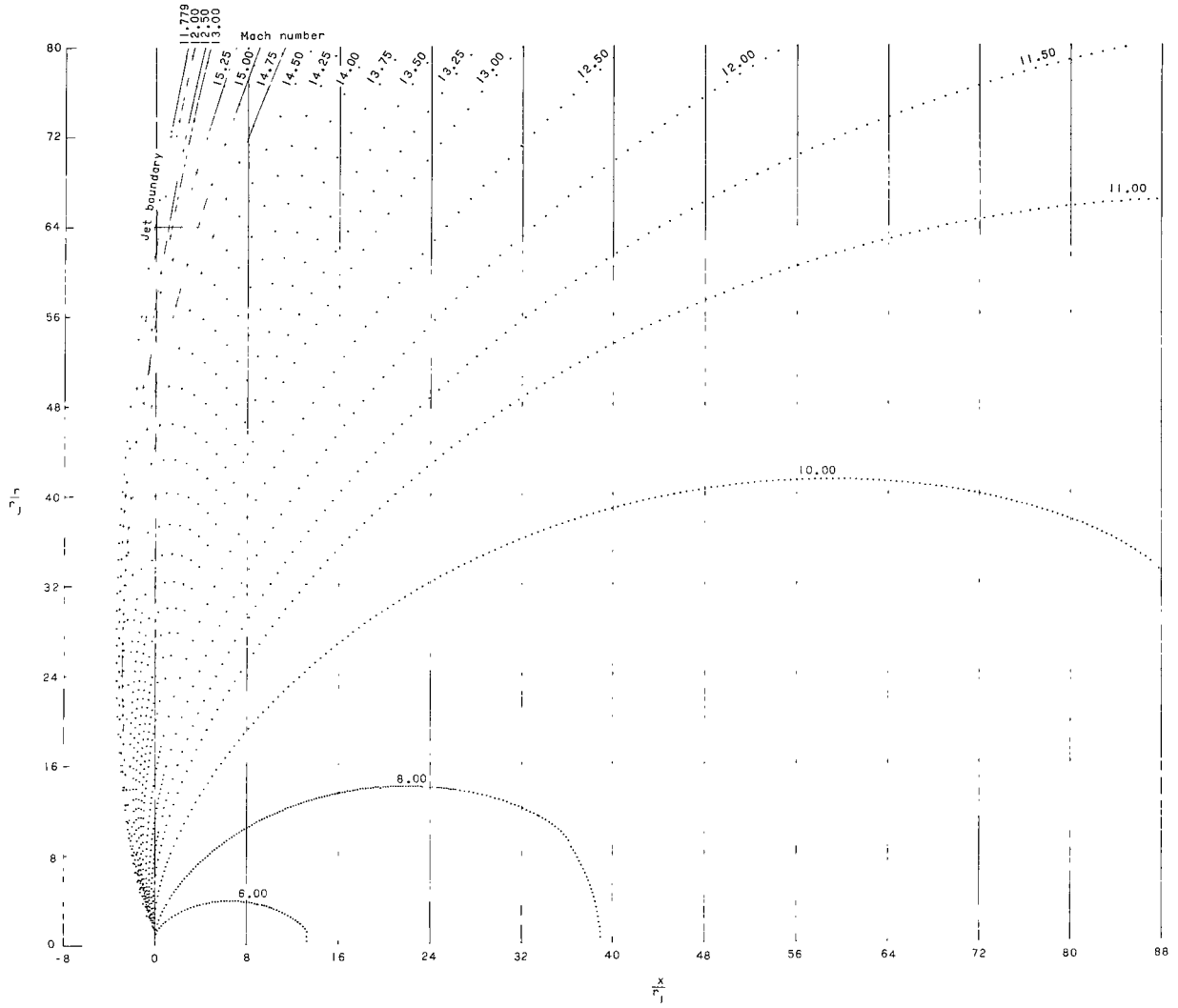

(d) $p_j/p_\infty = 2.38 \times 10^5$; $\alpha_n = 113.506^\circ$. Continued.

Figure 10.- Continued.

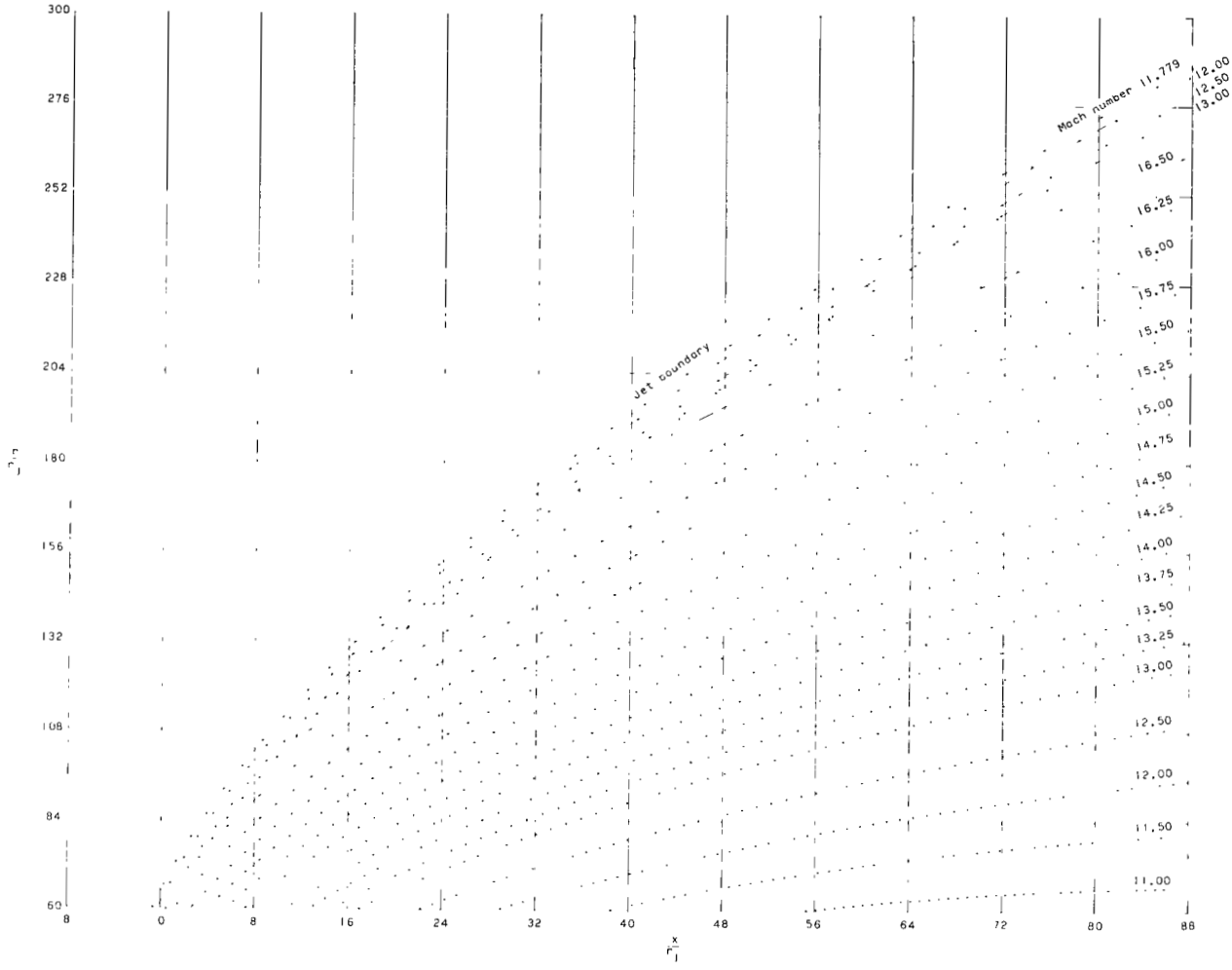

(d) $p_j/p_\infty = 2.38 \times 10^5$; $\alpha_n = 113.506^\circ$. Concluded.

Figure 10.- Continued.

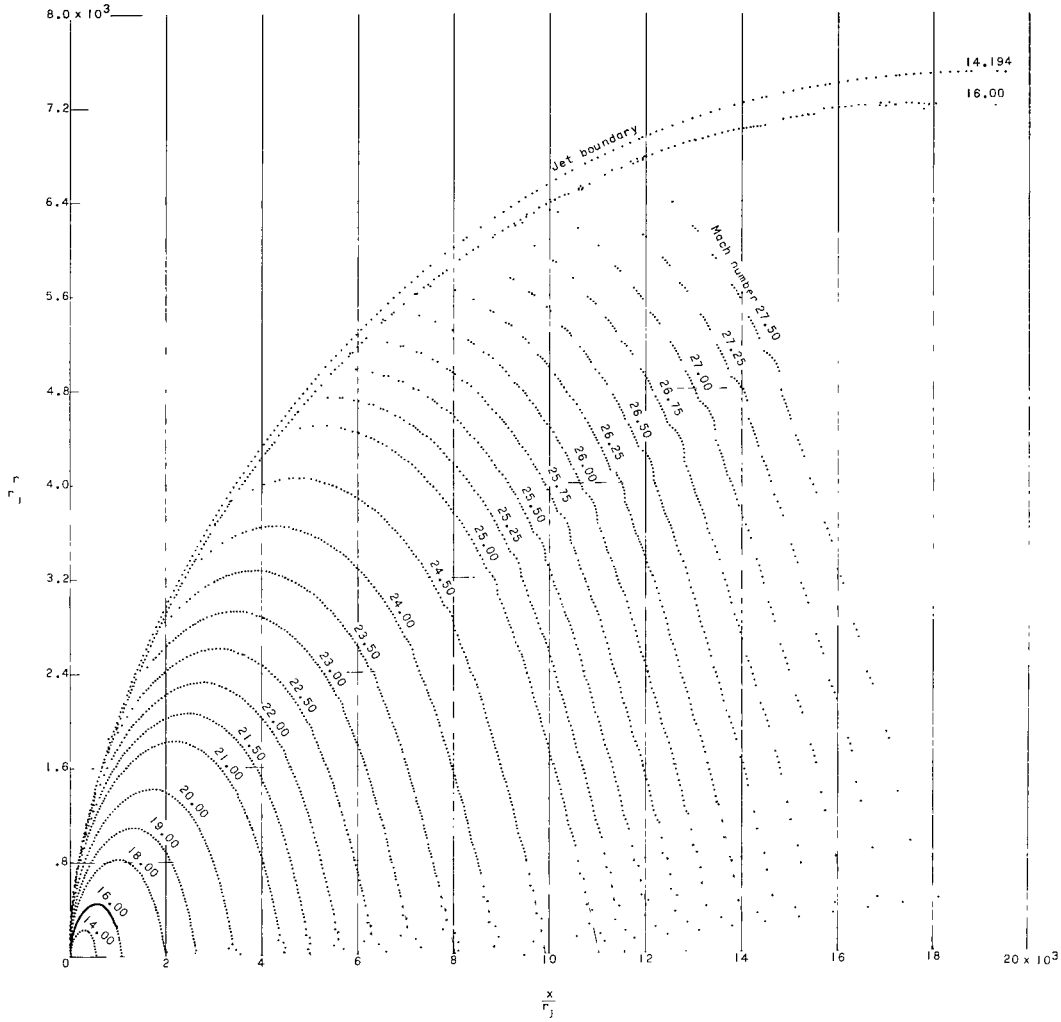

(e) $p_j/p_\infty = 2.38 \times 10^6$; $\alpha_n = 122.095°$.

Figure 10.- Continued.

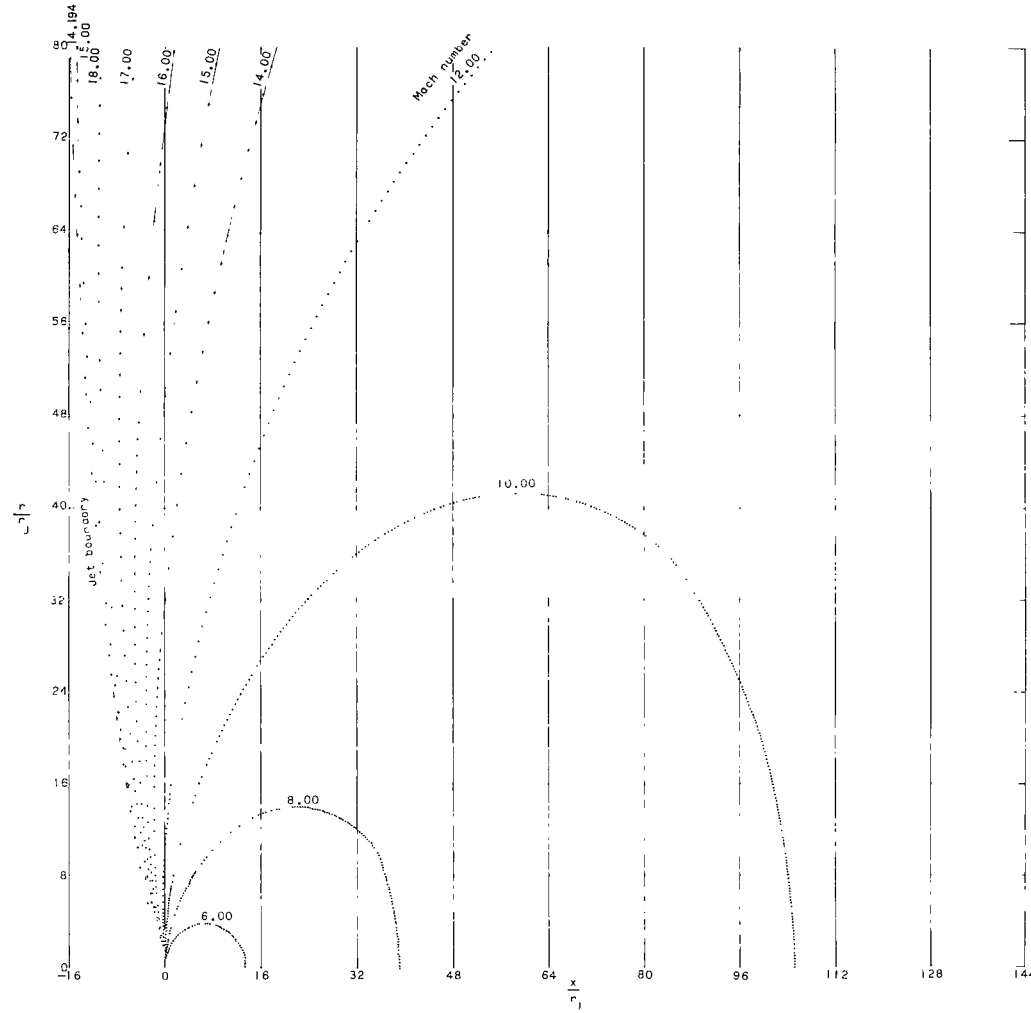

(e) $p_j/p_\infty = 2.38 \times 10^6$; $\alpha_n = 122.095^\circ$. Continued.

Figure 10.- Continued.

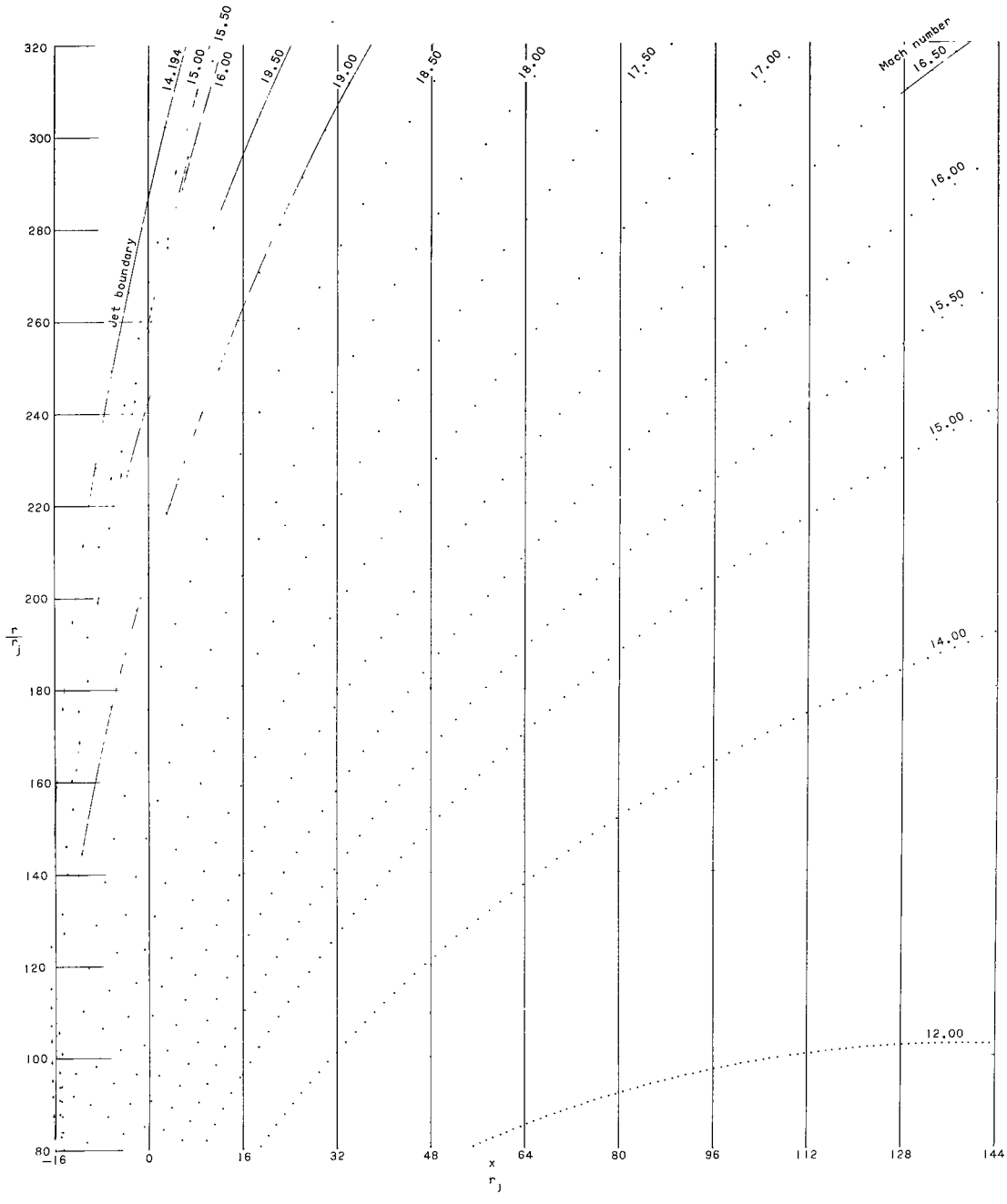

(e) $p_j/p_\infty = 2.38 \times 10^6$; $\alpha_n = 122.095^\circ$. Continued.

Figure 10.- Continued.

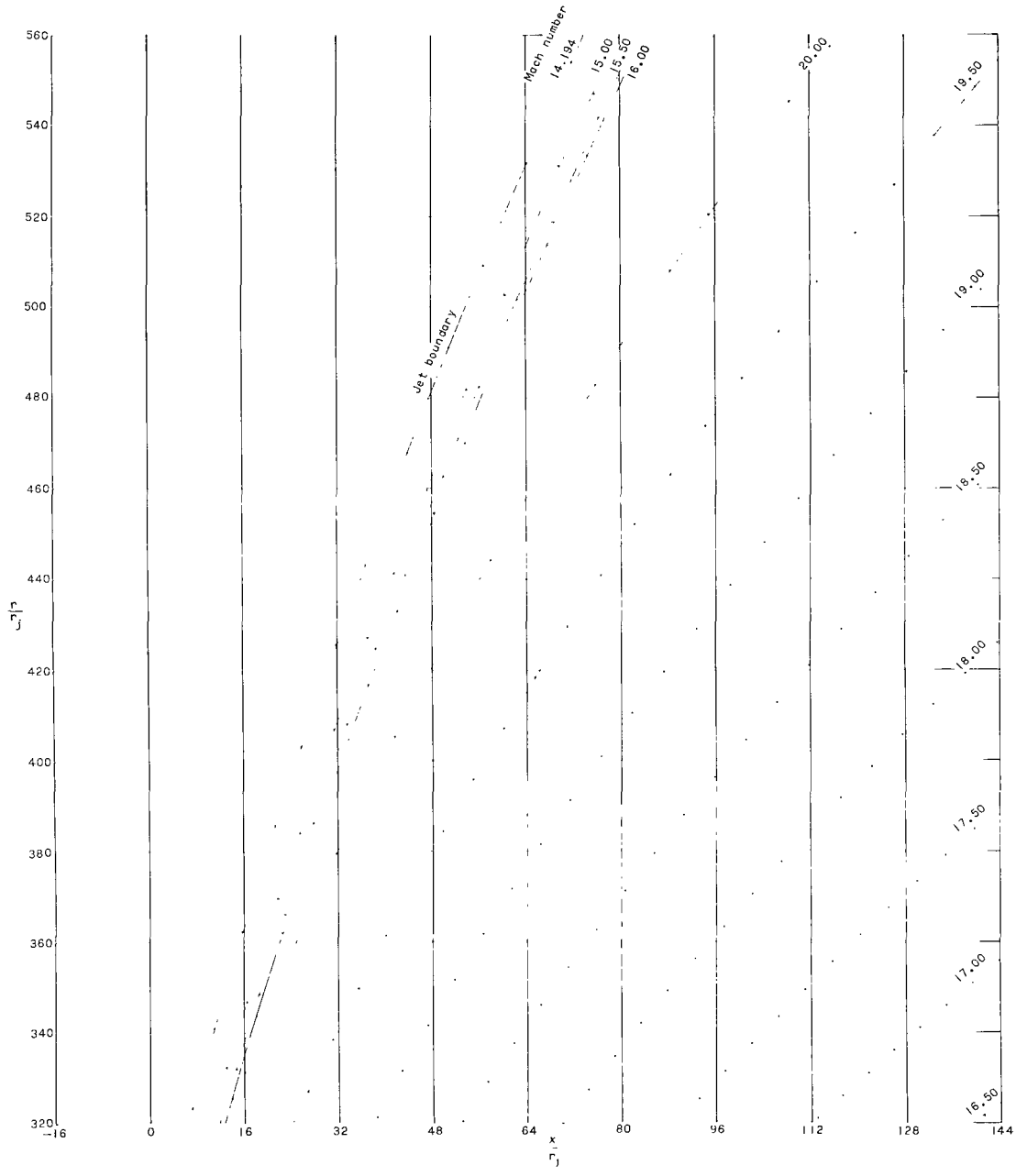

(e) $p_j/p_\infty = 2.38 \times 10^6$; $\alpha_n = 122.095^\circ$. Concluded.

Figure 10.- Concluded.

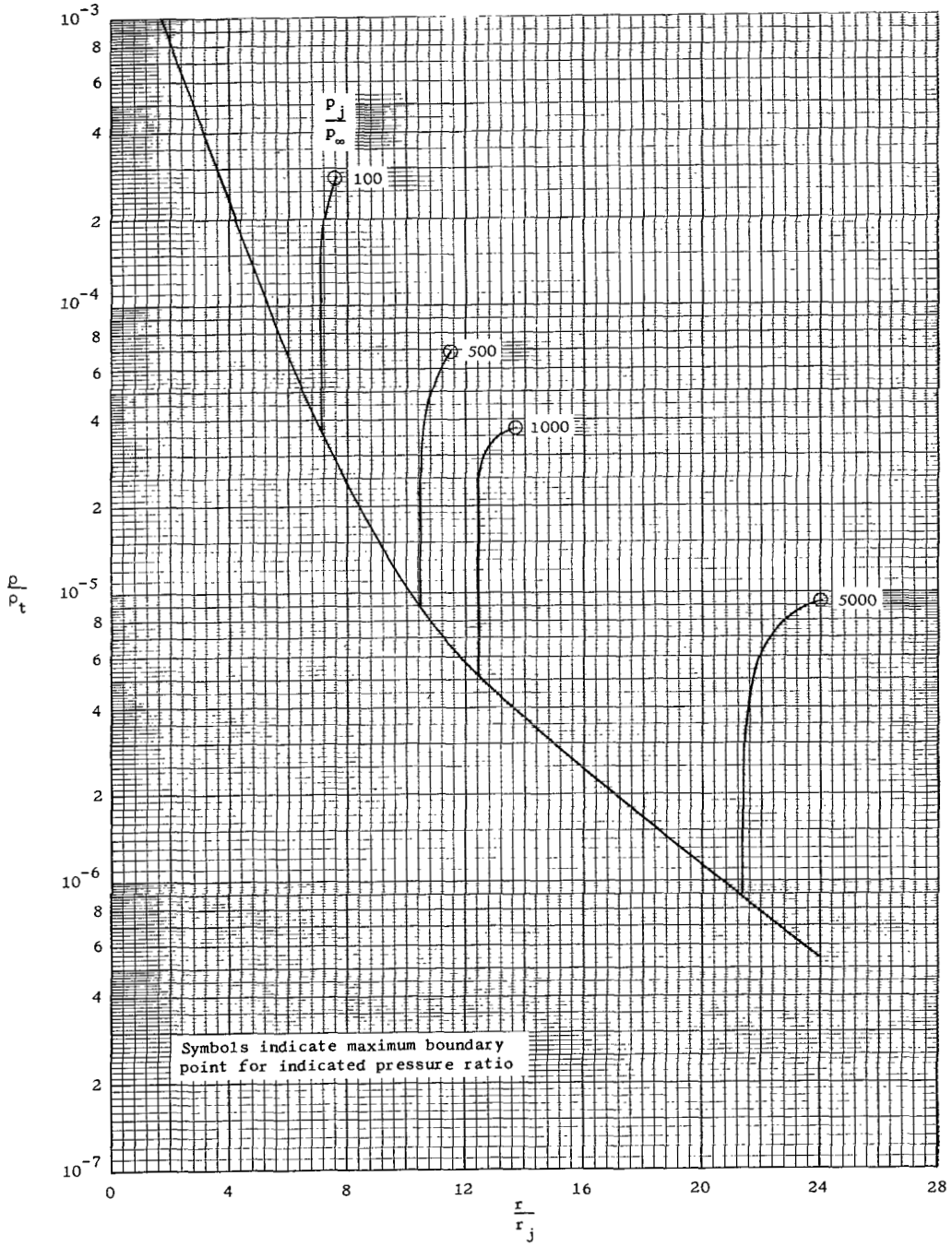

(a) $x/r_j = 5.$

Figure 11.- Variation of density ratio as radial distance is increased at constant distances downstream of nozzle exit for various pressure ratios of nozzle II.

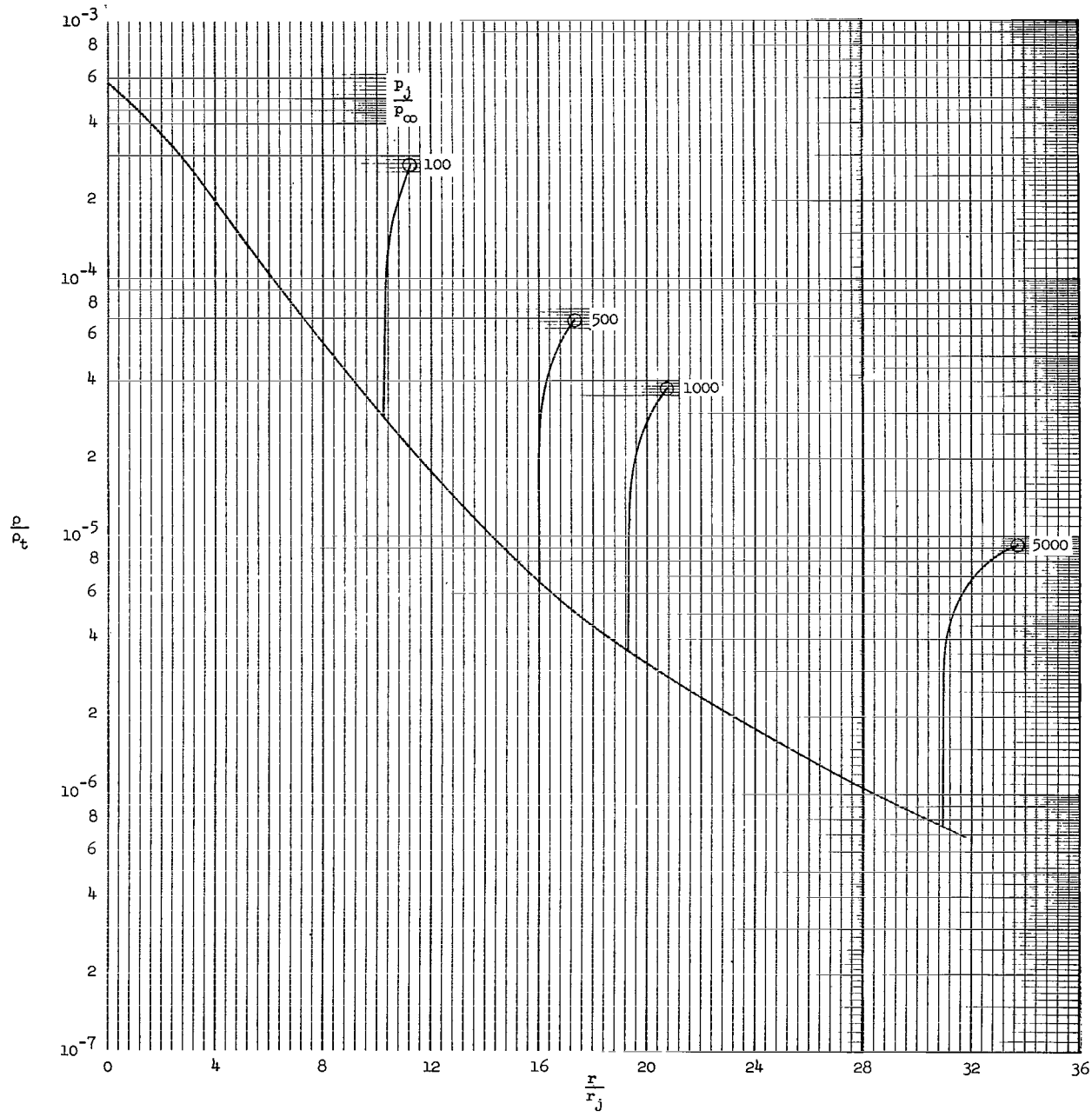

(b) $x/r_j = 10.$

Figure 11.- Continued.

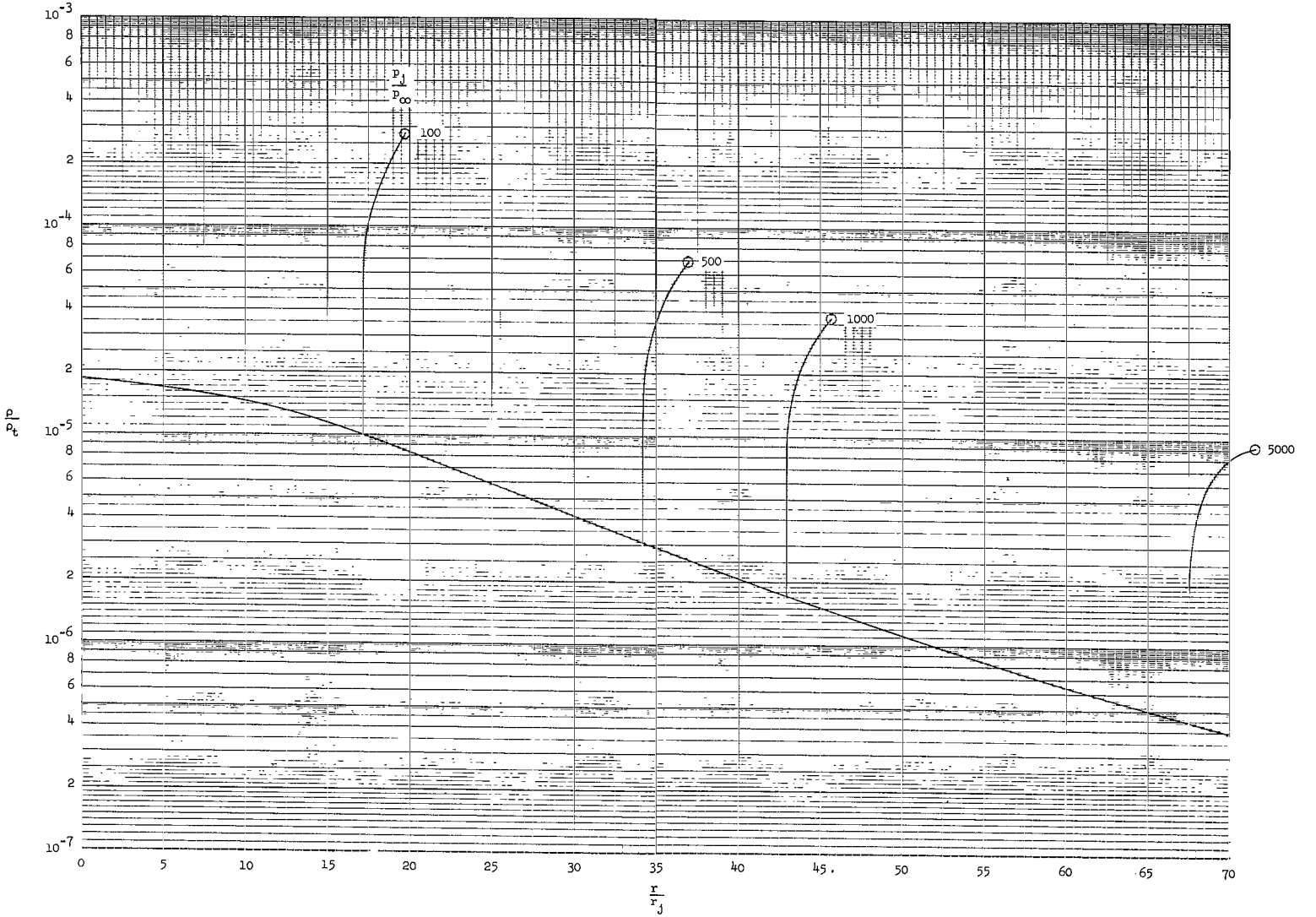

(c) $x/r_j = 40.$

Figure 11.- Continued.

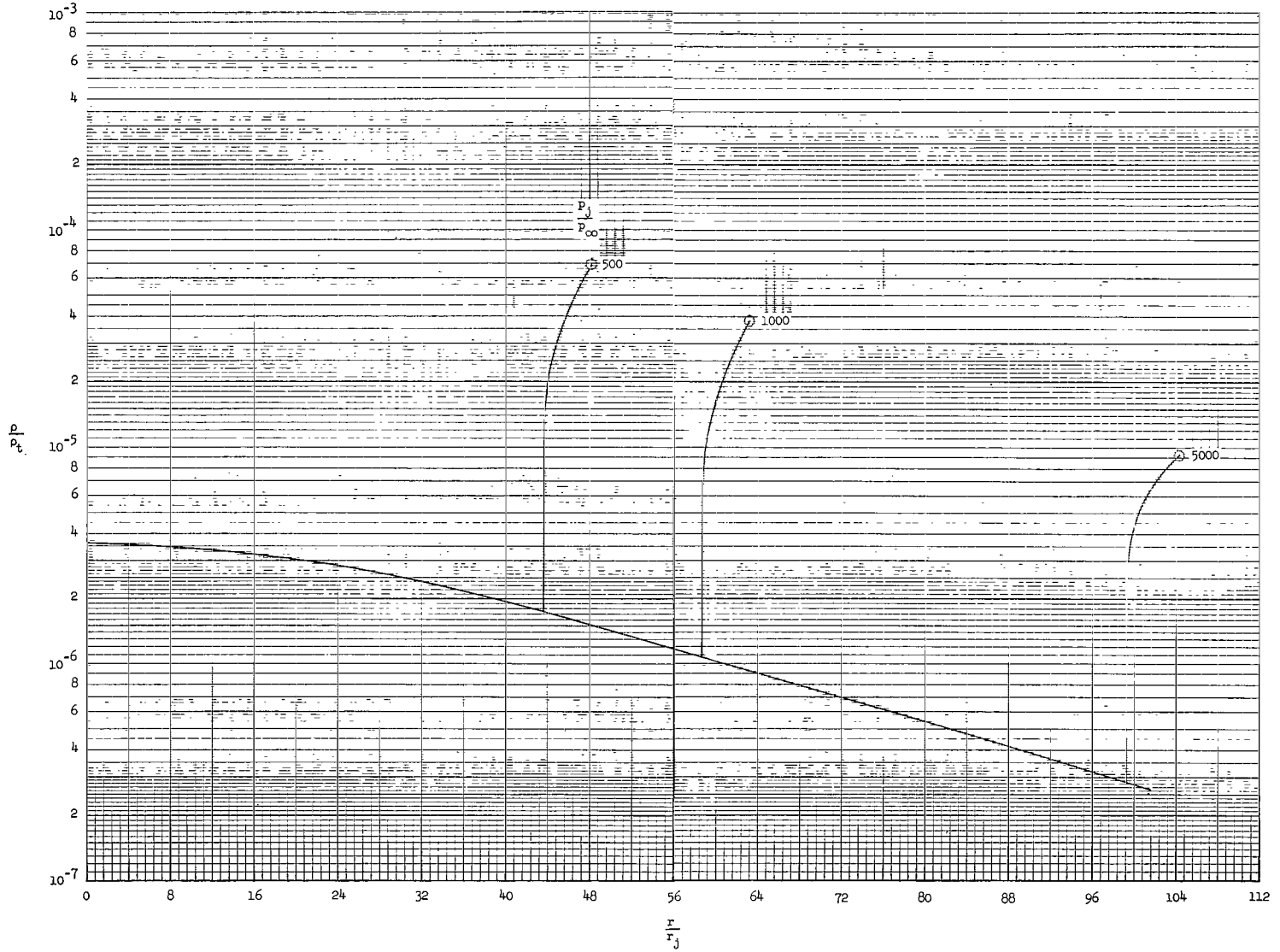

(d) $x/r_j = 80.$

Figure 11.- Concluded.

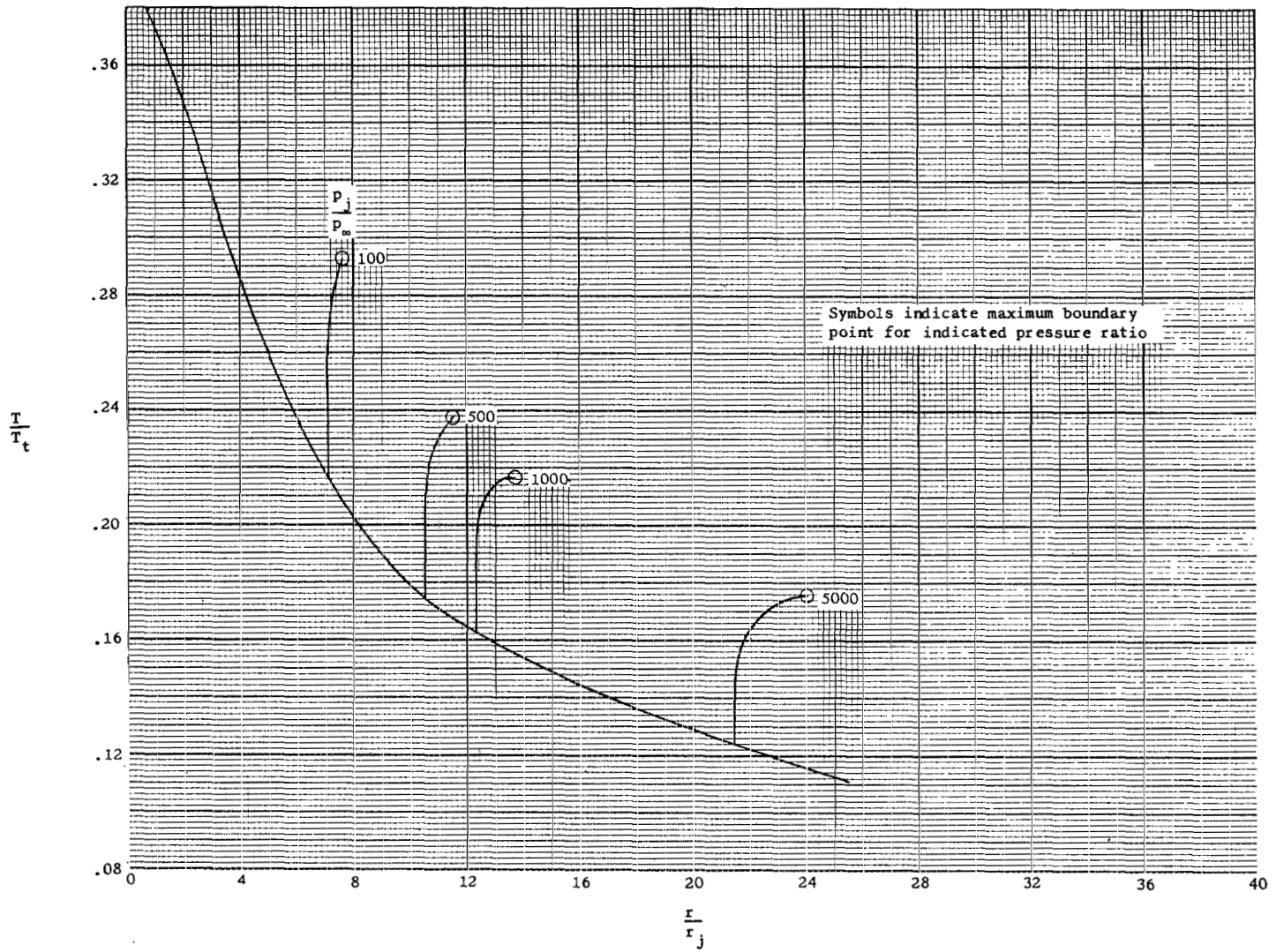

(a) $x/r_j = 5.$

Figure 12.- Variation of temperature ratio as radial distance is increased at constant distances downstream of nozzle exit for various pressure ratios of nozzle II.

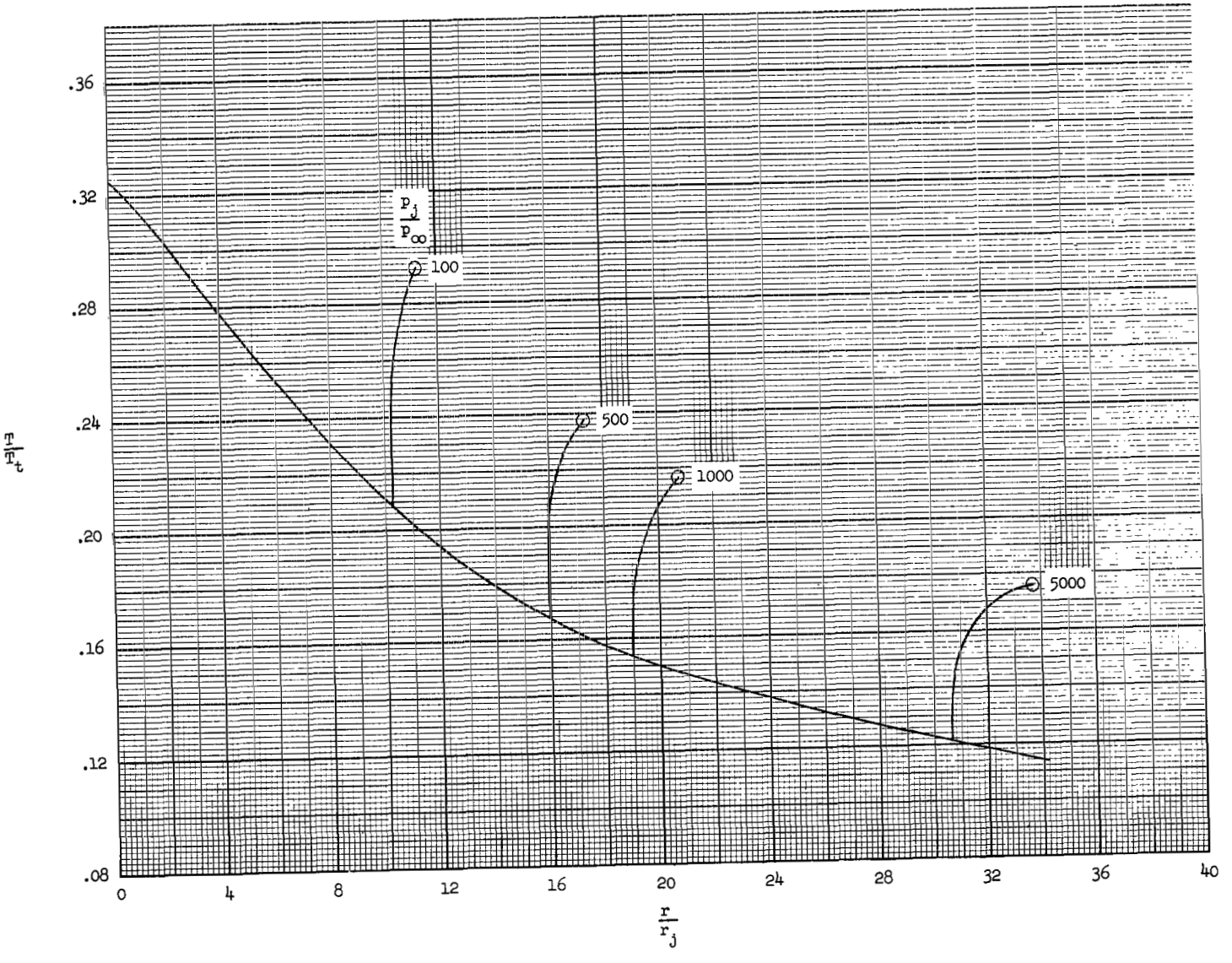

(b) $x/r_j = 10.$

Figure 12.- Continued.

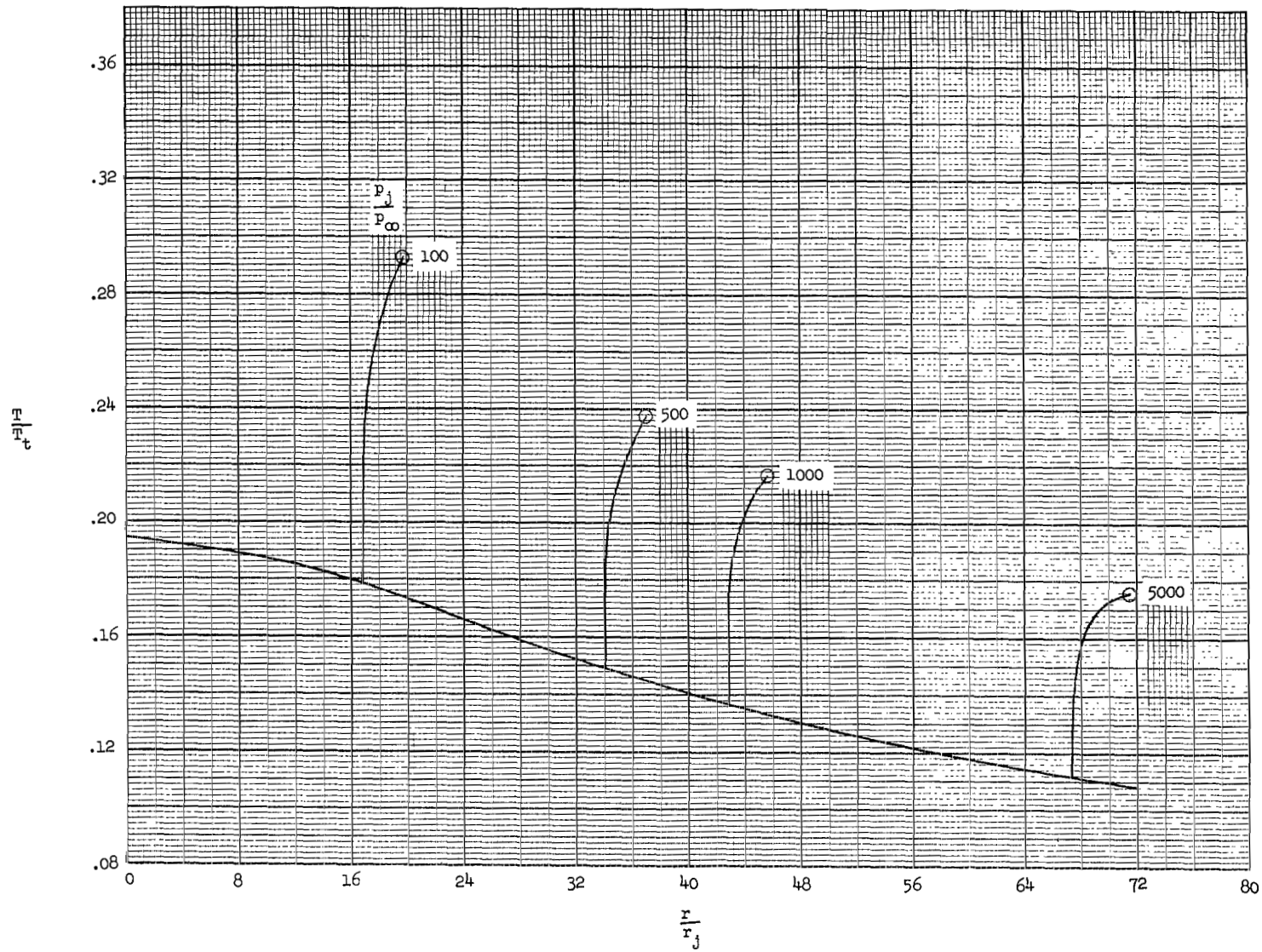

(c) $x/r_j = 40.$

Figure 12.- Continued.

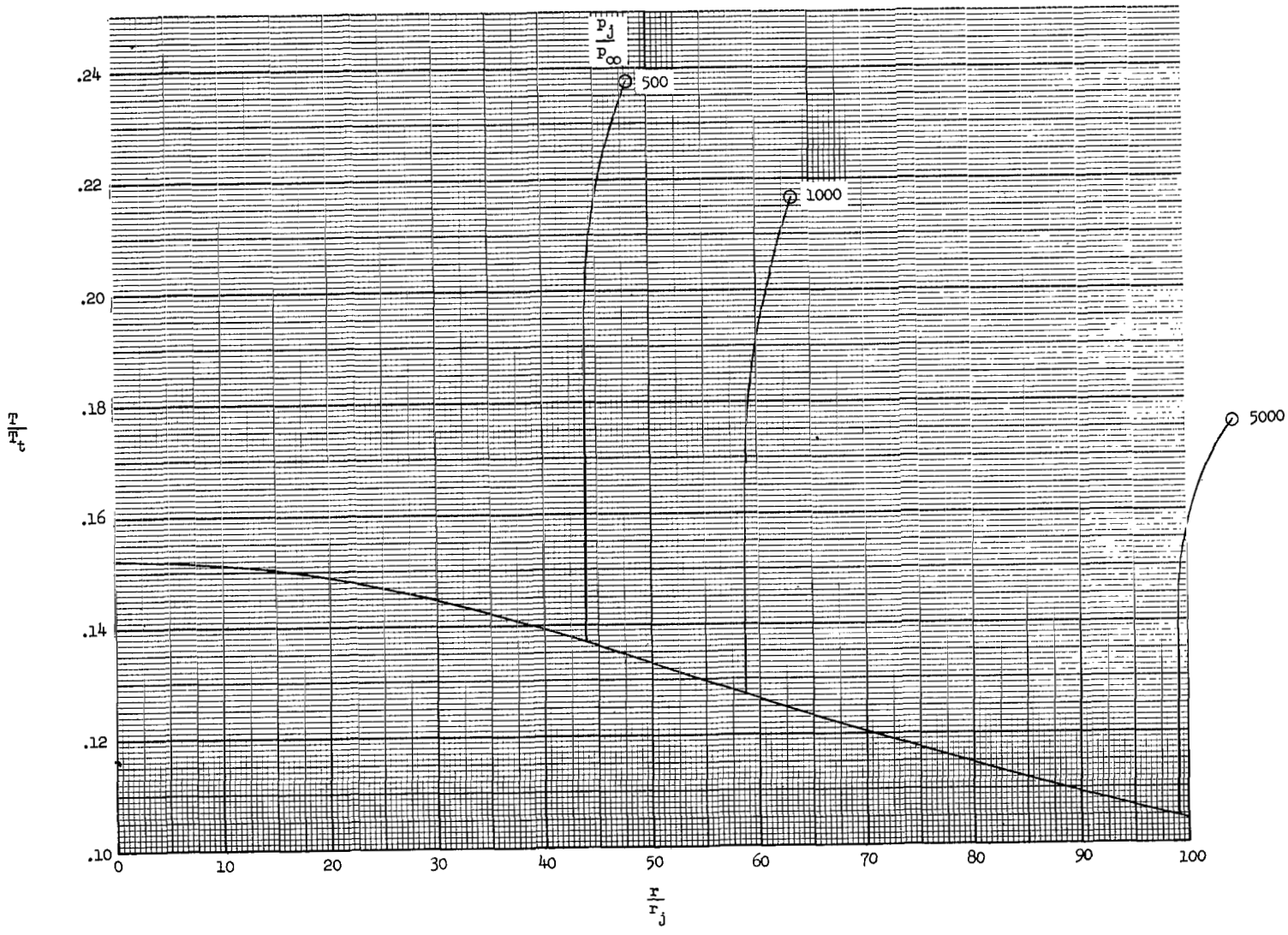

(d) $x/r_j = 80.$

Figure 12.- Concluded.

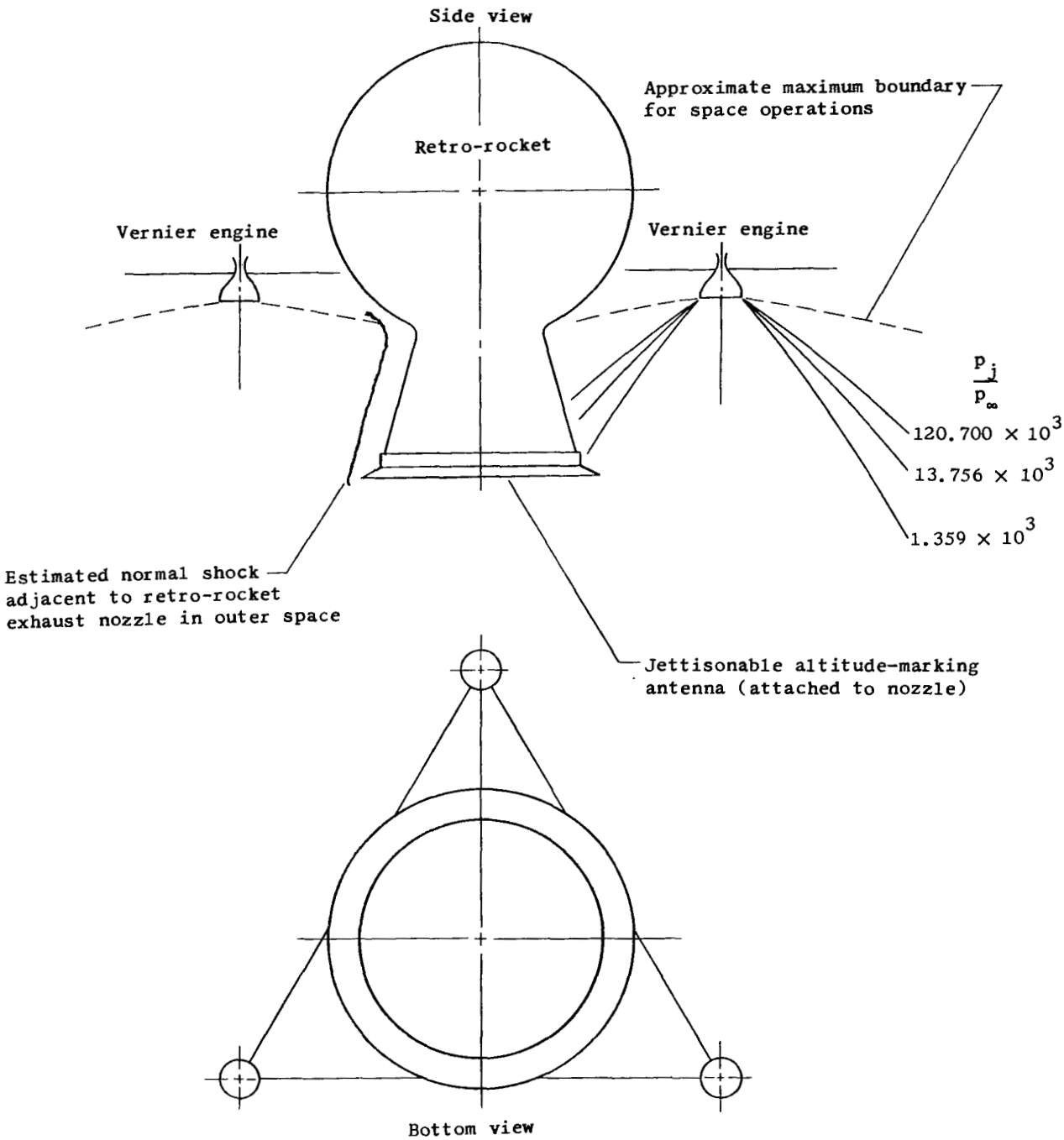

Figure 13.- Sketch showing possible location of vernier engines in relation to a retro-rocket.

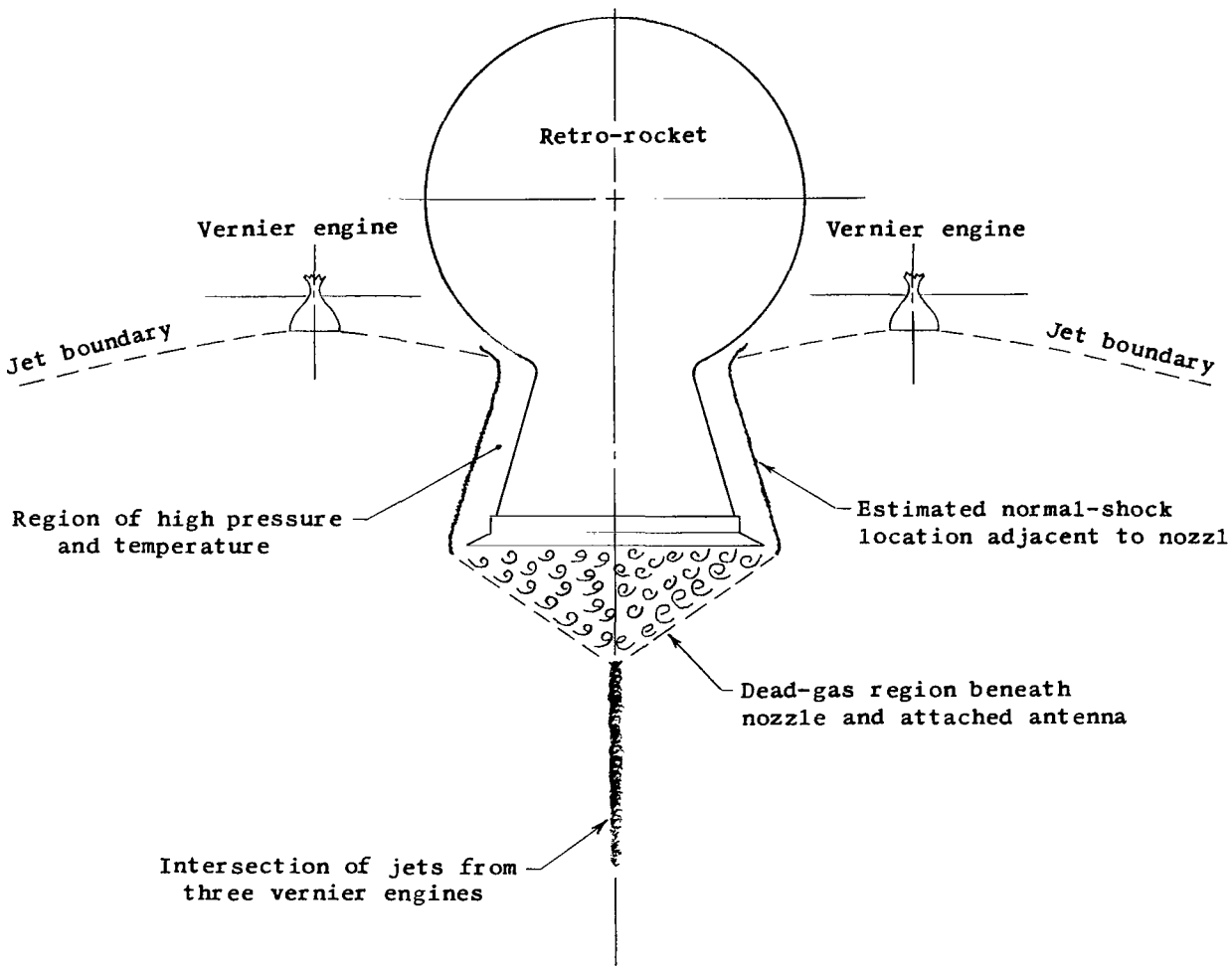

Figure 14.- Side-view sketch with jet impingement on retro-rocket nozzle.

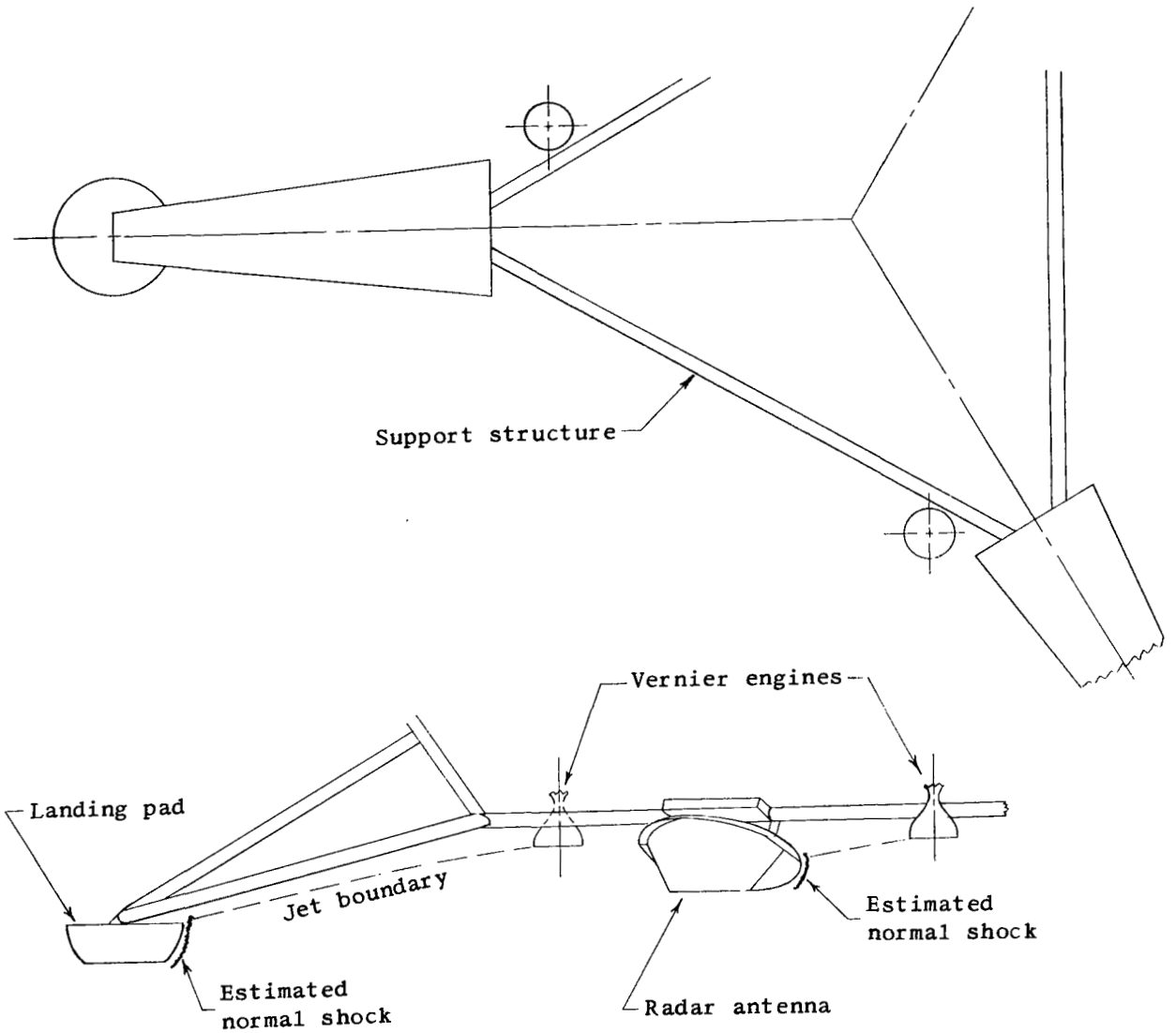

Figure 15.- Sketch showing intersection of vernier-exhaust plumes with radar antenna and landing pad.

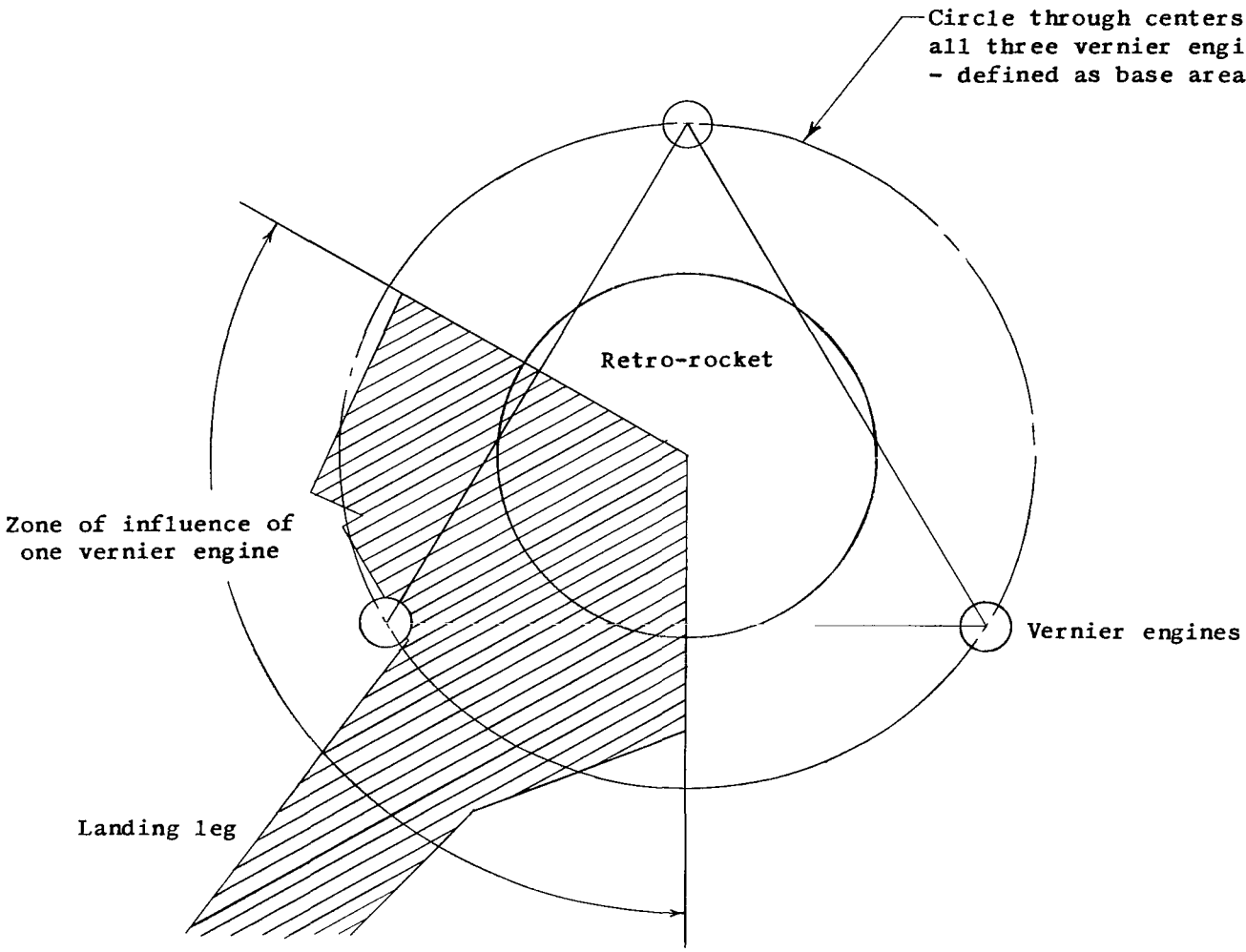

Figure 16.- Sketch showing an approximate blocked-base area.

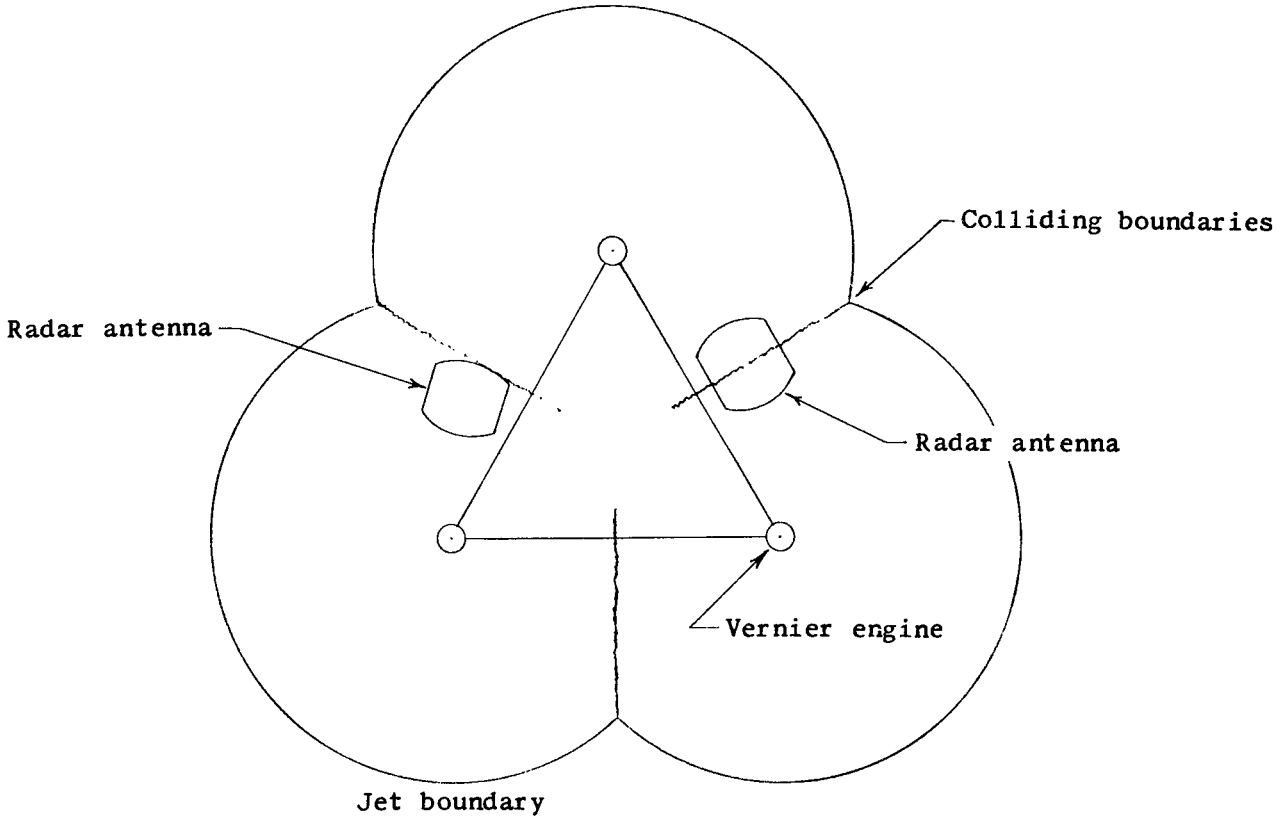

Figure 17.- Sketch of approximate location of radar antennas with respect to zones of exhaust-jet boundary collisions.

"The aeronautical and space activities of the United States shall be conducted so as to contribute . . . to the expansion of human knowledge of phenomena in the atmosphere and space. The Administration shall provide for the widest practicable and appropriate dissemination of information concerning its activities and the results thereof."

—NATIONAL AERONAUTICS AND SPACE ACT OF 1958

NASA SCIENTIFIC AND TECHNICAL PUBLICATIONS

TECHNICAL REPORTS: Scientific and technical information considered important, complete, and a lasting contribution to existing knowledge.

TECHNICAL NOTES: Information less broad in scope but nevertheless of importance as a contribution to existing knowledge.

TECHNICAL MEMORANDUMS: Information receiving limited distribution because of preliminary data, security classification, or other reasons.

CONTRACTOR REPORTS: Technical information generated in connection with a NASA contract or grant and released under NASA auspices.

TECHNICAL TRANSLATIONS: Information published in a foreign language considered to merit NASA distribution in English.

TECHNICAL REPRINTS: Information derived from NASA activities and initially published in the form of journal articles.

SPECIAL PUBLICATIONS: Information derived from or of value to NASA activities but not necessarily reporting the results of individual NASA-programmed scientific efforts. Publications include conference proceedings, monographs, data compilations, handbooks, sourcebooks, and special bibliographies.

Details on the availability of these publications may be obtained from:

SCIENTIFIC AND TECHNICAL INFORMATION DIVISION

NATIONAL AERONAUTICS AND SPACE ADMINISTRATION

Washington, D.C. 20546